MULTICOMPONENT CATALYSTS FOR METHANOL ELECTRO-OXIDATION PROCESSES SYNTHESIZED USING ORGANOMETALLIC CHEMICAL VAPOUR DEPOSITION TECHNIQUE

By

Qiling Ying Naidoo

A thesis submitted in fulfilment of the requirements for the Degree of Doctorate in the Department of Chemistry, University of the Western Cape

Supervisor: Prof. L. Petrik

Co-supervisor: Dr. A.N. Nechaev

May 2011

KEYWORDS

Nanostructure

Electrocatalysts

Platinum

Platinum group metal

Hybrid structured support

Carbon nanotubes

Titanium oxide

Organometallic chemical vapour deposition method

Methanol oxidation activity

Metal alloy structure

Multicomponent electrocatalysts for methanol electro-oxidation processes synthesized using organometallec chemical vapour deposition technique

Q.Y. Naidoo

PhD Thesis

Department of Chemistry

University of the Western Cape

In modern society there is an enormous demand for energy. The dependence on oil for transportation fuels is the major cause of air pollution in the growing urban areas of the world. Emerging trends suggest that the present oil-dependent transportation system should be moved to one that favours cleaner fuel such as natural gas in the short term, while aiming to shift over in the longer term to pollution-free fuels such methanol and hydrogen produced from renewable energy resources. Platinum has outstanding properties, such as high melting temperature, good conductivity and electronic and catalytic properties. Nanophase platinum catalysts play a vital role in hydrogen production and many other chemical production processes. The purpose of this study was tosuccessfully produce multicomponent nanophase platinum group metal (PGM) electrocatalysts with high uniform particle size, high dispersion and high electrochemical activity using an efficient one-step Organometallic Chemical Vapour Deposition(OMCVD) method for methanol electro-oxidation process.

In this study, the OMCVD method is demonstrated as a powerful, fast, economic and environmental friendly method to produce a set of PGMelectrocatalysts with different supports, metal content and metal alloys in one step and without the multiple processing stages of impregnation, washing, drying, calcinationsand activation.

ABSTRACT

The prepared electrocatalysts were characterized by physico-chemical and electrochemical techniques, such as EDS/SEM, ICP, BET, FTIR, HRTEM, XRD, TPR and CV.

In the investigation of different supports, it was found that carbon nanotubes (CNTs) are a better support than Vulcan XC-72 for preparing the Pt electrocatalysts. The Pt catalyst supported on CNTs showed a larger chemical-surface area (153m^2/g) and better methanol oxidation activity (115mA/cm^2) due to the highly crystalline structure of CNTs while the Pt catalyst supported on Vulcan XC-72 displayed the chemical-surface of 138 m^2/g and methanol electro-oxidation current densities of 99 mA/cm^2.The effect of Pt content was also investigated for the purpose of achieving optimal Pt wt. % with the highest electro-catalytic activity. It was found that the particle size of Pt was increased by increasing wt.%of Pt loaded onto the support. The 40 wt. % Pt/CNT catalyst obtained the largest electrochemical surface area (201 m^2/g) and the highest methanol oxidation activity (200 mA/cm^2), which was higher than 20 and 60 wt.% Pt catalysts as well as that of the commercial standard Johnson Matthey(JM) Pt/C catalyst (190 m^2/g and 182 mA/cm^2).

An investigation into the influence of Pt in binary and ternary combinations of metal alloys (PtRu/CNT, PtRuFe/CNT, PtRuCu/CNT and PtRuV/CNT) was undertaken for the purpose of reducing CO poisoning and enhancing catalytic performance by advanced electro-catalyst design relying on the bi-functional mechanism. It was found that the added metals in platinum alloys could reduce the particles size of the catalysts and resulted in the larger chemical-active surface area and higher methanol electro-oxidation current. Catalyst PtRuV/CNT showed the largest electrochemical surface area (238 m^2/g) and the highest methanol oxidation activity (228 mA/cm^2)compared to other home-made PGM catalysts.The activity obtained was also significantlybetter than that of the commercial standard JM PtRu/C catalyst (159 m^2/g and 140 mA/cm^2).

ABSTRACT

A new approach was adopted in which a TiO_2 coating on CNTs was introduced as a composite support for dispersing the PGM catalysts. The results showed that TiO_2 is a good surface promoter for the catalysts as the added additional TiO_2 resulted in a smaller PGM particle size and higher particle size dispersion of the PGM catalysts when compared with the catalysts supported only on CNTs. Catalyst PtRuV/TiO_2/CNT was found to achieve the largest chemically-active surface area (260 m^2/g) and the highest methanol oxidation current density (280 mA/cm^2), which was significantly better than other home-made electrocatalysts as well as the commercial standard JM PtRu/C catalyst (159 m^2/g and 140 mA/cm^2).

All the home-made catalysts with different metals and TiO_2 coatings were successfully produced by OMCVD method. Knowledge gained from the project is expected to allow the directed design of electrocatalysts with uniform particle size, high dispersion and high electrochemical activity using OMCVD method.

May, 2011

DECLARATION

"I declare that "*Multicomponent electrocatalysts for methanol electro-oxidation processes synthesized using organometallec chemical vapour deposition technique*" is my own work, that it has not been submitted for any degree of examination in any other university and that all the sources I have used or quoted have been indicated and acknowledged by means of complete references".

Full name: Date: _____ _____

Signed: _____

ACKNOWEDGEMENTS

I want to express my deepest gratitude to my family, whose support has been invaluable to me. A special thanks to my husband and my daughter.

I would like to thank the NRF for the financial support and for promoting this research direction.

I would like to express my deepest appreciation to Prof. L. Petrik for her support and affording me a chance to be a member of ENS group.

I am most grateful to Dr A. Nechaev and Dr. P. Ndungu, my co-supervisors, for providing valuable experimental idea, guidance and supervision.

Many thanks to Dr. N. Young at University of Oxfard for his contribution to HRTEM analysis.

I would also like to acknowledge Prof. B. Julies and Mr. A. Josephs in the Physics Department of UWC and Dr. R. Bucher in Ithemba Labs, for their excellent work with EDS/SEM, HRTEM and XRD analysis, especially thanks to Dr. Malik Maaza for supplying the Auto Lab system to support my experimental work.

A special thanks to all my colleagues at the ENS group for all their help during this study. In particular, I would like to thank Miss A. Abbott and Mrs. V. Kellerman for their assistance.

LIST OF FIGURES

LIST OF FIGURES

LIST OF TABLES

LIST OF TABLES

LIST OF ABBREVIATIONS

ALD Atomic layer deposition

BET Brunauer-Emmett-Teller

CNT Carbon Nanotube

CV Cyclic Voltammetry

CVD Chemical Vapor Deposition

DMFCDirect methanol fuel cells

EBCVD Electron beam chemical vapour deposition

EC Electrochemical

EDS Energy Dispersive Spectroscopy

EG Ethylene glycol

FBCVD Fluidized bed chemical vapour deposition

FTIRFourier Transform Infrared

HRTEM High resolution Transmission Electron Microscopy

IACVDFocused ion-assisted chemical vapour deposition

ICP-MSInductively Coupled Plasma Mass Spectroscopy

JM Johnson Matthey™

LCVD Laser induced CVD

LSV Linear Sweep Voltammetry

MEAMembrane Electrode Assembly

SWNT Single-wall Nanotube

MWNT Multi-wall nanotube

OMC Ordered mesoporous carbon

OMCVD Organometallic Chemical Vapour Deposition

ORR Oxygen Reduction Reaction

PAFC Phosphoric acid fuel cell

PECVD Plasma enhanced platinum chemical vapour deposition

PEM Proton Exchange Membrane

LIST OF ABBREVIATIONS

PEMFC Proton Exchange Membrane Fuel Cell

PGMPlatinum group metal

SEM Scanning Electron Microscopy

TPRTemperature Programmed Reduction

XRD X-Ray diffraction

UVCVD UV induced chemical vapour deposition

WC Wet-chemical

CHAPTER 1:

Introduction

This chapter introduces the dissertation topic and specifies the main perspective, from which the topic was researched, and the rationale and motivation of the study. The main research questions and problem statements are set out and the research approach and design and the methodology that was used in then described. The dissertation outline is finally given in this chapter with an overview of the structure of the dissertation showing how the dissertation will unfold and describing the main topic of each chapter of the dissertation.

1.1 Background

In modern society there is an enormous demand for energy. The dependence on oil for transportation fuels is the major cause of air pollution in the growing urban areas of the world. Emerging trends suggest that the present oil-dependent transportation system should be moved to one that favours cleaner fuel such as natural gas in the short term, while aiming to shift over in the longer term to pollution-free fuels such methanol and hydrogen produced from renewable energy resources [1]. Nanotechnology provides clean energy solutions to manyapplications and may have a profound effect on energygeneration, storage and utilization. Thus, understanding differences in energy states and transport mechanisms ofnanostructures compared to macrostructures is important [2].

Platinum has outstanding unique properties, such as high melting temperature, good conductivity and electronic and catalytic properties [3].Nanophase platinum catalysts play a vital role in hydrogen production and many other chemical production processes. For example, Pt serves as a catalyst in catalytic converter (autocatalyst), which converts over 90 per cent of hydrocarbons, carbon monoxide and oxides of nitrogen from gasoline engines into less harmful carbon dioxide, nitrogen and water vapor. Pt is also a critical component of fuel cell, where the platinum is using as an electrocatalyst to generate energy for portable and auxiliary power units and for powering vehicles [4].

South Africa holds about 88% of the total known of platinum reserves [5].The future economic growth is tied of South Africa to a transition towards innovation, benificication and high technology development rather than simply just speeding up the extraction of non-renewable resources. This is the only way of building an effective and sustainable basis for South Africa over the long-term.

1.2 Rational and Motivation

As South Africa is the one of the world's leading exporters of platinum group metals, the beneficiation of platinum group metals (PGM) holds great promise. Thus, a fundamental research investigation of nanostructured PGMcatalysts therefore is vital.

Catalytic activity strongly depends on particle size. For two reasons catalysts are more effective when they are small enough to fall within the range of 1-100 nanometers (nm) in size (the nanoscale) than conventional catalysts. First, their extremely small size yields a tremendous surface area-to-volume ratio. Second, when materials are fabricated on the nanoscale, they achieve properties not found within their macroscopic counterparts. Both of these reasons account for the versatility and effectiveness of nano-catalysts [6]. A fundamental research investigation is needed to identify and understand how to engineer and fabricate functionally designed nanostructured PGM metal alloys with specific architectures.Further understanding of the particle-to-particle or intermetallic interactions on the nanoscale and how these interactions translate to the bulk material will allow for intelligent and targeted design of novel metal alloys. Methodologies must be developed to evaluate the performance of designed materials and to understand the behaviour observed.

In conclusion, for the successful beneficiation and application of PGM to be realized, which holds great promise for SA, the development of novel nanostructured PGM catalysts is very important.

1.3 Research Approach

Platinum is a nobel metal of limited supply. To enhance catalytic performance [7-8], stability [9-10], durability [11-12] and reduce operational costs [13] of platinum

electrocatalysts, advanced electro-catalyst design relying on the bi-functional mechanism, and using hybrid support carbon materials has been proposed. The benefit of a bi-functional nanophase containing catalyst is that the reaction mechanism involves both the metal alloy and the support. The important factors are the dispersion of the metal alloy on the support and the overall sizeand composition of the metal alloy.

Also, to deposit the TiO_2 on CNTs as a support for Pt catalysts has become a new approach in current study. Recently, researchers have reported that systems combining platinum, metal oxides and carbon exhibited excellent catalytic activity for electrooxidation of methanol and CO. The so-called “hypo-hyper-d-concept” is very important for the development of multi-component platinum electrocatalysts.

Furthermore, the deposition of precious metals either chemically or electrochemically plays an important role in the development of technologies where these metals are used.The greatest challenge at present is to find effective nano synthesis procedures to prepare and apply nanoscale components [14].There is significant interest to improve the functionality of the catalyst by Pt-alloying with high dispersion and great electrochemical activity.

By taking into account both size and surface structure, one can tailor the catalytic activity of PGM and non-platunum catalysts at the nanoscale by controlling the shape of nanocrystals during their chemical synthesis. Developing the optimal

synthesis routs for the electrocatalysts with well-defined and selectivity at lower cost should be investigated.

1.4 Research Hypothesis

The problem statement of the study can be hypothesized as follows:

Development of synthesize method, based on the Organometallic Chemical Vapour Deposition technique, for the preparation of advance multicomponent electrocatalysts, based on Pt and Pt alloys, for the methanol electro-oxidation process. The fabrication method should beefficient and produce electrocatalysts that should exhibit uniform particle size, high dispersion and high electrochemical activity.

In addressing the hypothesis the following research questions of the study were included:

i. What is the most efficient fabrication method?
ii. Which fabrication method produces the best catalytic behavior?
iii. Can multicomponent catalysts be prepared by using the simple synthesis method?
iv. Can the catalysts be prepared without agglomeration and with high dispersion and high catalytic activity?
v. Will the CNTs be a better support than Vulcan for the catalysts?
vi. What is the optimal content for Pt catalysts

vii. Will the electrochemical activity of Pt catalyst be enhanced by adding the additional second or third metals?

viii. Will the added additional metals reduce the cost of Pt catalysts?

ix. What is the structure of prepared binary and ternary PGM catalysts?

x. Can TiO_2 modify the CNTs as a new support for electrocatalysts?

xi. Will the catalytic activities of the catalysts be enhanced by being supported on TiO_2/CNT

1.5 Characterization of Catalysts

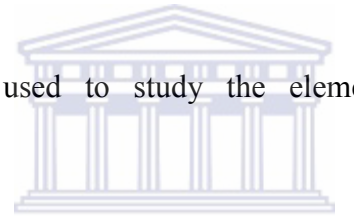

i. EDS/SEM will be used to study the elemental composition of the electrocatalysts

ii. FTIR will be used to determine the structural configuration

iii. BET will be used to study the information of total surface area, pore size distribution andporosity of support

iv. ICP will be used to determine the composition of the catalysts

v. XRD will be carried out to confirm the PGM particle size and crystalline structure of the PGM/CNT electrocatalysts.

vi. HRTEM will be used in the investigation of average particle size, particle shape, surface morphology and particle size distribution of electrocatalysts.

vii. TPR will be used to determine the reducibility and catalyst structure of the prepared electrocatalysts.

viii. Cyclic votammetry (CV) will be carried out to determine the electrochemically-active surface area and catalytic activity of the measurement for electronic properties

1.6 Structure of Thesis

- ✧ Each chapter opens with an overview of the literature related to the specific topic covered in that chapter, followed by experimental section, results and discussion and a concluding section.
- ✧ Chapter 2: Literature review. Presents a theoretical overview and background information of research, undertaken to date
- ✧ Chapter 3: Experimental. Outlines the principles supporting the characterization techniques when testing the catalysts
- ✧ Chapter 4: Synthesize platinum group metal catalysts with different preparation conditions
- ✧ Chapter 5: Synthesize platinum group metal catalysts supported on TiO_2/CNT by OMCVD method
- ✧ Chapter 6: Determination of Reducibility of PGM/TiO_2/CNT Electrocatalysts
- ✧ Chapter 7: Conclusions and Recommendations for future research

Scope and delimitations of the study will be presented by the end of Chpater 2.

CHAPTER 2:

Literature Review

The literature review presented in this chapter informed and defined the thesis topic and main perspective, rationale and motivation, research tasks and objectives of study as well as the delimitation of the study. The researchdesign and refinement of approach and research hypothesis as well as thedelimitations of the research and the main perspective from which the topic wasresearched were also developed from the perspective gained from the literaturereview.

2.1 Introduction

A catalyst is defined as a substance, usually used in small amounts relative to the reactants, that modifies and increases the rate of a reaction without being consumed in the processes [15]. The catalyst can perform reaction in one of three ways, which are it can lower the activation energy for the reaction, act as a facilitator and bring the reactive species together more effectively, or create a higher yield of one species when two or more products are formed. Depending on the application, nano-catalysts can be used in all the ways listed above [16].

Catalysts play an essential role in many chemical production processes. They work by providing an (alternative) mechanism involving a different transition state and lower activation energy. The effect of this is that more molecular collisions have the

energy needed to reach the transition state. Hence, catalysts can perform reactions that, albeit thermodynamically feasible, would not run without in their absence, or perform them much faster, more selectively, or at lower temperatures [17]. This effect can be illustrated with a Boltzmann distribution and energy profile diagram in Figure 2.1, which shows a generic potential energy diagram of the effect of a catalyst in a hypothetical exothermic chemical reaction X + Y to give Z. The presence of the catalyst opens a different reaction pathway (shown in red) with lower activation energy. The final result and the overall thermodynamics are the same.

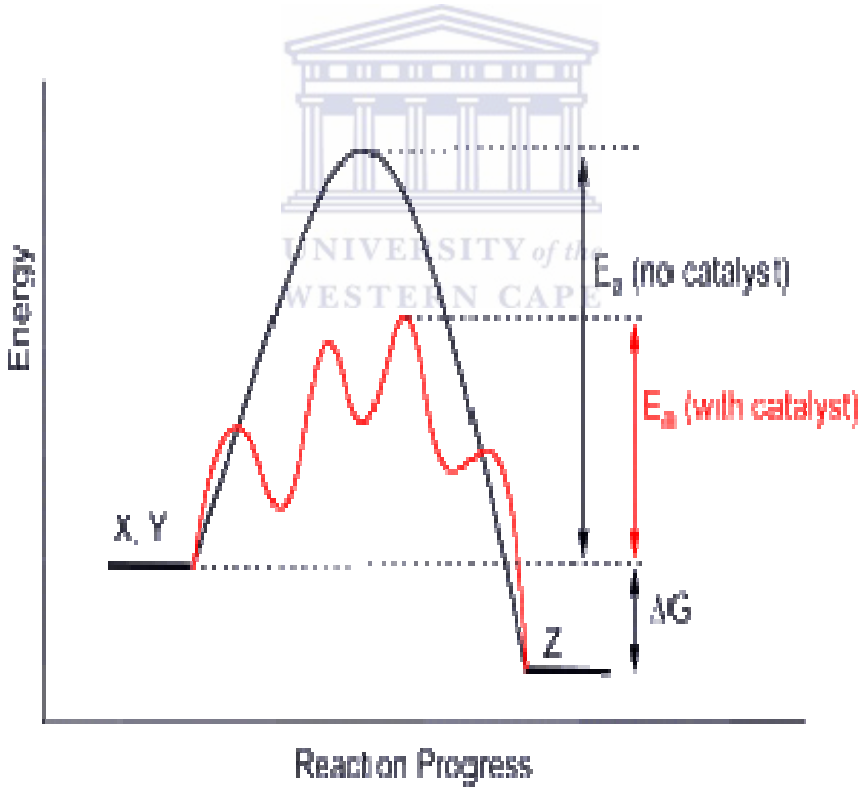

Figure 2.1 Energy profile diagram with catalyst and without catalyst [17]

The general purpose of catalysts is to increase the speed of a given reaction. This is achieved through kinetic means and does not directly affect the thermodynamic

properties of a chemical system. Introducing a catalyst increases the speed of a reaction in one of three ways: 1) it can lower the activation energy for the reaction; 2) act as a facilitator and 3) bring the reactive species together more effectively [6].

Materials reduced to the nanoscale can suddenly show very different properties compared to what they exhibit on the macroscale, enabling unique applications. For instance, opaque substances becomes transparent (copper); inert materials become catalysts (gold); stable material turn combustible (aluminum); insulators become conductors (silicon). Materials such as platinum, which is chemically inert at normal scales, can serve as a potent chemical catalyst at nanoscale. Much of the fascination with nanotechnology stems from these unique quantum and surface phenomena that matter exhibits at the nanoscale [18]. The active sites of a catalyst increase or are more readily available in nanoscale structures, causing chemical reactions to speed up. An active site is the area of the catalyst where reactants combine and a new product forms. Not all the surface of nanoparticle serves as an active site, though. In some cases, the active site may be at the edge or surface. Catalysts are deemed improved if products form faster than before, and it is not as expensive to make the product as before [19].As a result, physical and chemical properties of the electrocatalystic materials are altered compared to the original properties of the associated bulk materials. With the shift of PGM catalyst particle size into the nanometer domain the characteristics of altered electrocatalystic properties (e.g. surface reactivity) gains significant importance. This significance stems from the

fact that most engineered nanophase PGM catalysts have a functionality based on their structural physicochemistry.

In the context of electrochemistry, specifically in fuel cell engineering, various metal-containing catalysts are used to enhance the rates of the half reactions that comprise the fuel cell. One common type of fuel cell electrocatalyst is based upon nanoparticles of platinum that are supported on slightly larger carbon particles. When this platinum electrocatalyst is in contact with one of the electrodes in a fuel cell, it increases the rate of oxygen reduction to water (or hydroxide or hydrogen peroxide) [17].

Electrocatalysis entails increasing the reaction rate and selectivity at electrodes, in electrochemical cells, using materials exhibiting high catalytic activity towards the electrode processes. Electrocatalysts act directly at interfaces by anchoring reagent species to their catalytic centres or active sites. Suitable electrocatalysts have good corrosion stability over extended periods, good electrical conductivity to minimize resistance loss, and low cost [16].

The requirements for a practical electrocatalyst include high intrinsic activity for the electrochemical oxidation of a fuel at the anode side and for the reduction of di-oxygen at the cathode side. It also requires good durability and electrocatalysts should have good electrical conductivity to minimize resistive losses in the catalyst layer, be inexpensive to fabricate, and be manufacturable at high volume with good reproducibility [20].

If an electrocatalyst is to be commercially useful it must possess several desirable features. Key electrocatalysts properties are high activity, high selectivity, high-recycle capability and filterability. Important process components include choice of catalytic metal, choice of support, reactor design, heat and mass transport, catalyst design, catalyst separation, and spent catalyst recovery and refining [21].Considering the requirements of a suitable catalyst material, platinum and platinum metal group (PGM) catalysts supported on carbon nano-structure materials are found to accord with these requirements, in both activity and stability [20].

2.2 Overview of Platinum Group Metal Electrocatalysts

In materials science, the range of properties of metallic systems can be greatly extended by using mixtures of elements to generate intermetallic compounds and alloys. In many cases, there is an enhancement in specific properties upon alloying due to synergistic effects, and the rich diversity of compositions, structures, and properties of metallic alloys has led to widespread applications in electronics, engineering, and catalysis. The desire to fabricate materials with well-defined, controllable properties and structures on the nanometer scale coupled with the flexibility afforded by intermetallic materials has generated interest in bimetallic and trimetallic nanocluster.

To enhance catalytic performance and reduce operational costs of platinum electrocatalysts, advanced electro-catalyst design relying on the bi-functional mechanism has been proposed. Various kinds of catalystshave been investigated.

2.2.1 Pt-Based Binary Electrocatalysts

In Pt-electrode applications in fuel cells, Pt-Ru nanoparticles, supported on carbon, have found widespread use for catalyzing a variety of fuel cell reactions [22-27]. Alloyed Pt-Ni nanoprticles are of interest as electrocatalysts for oxygen reduction in low-temperature polymer electrolyte fuel cells. Depending upon the method of surface preparation, Carbon supported Pt-Ni nanoparticles may even have enhanced activity over pure Pt catalysts for oxygen reduction [28]. Pt-Pd nanoalloys also have been widely studied due to their importance in catalysis [29]. An important catalytic application of Pt-Pd is in the reduction (by hydrogenation) of aromatic hydrocarbons in fuel. It has been claimed that Pt-Pd alloy particles are more catalytically active for aromatic hydrocarbon hydrogenation and more resistant to sulfur-poisoning than either of the pure metals [30]. Pt-Cu nanoparticles were investigated with regard to their catalytic activity for NO reduction [31]. Compared with pure Pt nanoparticles, intermixed Pt-Cu particles exhibited higher selectivity for N_2 formation but reduced overall activity. Pt-Au nanoparticles can be used for the electrocatalytic oxidation of methanol and CO with the reaction studied by cyclic voltammetry [32-34]. It is believed that CO oxidation takes place at surface Au sites, while methanol oxidation takes place at Pt. Pt-Co alloys were investigated with the electrocatalytic activity in

alkaline electrolyte and proton exchange membrane fuel cells [35-36]. The driving force behind this work was to reduce the costs of electrocatalysts by alloying Pt with less expensive metals (e.g., Fe, Co, Ni or Cu). Ross and co-workers also investigated carbon-deposited Pt-Co nanoalloys for oxygen reduction in fuel cell applications [28]. Pt-Os, however, as found to have low catalytic activity for methanol oxidation catalysis [37-38]. Pt-Rh alloys have been used tocatalyze the reduction of NO with Pt-rich clusters having higher catalytic activity and also being more active than pure Pt particles [39]. Pt-Mo alloys are even better electrocatalysts for oxidation of H_2/CO mixtures than the 50% Pt-Ru surface, perhaps because there is significantly less segregation of Pt to the surface than in the other systems, which is driven by the more exothermic Pt-Mo mixing [40].

Bimetallic nanoparticles are of considerable interest from both scientific and technological points of view [41-45]. Recently, the investigation of the mechanism of promotion as well as the search for more active or less expensive PtRu catalysts has been reported. In particular, M.T.M. Koper et al. [46] showed that of PtRu, where enhanced tolerance could be ascribed to a decrease in CO binding energy on platinum due to electronic substrate effects, and to the oxidation of chemisorbed CO being catalyzed at low potentials by the activation of H_2O [47]. Herrero et al. [48] also found that OH adsorption on Ru site on a Pt (110) surface could be identified as active in the bifunctional mechanism. Evidence of local electronic modification of Pt atoms near Ru atoms on a modified surface has also been provided by such studies [49-51]. Further, U.A. Paulus et al. [52] proved that the methanol

electrotro-oxidation activity on the PtRu/C catalyst can be enhanced if the PtRu alloy particles are produced in a nanoscale range 2-4 nm. There has also been an effort to improve the behavior of the PtRu binary catalyst by incorporation of a third metal exhibiting facile oxide formation characteristics.

2.2.2 Pt-Based Ternary Electrocatalysts

Regarding the Pt-based binary catalysts, the question is whether the catalytic activity can be further improved by using ternary systems with elements such as W, Mo, Co, Ni, Os, Sn, etc., having aco-catalytic activity for the anodic oxidation of methanol orCO, if used either as platinum alloys or as adsorbate layers onplatinum [53].

Chen, *et. al.* [54-56] tested the activity for CO and methanol oxidation with H_2/CO or methanol showed that many ternary Pt-Ru-M catalysts (M = W in WOx or W_2C form, Mo, Ir, Ni, Co, Rh, Os, V) performed better than commercial standard Pt-Ru catalysts, however, Pt-Ru-Nb, Pt-Ru-Au and Pt-Ru-Ag systems showed no improvement in CO tolerance [57-59]. With the methodology of high-throughput screening, the Co, Ni, Fe, Ir, Rh and W were proved as suitable elements to form ternary Pt-Ru-based catalysts with improved activity for CO and methanol oxidation [60-61]. All ternary Pt-Ru-based catalysts were tested by Zhou *et. al.* [62-64] and showed better perform than Pt-Ru. Ternary Pt-Sn-based catalysts were also proved have better perform once than Pt-Sn [65-67]. Luczak and Landsman [68] found that carbon supported Pt-Cr-Co alloys have a catalytic activity for the ORR of at 20% more with respect to the binary Pt-Cr catalyst. Conversely, Shukla *et. al.* [69-70]

found that Pt-Co/C has a superior activity relative to Pt-Co-Cr/C. The same conclusion was also found by Cho *et. al.* [71] that Pt-Cr/C possessed an enhanced electrocatalytic activity compared to ternary Pt-Cu-Fe/C catalysts. A high stability of the ternary Pt-M1-M2 alloys catalysts was observed both in phosphoric acid fuel cell (PAFC) and proton exchange membrane fuel cell (PEMFC) conditions. Pt-Ga-Cr showed resistance to both sintering and chemical dissolution during operation in PAFC [71-72]. Pt-Rh-Fe/C showed high physical and chemical stability, as well as high activity of fuel cell tests [73]. During a long-term stability test in single PEMFC, the Pt-Co-Cr/C catalyst did not show a significant decay in performance [74]. A higher ORR activity of Pt-Cr-Cu/C than that of the Pt/C catalyst was found by Tamizhmani *et. al.* [75]. Cho *et. al.* [76] also found that the ORR activity of Pt-Cu-Fe catalysts increased with increasing the degree of ordering. In the case of PtRuMo, promising results were attained for PEMFC operation on hydrogen [77-78] or reformate gas [79-80]. The inclusion of W was also found to be beneficial [80], while partial substitution of Ru in PtRu by Cr, Zr, or Nb, resulted in a decrease in activity for H_2 oxidation in the presence of 10 or 100 ppm CO [81].

2.2.3 Oxidation of methanol on thePt electrocatalysts

The methanol oxidation reaction can be used to study the activities of the platinum electrocatalysts. It has been found that platinum is the best catalyst for methanol oxidation. Methanol oxidation is a slow reaction that requires multiple active sites for methanol adsorption and oxidation and it can be summarized in terms of two

basic functionalities: (1) electrosorption of methanol onto the substrate and (2) addition of oxygen to adsorbed carbon-containing intermediates to generate CO_2 [82]. The mechanism of methanol oxidation of the Pt catalyst is commonly written as:

$$Pt + CH_3OH \rightarrow Pt—CH_2OH + H+ e^- \quad [2\text{-}1]$$

$$Pt + CH_2OH \rightarrow Pt—CHOH + H^+ + e^- \quad [2\text{-}2]$$

$$Pt + CHOH \rightarrow Pt—COH + H^+ + e^- \quad [2\text{-}3]$$

$$Pt + COH \rightarrow Pt—CO + H^+ + e^- \quad [2\text{-}4]$$

$$Pt + H_2O \rightarrow Pt—OH + H^+ + e^- \quad [2\text{-}5]$$

$$Pt—CO + Pt—OH \rightarrow 2Pt + CO_2 + H^+ + e^- \quad [2\text{-}6]$$

Reactions [2-1] to [2-4] are the methanol electrosorption processes and [2-5] to [2-6] are the processes of oxygen removal or oxidation of intermediates. Figure 4.6 shows the mechanism of methanol oxidation on platinum.

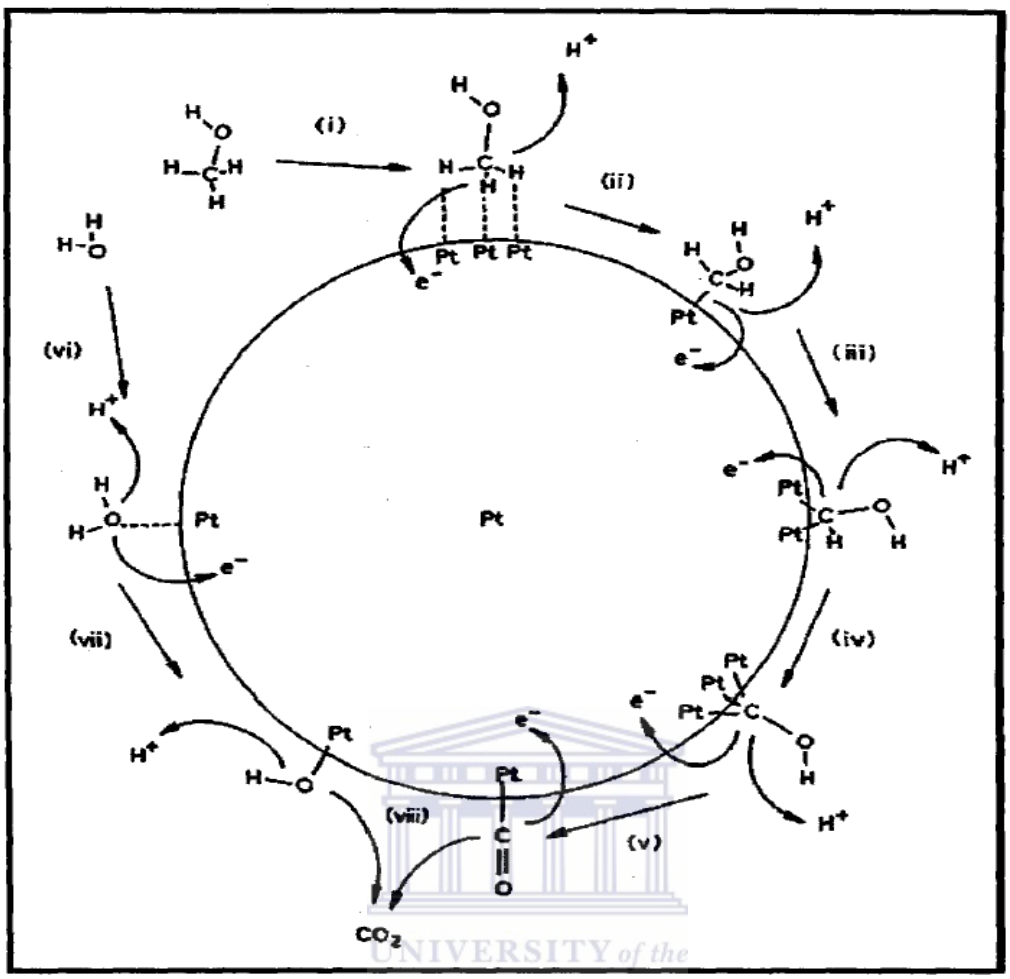

Figure 2.2: Mechanism of methanol oxidation reaction on Pt catalyst [83]

Bimetallic PtRucatalysts are promising anodic catalysts forcommercial direct methanol fuel cells (DMFC). The role of Ru inPtRu catalysts for CO oxidation is commonly explained by theelectron effect or a bi-functional mechanism. According to theelectron effect, Ru alters the electronic state of Pt, causing CO tobecome more weakly adsorbed. Loss of CO binding intensityleads to a decrease in oxidation overpotential of the cell.The mechanism of methanol oxidation of the PtRu catalyst is commonly written as [84]:

$Pt + CH_3OH \rightarrow Pt - CH_3OH$ [2-7]

$Pt - CH_3OH \rightarrow Pt - CO_{ads} + 4H^+ - 4e^-$ [2-8]

$Ru + H_2O \rightarrow Ru - OH_{ads} + H^+ + e^-$ [2-9]

$Pt - CO_{ads} + Ru - OH_{ads} \rightarrow Pt + Ru + CO_2 + H^+ + e^-$ [2-10]

2.3 Structures of Platinum Nanoalloy

Nanoalloys can be generally classified according to their chemical ordering (mixing pattern) and geometric structure.

2.3.1 Mixing Patterns

There are four main types of mixing patterns can be identified for nanoalloys, see Figure 2.3.

i. Core-shell Segregated Nanoalloys
ii. Subcluster Segregated Nanoalloys
iii. Mixed A-B Nanoalloys
iv. Multishell Nanoalloys

Core-shell structures (Figure 2.3 a) consist of a shell of one type of atom (B) surrounding a core of another (A), though there may be some mixing between the shells. This mixing pattern is common to a large variety of systems.Subcluster segregated (Figure 2.3 b) nanoalloys consist of A and B subclusters, which may share a mixed interface (left) or may only have a small number of A-B bonds

(right).The mixing structure will be either ordered (left) or random (right) (Figure 2.3 c). Random mixed nanoalloys (Figure 2.3 d) are often termed "alloyed" nanoparticles and multishell pattern may present layered of onion-like alternating –A-B-A- shells.

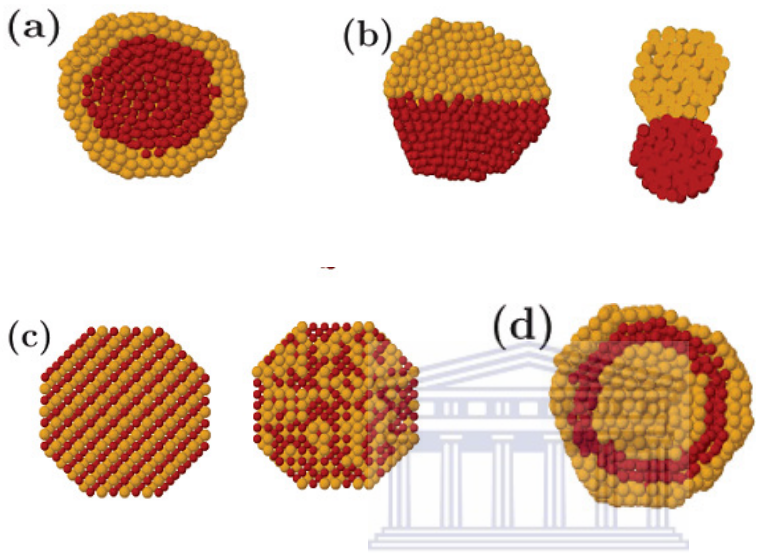

Figure 2.3: Different mixing patterns of (a) core-shell, (b) subcluster, (c) mixed, (d) mutilshell [74]

2.3.2 Geometric Structures

By analogy with pure metal cluster, for nanoalloys, crystalline structure and noncrystalline structures are possible. Crystalline structures are fragments of bulk crystal (Figure 2.4). In the case of the fcc bulk lattice, crystalline clusters may take the form of octahedral or truncate octahedral [85].

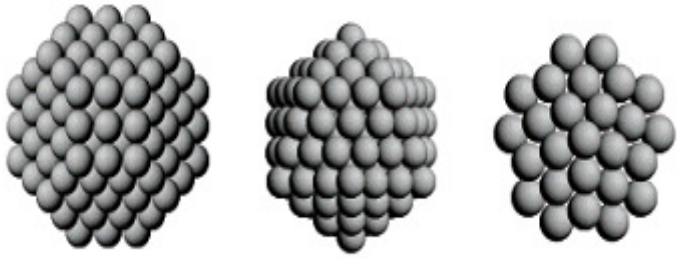

Figure 2.4: Crystalline structures (from left to right) fcc truncated octahedron, icosahedron, and truncated decahedron

2.3.3 Factors Influencing Atomic Ordering in Nanoalloys

Structures and degree of A-B segregation/mixing can depend on the method of nanoparticle generation. Normally, nanoalloys can be generated in cluster beams or as colloids or by decomposing bimetallic organometallic complexes. Bimetallic nanolloys (A_aB_b) can be generated with controlled size (a+b) and composition (a/b) [86].

The degree of segregation/mixing and atomic ordering in AaBb nanoalloy depends on the following factors:

i. Relative strengths of A-A, B-B and A-B bonds
ii. Surface energies of bulk elements A and B
iii. Relative atomic sizes
iv. Charge transfer
v. Strength of binding to ligands (surfactants) or surfaces
vi. Specific electronic/magnetic effects

2.4 Structural Effect of Electrocatalysts

The common criteria for a high performance catalyst are: (1) narrow nanoscale size distribution; (2) uniform composition throughout the nanoparticles; (3) high dispersion on carbon support [87]. The basic function of a catalyst layer is to provide a environment conductive for electrochemical reactions. The main processes that occur in the catalyst layer include mass transport, interfacial reactions at electrochemically active sites, proton transport in the electrolyte phase, and electron conduction in the electronic phase [2].

2.4.1 Particle Size Effect

The size of the deposited noble metal particulates and their location on the support material affect the properties and performance of a heterogeneous catalyst. Increased metal dispersion and decreased metal particle size generally result in increased catalyst activity.

The first investigation of the relation between particle size and structure of platinum black and platinum on carbon and the electrochemical activity of oxygen reduction reaction (ORR) was reported by H. Zeliger and Bett *et. al.* [88-89]. They found that there is no relationship between the particle size (between 3-40nm) and the structure of commercial Pt black and Pt/C catalysts with ORR activity. Vogel *et. al.* [90] also came to a similar conclusion when correlating ORR activity and particle size. Kunz *et. al.* [91] found that smooth Pt has the equivalent ORR activity to carbon supported

Pt catalyst at 160 °C in an electrolyte composed of 96% H_3PO_4 and at 70 °C in 20% H_2SO_4. As a result, they deduced that the contact between the noble metal and the carbon support was inadequate and thus concluded that ORR activity is not related to Pt particle size.

On the other hand, Bluton [92], Bregoli [93] and Peuckertdeng [94] *et. al.* found a decrease in the specific activity for oxygen reduction with diminishing particle size from 12 to 2 nm. Blutons study involved highly dispersed platinum on carbon in 20% H_2SO_4at 70 °C and he attributed the results to either a particle size effect or an effect of the support interaction or a combination of both. Bregoli *et. al*. found the activity of ORR to vary by a factor of 2 in the range of particle size study (12-2nm) with highly dispersed catalyst at 177 °C in 99% H_3PO_4. In the Peuckertdeng investigation, where the platinumparticle size range was between 12-1nm and in 0.5M H_2SO_4, a constant site time yield for particle size above 4nm was shown. In the investigation of the interaction of oxygen with Pt particles sputtered on Teflon, Parmigiani *et. al.* [95] found by XPS measurements that Pt is more easily oxidized when the particle size is decreased. This is confirmed by Takasu [96], Myoung-ki [97] and L. Geniès [98] *et al*., who observed that the potential was shifted negatively with decreasing Pt particle size. This could imply that the oxidation occurs at lower potentials for smaller Pt particles.

An alternative viewpoint to the observed particle size effect was presented by Ross [99] that the optimal Pt particle size was around 3.0-5.0 nm. In a study of PEMFCs,

Wilson [100] also found that the optimal Pt particle size for the cathode reaction was around 4 nm. In this range, the Pt/C catalyst obtains the highest specific electroactivity. S. Y. Cha *et. al.* [101] also came to the same conclusion, they used plasma sputtering technology to directly disperse the Pt particles on the Nafion membrane, and found that when varying size from 1 – 20 nm, the Pt electrocatalyst showed the best specific activity when the particle size was 5 nm.

2.4.2 Crystal Form Effect

It is known that not only the particle size but also the crystal form of metal plays an important role in terms of the electrocatalytic activity and stability of the electrocatalyst. The different crystal faces forms are shown in Figure 2.5 [102].

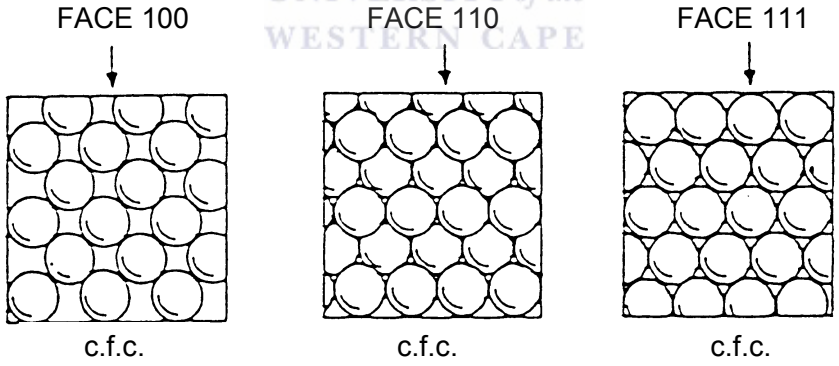

Figure 2.5: Different crystal faces forms of Pt

Sun *et. al* [103] and Beden *et. al.* [104] found that different crystal faces of Pt showed different specific activity under the same conditions by the dissociative adsorption behaviour study of a series of Pt single crystal electrodes in formic acid

and methanol. The Pt was easier to dissociatively adsorb on the (100) and (110) crystal faces than on the (111) face. This could be caused by the different interplanar spacings. Kinomoto *et. al.* [105] also showed that surface structures of Pt (100), Pt (111) and Pt (110) were changed under the electrochemical condition. Pt (100) and Pt (110) were easily to recombine and turned to more stable surface structures.

2.4.3 Surface Morphology Effect

The most efficient ways to reduce the Pt loading and enhance the activity of electrocatalyst are not only reducing the particle size and improving the metal dispersion but also increasing the surface roughness of the catalyst.There are more fractures on vertices, edge and corner sites of Pt particles with increasing surface roughness. As the fractures increase, the electrocatalytic activity increases with respect to the number of Pt atom located at vertices, edges and corners. Y. Morimoto *et al.* [106] investigated the electrochemical characteristics of Pt electrodes and found that the CO oxidation characteristics on rough Pt electrode surfaces are much better than upon smooth ones. Hoster *et al.* [107] also came to the same conclusion. They compared the different electrochemical activities of smooth PtRu and multi-pore rough PtRu catalysts and found that the rough PtRu catalyst had higher electrocatalytic activity for fuel cell application than the smooth one.

2.4.4 Structural Effect of Pt Alloy

Surface structures, compositions, and segregation properties of nanoalloys are of interest as theyare important in determining chemical reactivity and especially catalytic activity [108-111]. Oneofthemajorreasonsforinterestinalloynanoparticlesis the fact that their chemical and physical properties maybe tuned by varying the composition and atomic orderingas well as the size of the clusters. In fact, nanoalloys maydisplay not only magic sizes but also magic compositions,i.e., compositions at which the alloy nanoclusters present aspecial stability. Nanoalloys are also of interest as they may display structures and properties which are distinct from those of the pure elemental clusters: the structures of binary clusters may be quite different from the structures of the corresponding pure clusters of the same size; synergism is sometimes observed in catalysis by bimetallic nanoalloys [85].

Toshima *et. al.* [112] found that core-shell Pd-Pt with ratio of 4:1 exhibited much higher catalystic activity for olefin hydrogenation than monometallic Pt clusters. Core-shell and intermixed Cu-Pt nanoparticles were investigated by Eichnorn *et. al.* [113] with regard to their catalytic activity for NO reduction. Intermixed Cu-Pt exhibited higher selectivity than pure Pt.

2.5 Carbon Supports for Electrocatalyst

In order to increase catalytic activity, it is necessary increase catalyst utilization. This will not only increase performance but also lead to a lowering of the required

Pt loading. One very successful method to increase catalyst utilization is to employ a support. The requirements of a support for an active electrocatalyst are rigorous. It must provide structural, conductive and durable support for the active metal particles. Interest has focused on the development of the supporting material – one of the key factors in increasing the utilization of noble metal electrocatalysts, which means the nanoparticles should be well dispersed over a conductive and high surface area support [114].

Currently, nanostructured conducting carbon materials, such as carbon black [115-118], carbon nanofibre [119], ordered mesoporous carbon (OMC) [120-122] and carbon nanotubes (CNTs) [123-132] are being used as support for Platinum Group Metal (PGM) catalysts to minimize the use of precious metal. The requirements of carbon materials for their applications as supports for platinum-based electrocatalsyts are as follows: a high surface area for a high level of dispersion of nanosized catalysts, excellent crystallinity of low electrical resistance to facilitate electron transport during the electrochemical reactions, a pore structure suitable for maximum fuel contact and by-product release, and good interactions between the catalyst nanoparticles and carbon support. The role of carbon is to serve as an electrical connection between the dispersed catalysts and the porous backing materials. In addition, metal nanoparticles are physically separated by carbon, which decreases the rate of their degradation due to agglomeration [114].

Various studies have been published on the effect of different carbon supports on catalyst properties. As expected, increasing the surface area of the carbon leads to greater Pt dispersion at a given loading. Uchida *et al*. showed that Pt crystallite size decreased from 3.7 to 1.0nm when the carbon surface area increased from 58 to 1500m^2/g for a series of 23 to 24nm Pt catalysts. Similarly, Tokumitsu *et al*. reported that increasing the carbon surface from 60m^2/g to over 1300m^2/g leads to a reduction in Pt particle size from 2.5 to 1.5nm for 10wt. % catalyst. However, despite the increase in Pt surface area achieved by higher-area carbon support, both these studies showed little effect of carbon support on activity. It was suggested that both the Pt particle size effect and the interaction of the ionomer with the carbon support played important roles in determining activity [133].

2.5.1 Carbon Black

Carbon black is currently considered as the main catalyst support because of its long life. It is a material produced by the aromatic residue oil from petroleum refineries and thermal decomposition of acetylene [20]. Carbon black is a form of amorphous carbon that has a high surface-area-to-volume ration.

Vulcan® XC-72 is powdered form of highly dispersed elemental carbon manufactured by controlled vapour-phase pyrolysis of hydrocarbons [134] and consists of primary carbon particles which are spherical and of colloidal size. Vulcan® XC-72 was found to have particle size 30-50nm and surface area ranging

from 250-300 m^2/g surface areas [135] and it is a popular catalyst support material for high specific surface area, good conductivity and better pore structure.

2.5.2 Carbon Nanotubes

CNTs have attracted great attention due to their unique structural and electrical characteristics. As catalyst carriers, these materials could provide not only for a higher chemical and mechanical stability, and higher electrical conductivity, but also relatively large surface area [136].

CNTs are allotropes of carbon with a nanostructure that can have a length-to-diameter ratio greater than 1,000,000.Since the discovery of carbon nanotube (CNT) by Iijima [137], it has become a potential candidate for a wide range of applications such nanoelectronics [138], composite fabrication [139] and gas storage [140] as their cylindrical carbon molecules have novel properties. They exhibit extraordinary strength and unique electrical properties, and are efficient conductors of heat.

Nanotubes are member of the fullerene structural family. They are seamless cylinders composed of carbon atoms in a regular hexagonal arrangement, closed at both ends by hemispherical endcaps. Nanotubes are categorized as either a single-wall (SW) or multi-wall (MW) configuration. Each type of nanotube has a distinct set of material characteristics that make it suitable for different target applications. For instance, individual single-wall carbon nanotubes (SWNTs) can

function as either metallic conductors or semiconductors, while multi-wall carbon nanotubes (MWNTs) inevitably have a mixed suite of such properties due to the alternating characteristics of its layered structure.

2.5.2.1 Structural Features of Carbon Nanotubes

The chemical bonding of nanotubes is composed entirely of sp^2 bonds, similar to those of graphite. This bonding structure, which isstronger than the sp^3 bonds found in diamond, provides the molecules with their unique strength [114]. Figure 2.6 shows the bond models of sp^2 and sp^3.

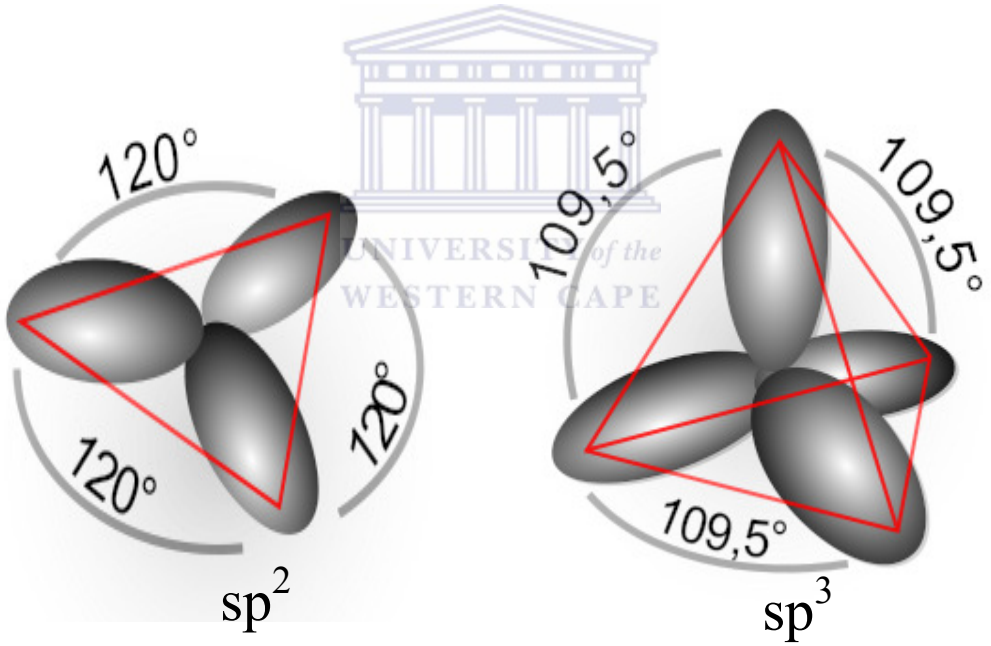

Figure 2.6: Bond Structure of sp^2 and sp^3

Ideally, Single-walled nanotubes consist of a single graphite sheet seamlessly wrapped into a cylindrical tube (see Figure 2.7 A to C) [141].Most single-walled nanotubes (SWNT) have a diameter of close to 1 nanometer, with a tube length that can be many thousands of times longer.Single-walled nanotubes are still very

expensive to produce, and the development of more affordable synthesis techniques is vital to the future of carbon nanotechnology [142].

MWNTs (See Figure 2.7 D) are basically made-up of SWNT-concentric cylindrical graphitic tubes, one within the other; the separation between them is about equal to that between the layers in natural graphite. In these more complex structures, the different SWNTs that form the MWNT may have quite different shapes (length and chirality). The aspect ratio of MWNTs is typically 100 times longer than its width with outer diameters mostly in the tens of nanometers [114]. Many of the nanotube applications now being considered or put into practice,use MWNTs because they are easier to produce in large quantities at a reasonable price and are available in useful amounts [142].

2.5.2.2Strength

Carbon nanotubes are the strongest and stiffest materials on earth, in terms of tensile strength and elastic modulus respectively. This strength results from the covalent sp^2 bonds formed between the individual carbon atoms [142].Under excessive tensile strain, the tubes will undergo plastic deformation, which means the deformation is permanent. This deformation begins at strains of approximately 5% and can increase the maximum strain the tube undergo before fracture by releasing strain energy. CNTs are not nearly as strong under compression. Because of their hollow structure and high aspect ratio, they tend to undergo buckling when placed under compressive, torsional or bending stress [142].

2.5.2.3 Kinetics

Multi-walled nanotubes, multiple concentric nanotubes precisely nested within one another, exhibit a striking telescoping property whereby an inner nanotube core may slide, almost without friction, within its outer nanotube shell thus creating an atomically perfect linear or rotational bearing. This is one of the first true examples of molecular nanotechnology, the precise positioning of atoms to create useful machines [142].

2.5.2.4 Electrical Properties

Electronic properties are mainly governed by two factors: the tube diameter and the helicity, which is defined by the way in which the graphene layer is rolled up. When used in catalysis, carbon nanotubes as conductive supports present clear difference with respect to activated carbon [143]. For a given (n,m) nanotube, if n − m is a multiple of 3, then the nanotube is metallic, otherwise the nanotube is a semiconductor. Thus all armchair (n=m) nanotubes are metallic, and nanotubes are semiconducting. In theory, metallic nanotubes can have an electrical current density more than 1,000 times greater than metals such as silver and copper [142].

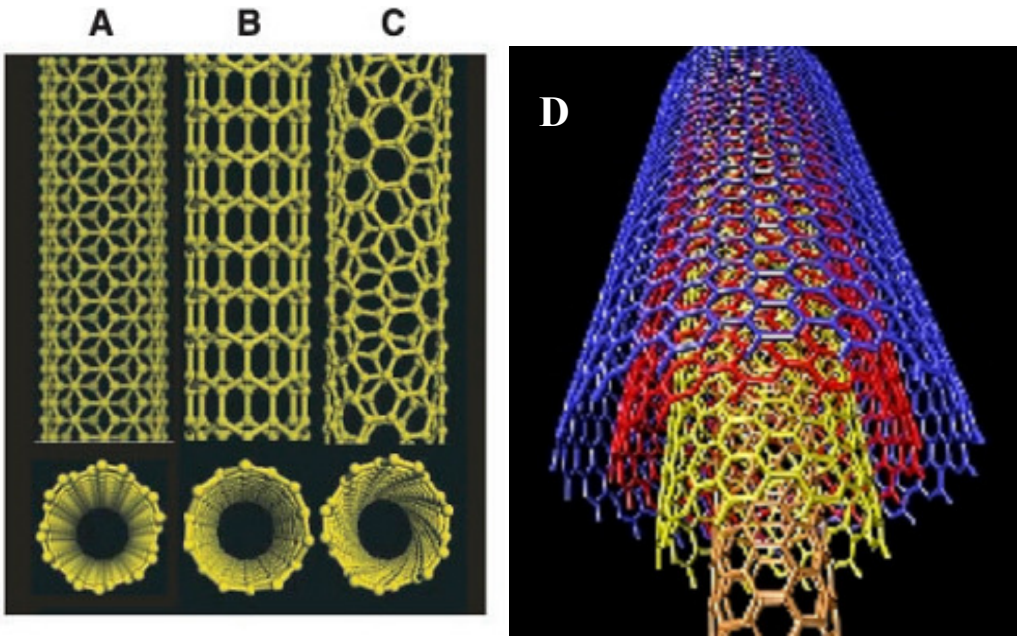

Figure 2.7: Schematic illustrations of the structures of (A) armchair, (B) zigzag, (C) shiral SWNTs [141] and (D) Mutil-walled carbon nanotubes [114]

2.6.3.5 Thermal Properties

All nanotubes are expected to be very good thermal conductors along the tube, exhibiting a property known as "ballistic conduction," but good insulators laterally to the tube axis. It is predicted that carbon nanotubes will be able to transmit up to 6000 watts per meter per kelvin at room temperature; compare this to copper, a metal well-known for its good thermal conductivity, which only transmits 385 $W \cdot m^{-1} \cdot K^{-1}$. The temperature stability of carbon nanotubes is estimated to be up to 2800 °C in vacuum and about 750 °C in air [142].

2.5.3 Metal Oxide as Support

Recently some papers have been reported that the addition of oxide is efficient to improve catalytic activity of platinum and its CO-tolerance. Qiu [144-145] and Vatistas et al. [146] have found that RuO_2 can enhance the catalyst activity in acid solution for methanol electro-oxidation. Olivi [147] and Xin [148] have reported, respectively, that the addition of SnO_2 can promote the catalyst activity for methanol and ethanol oxidation. ZrO_2 [149], CeO_2 [150] and MgO [151] were also studied and it was found that they could improve the catalytic activity and CO-tolerance in alkaline solution for ethanol electro-oxidation.

2.5.3.1 Titanium Oxide

Titanium oxide (TiO_2) was first produced commercially in 1923 [152].The bulk material of $TiO_2$is widely nominated for three main phases of rutile,anatase and brookite [153]. Amongthem, the most important of TiO_2 crystalline forms are rutile and anatasephases which both of them have the tetragonalstructures. TiO_2 is mainly applied as pigments,adsorbents, catalyst supports, filters, coatings,photoconductors, and dielectric materials [154]. Pure titanium dioxide does not occur in nature but is derived from ilmenite or leuxocene ores. The physical and mechanical properties of sintered titania are summarized in Table 2.1.

Table 2.1: Typical physical and mechanical properties of titania [154]

Property	
Density	4 gcm^{-3}
Porosity	0%
Modulus of Rupture	140MPa
Compressive Strength	680MPa
Poisson's Ratio	0.27
Fracture Toughness	3.2 $Mpa.m^{-1/2}$
Shear Modulus	90GPa
Modulus of Elasticity	230GPa
Microhardness (HV0.5)	880
Resistivity (25°C)	10^{12} ohm.cm
Resistivity (700°C)	$2.5x10^{4}$ ohm.cm
Dielectric Constant (1MHz)	85
Dissipation factor (1MHz)	$5x10^{-4}$
Dielectric strength	4 $kVmm^{-1}$
Thermal expansion (RT-1000°C)	9 x 10^{-6}
Thermal Conductivity (25°C)	11.7 WmK^{-1}

$TiO_2$is known for its higher value of efficiency than any other metal oxide and high catalytic activity and stability in acidic or alkaline solutions and non-toxic properties, thus has been widely studied for its special photoelectric properties [155]. In

addition, it has been reported that Pt [156] or PtRu [157] catalysts supported on TiO_2 exhibited excellent catalytic activity for methanol electro-oxidation because of the synergetic interaction between Pt and TiO_2.

TiO_2 exists in four mineral forms that are, anatase, rutile, brookite and titanium dioxide (B) or TiO_2(B). Anatase type TiO_2 has a crystalline structure that corresponds to the tetragonal system which is the same with rutile type TiO_2. Brookite type TiO_2 has an orthorhombic crystalline structure while TiO_2(B) is a monoclinic mineral and is a relatively newcomer to the titania family [158].

2.6 Methods for Preparation of Pt-based Electrocatalyst

Methods of catalyst preparation are very diverse and each catalyst may be produced via different routes. Preparation usually involves several successive steps. Many supported metal and oxide catalysts are prepared by the succession of impregnation, drying, calcinations, and activation [161].

Three fundamental stages of catalyst preparation may be distinguished [161]:

1. Preparation of primary solid associating all the useful components;
2. Processing of that primary solid to obtain the catalyst precursor;

3. Activation of the precursor to give the active catalyst: reduction to metal, formation of sulphides, deammoniation. Activation may take place spontaneously at the beginning of the catalytic reaction.

In recent years, methodological development for Pt-based catalyst preparation has been one of the major topics catalyst explorations. Four main routes exist for preparing the primary solid: deposition, precipitation and co-precipitation, gel formation and selective removal.

2.6.1 Wet-Chemical Synthesis Methods

Many methods have been applied to the preparation of carbon-supported fuel cell catalysts. If the discussion is restricted to the preparation of Pt-based fuel cell catalysts, five general methods have been employed [159]:

i. Impregnation-reduction method
ii. precipitation method
iii. Sulphite method
iv. Colloidal Method
v. Electrochemical Deposition method

2.6.1.1 Impregnation

The simple method of catalyst deposition on a support is by approaches wet impregnation. In this method, a solution of metal salt(s) is prepared and mixed with

the preferred support, e.g Carbon. The resulting slurry is dried to remove the solvent and the material is usually heat-treated and/or reduced to decompose the salt to give the desired metal form of the catalyst. The method has the advantage that metal is only deposited within the pore structure of the carbon. However, impregnation is not favored as a large-scale preparation method due to difficulties associated with dry mixing of carbon black and the poor wetting of carbons by aqueous solutions [114].

2.6.1.2 Precipitation

The majority of methods used for the preparation of Pt-based catalysts in the patent literature are based on precipitation. These are generally based on the precipitation of a soluble species (e.g. chloroplatinic acid, platinum nitrate) by chemical transformation. This can be in the form of a change in pH (e.g. from acidic to basic) or the addition of a reducing agent (e.g. formaldehyde to precipitate metal) [114].

2.6.1.3 Sulphite Method

The sulphite method is based initially on sulphito chemistry: the basic chemistry involves formation of sulphito complexes of the general form $[H_xPt(SO_3)_4]^{-(6-X)}$ in solution and analogously for Ru. These complexes are then oxidized where the sulphito-ligands are converted to sulphate which does not coordinate under the conditions used. This leaves on unstable $[Pt(OH)_n]^{-(n-2)}$ species that aggregates to form small colloidal particles (2nm). The advantage of the method is that even at high loadings, the particles show little tendency to aggregate, but the pH must be

very carefully controlled, which is essential if uniform 2nm particles are to be obtained [114].

2.6.1.4 Colloidal Method

The development of colloidal methods to prepare Pt-based fuel cell catalysts has received more attention in recent years. Bönnemanns method [160] is based on surfactant shell stabilizing Pt colloid particles in organic solvent. A solution of the reducing agent, $Al(CH_3)_3$, was stirred with a solution of the metal salt, $Pt(acac)_2$ and kept at 60°C for 16 hours to optimize the reduction reaction, and then colloids were supported on high-surface-area carbon by adding the colloid dispersion in toluene. Finally, the solvent was evaporated and the catalyst was rinsed with pentane [114].

2.6.1.5 Electrochemical Deposition Method

Electrochemical deposition is a versatile technique by which a thin desired metallic coating can be obtained on to the surface of another metal by simple electrolysis of an aqueous solution containing the desired metal ion or its complex. In the electrochemical method, reduction takes place by supplying current externally and the sites for the anodic and cathodic reactions are separate. This is the only technique by shich metals with high melting points (e.g., Pt, Rh) can be deposited upon surface. Electrodeposits have fine structure and have valuable physical properties such as high hardness, high reflectivity etc. A great advantage of this method is that the thickness of the layer can be controlled to a fraction of micron

[162]. However, this method only applies to 2 dimensional low surface area not to particulate systems.

2.6.2 Chemical Vapour Deposition Method

Many studies have been devoted to liquid-phase methods to prepare supported catalysts and so [114, 162], according to the promising development, this thesis will focus on the chemical vapour deposition and related techniques.

2.6.2.1 Chemical Vapour Deposition Method

Chemical Vapour Deposition (CVD) is an advanced manufacturing technology for surface coating currently enjoying intense development. It is a chemical process used to produce high-purity, high-performance solid materials. In a typical CVD process, the wafer (substrate) is exposed to one or more volatileprecursors, which react and/or decompose on the substrate surface to produce the desired deposit. Frequently, volatile by-products are also produced, which are removed by gas flow through the reaction chamber [164].

The advantages of this method are: (1) the produced materials are mainly on the external surface of the support; (2) it has little effect on the porous structure of the support due to the use of gases as precursors; (3) many of the traditional steps in catalyst preparation, such as saturation, drying, and reduction, can be eliminated; (4) the properties of the deposited material are easily controlled [163].

The CVD method has been believed that it allows the production of deposits in a controlled manner and on a large scale; it could be applied to the preparation of supported catalysts.

2.6.2.2 Platinum Organometallica Chemical Vapour Deposition Method

Platinum Organometallic Chemical Vapour Deposition (OMCVD) is a technique allowing the formation of platinum thin films as a fine dispersion of platinum particles. The principle of an organic metal chemical vapour deposition process is to vaporize a metal-containing precursor, usually an organometallic complex which undergoes thermal decomposition, followed by deposition onto the substrate to form a metal layer. In practice, vaporization is performed under pressure andtemperature conditions that allow a precursor vapour pressuresufficient for film deposition to be obtained, while maintainingthe integrity of the precursor complex. The substrate isheated beyond this stability range, causing the decomposition ofthe organometallic species and the formation of metallic particles. In contrast, OMCVD is simple, fast, economic and environmental friendly method to obtain controlled deposits of high quality. It avoids the stages of washing, drying, calcinations and activation in wet-chemical method. Also avoided are surface poisoning and the material transformations activated during drying [163].

There are different techniques, such as Laser induced chemical vapour deposition (LCVD), UV induced chemical vapour deposition (UVCVD), Plasma enhanced platinum chemical vapour deposition (PECVD), Focused ion-assisted chemical

vapour deposition (IACVD), Electron beam chemical vapour deposition (EBCVD), Fluidized bed chemical vapour deposition (FBCVD) and Atomic layer deposition (ALD), use for platinum organometallic chemical vapour deposition [163].

A dry-mix method based on using $Pt(acac)_2$ as precursor has been studied since 1947 [165]. $Pt(acac)_2$because of the advantages of being not very expensive and not sensitive to water and air was choosed as precursor used in OMCVD method. A series of studies of the characteristics of $Pt(acac)_2$ decomposition at different temperature have been reported by Marboe *et.al* [165-169]. Also, a dry-mix method has been developed by Davis *et. al*[172] in 1999, catalysts $Pt/AlPO_4$ made by dry-mix method were compared to an $[Pt(acac)_2]$/acetone impregnated catalyst. The TEM observation showed that the localization of the particles with a mean particle size 2-3 nm for the dry-mix catalyst, while 20 nm for the impregnated catalysts with most of the particles being located on the outer surface. Jacobs*et.al* [170-171] also came with the same results. They prepared similar Pt/KL catalysts by the dry-mix method and compared to impregnated catalysts in the reaction of conversion of MCP. TEM and EXAFS showed that the dry-mixcatalysts results in smaller particles than the catalystprepared by impregnation with an aqueous solutionof tetraamine platinum(II) nitrate. Such morphologyinduces an improvement of the performance of thedry-mix catalyst under clean and sulfur-poisonedconditions, enhancing the catalyst resistance to cokeformation and decreasing the sintering.

2.7 Characterization Techniques for Electrocatalyst

The characterization of Pt-based electrocatalyst is the first major step after their preparation and prior to their application. The structural and chemisorptive characteristics are beloned to the physico-chemical properties of catalyst. The electrochemical properties subsequently characterized can be correlated to the physico-chemical characterizations. The following section gives a brief overview of the most commonly applied characterization techniques.

2.7.1 Diffraction

Powder X-ray diffraction (XRD) is a powerful tool in the study of structural identification lattice spacing, particle size, crystallinity, atomic structure and qualitative chemical composition information of materials and forms an integral part in a comprehensive characterization study of nanophase electrocatalysts.

Crystallite size in nanomaterials can be measured by XRD using the Scherrer equation and is performed by measuring the broadening of a particular peak in a diffraction pattern associated with a particular planar reflection from within the crystal unit cell. The breadth of the diffraction peak is related to the size of the crystals by the Scherer equation as below:

$$d = 0.9\ _{k} / (B \cos_{max}) \qquad [2\text{-}11]$$

Where, d = particle size (nm)

λ_k = wavelength (Cu-Kα, λ = 1.5406 A)

θ_{max} = half the angle of diffraction (2θ), (the peak position Pt (220) was chosen in this thesis)

B = radians (peak-width at half peak-height)

Furthermore, the lattice parameter (α) can be calculated by the equation [2-12]:

$$\alpha_{fcc} = 2^{1/2}\lambda_k / \sin\theta_{max} \qquad [2\text{-}12]$$

In addition, the atomic ration of Ru:Pt of PtRu/CNT alloy catalysts can also be investigated by the equation as given below:

$$X_{Ru} = (0.39155 - \alpha fcc)/k \qquad [2\text{-}13]$$

Where, X_{Ru}: atomic ration of Ru

0.39155 (nm): lattice parameter of pure Pt supported on CNTs

α_{fcc}: lattice parameter of PtRu alloy

K = 0.0124 nm, a constant

2.7.2 Microscopy

Microcopies of various types can be used to obtain morphological information, such as the degree of aggregation, particle size, size distribution and crystal morphology of the catalyst particles.

Transmission Electron Microscopy (TEM) is used in the investigation of surface morphology, average particle size, particle shape and particle size distribution of electrocatalyst. High-resolution TEM (HRTEM) offers resolution down to the Angstrom level and enables information to be obtained on the structure rather than just the morphology of the nanoparticles [173].

Scanning electron microscopy (SEM) is a versatile imaging technique capable of producing three-dimensional profiles of material surfaces. Although SEM images have lower resolution than TEM, SEM is better for imaging bulk samples and has great depth of view [174].

2.7.3 Spectroscopic Techniques

Energy Dispersive Spectroscopy (EDS) is often used in conjunction with scanning electron microcscope (SEM). EDS is used to investigate the surface elemental compositions and relative element concentrations of electrocatalysts. However, EDS is used as a qualitative rather than a quantitative technique.

The vibrational spectra of small molecules adsorbed on metallic clusters are widely studied by using Fourier transform infrared spectroscopy (FTIR). It is an analysis technique that provides information about the chemical bonding or molecular structure of materials. The technique works on the fact that bonds and groups of bonds vibrate at characteristic frequencies. A molecule that is exposed to infrared rays absorbs infrared energy at frequencies which are characteristic to that molecule.

The resulting FTIR spectral pattern is then analyzed and matched with known signatures of identified materials in the FTIR library [175].

Raman spectroscopy has been used to study the binding of adsorbates on metallic nanoparticles and the cluster formation process [175].

2.7.4 Other Characterization Techniques

The specific surface area, pore size, pore size distribution and pore volume of supported electrocatalyst can be determined by using Brunauer-Emmett-Teller (BET) technique.

Thermogravimetry (TGA) is used to investigate the thermal stability and weight loss character of electrocatalyst. It monitors the properties of materials as they change with temperature.

2.7.5 Electrochemical Characterization

The standard tool for the electrochemical characterization of electrocatalysts is cyclic volammetry. The basic instrumentation for the CV analysis requires controlled potential equipment and the electrochemical cell which consists of three electrodes. The analysis is normally carried out using electrochemical analyser connected to a three electrode cell, which are the working electrode, reference electrode and counter electrode.

The working electrode is the electrode at which the reaction of interest takes place. Materials that are used for the working electrode include platinum, gold and carbon. These are materials that are not susceptible to oxidation or reduction. The reference electrode provides a stable potential compared to the working electrode. Reference electrodes are used because their potentials are constant, such as Ag/AgCl. The counter electrode is usually made of platinum wire. Electrochemical activity of counter electrode does not affect that of the working electrode [176].

A typical cyclic voltammogram recorded for a reversible single electrode transfer reaction is shown below (Figure 2.8). In this figure, i_p^c and i_p^a are cathodic and anodic peak currents respectively. E_p^c and E_p^a are cathodic and anodic peak potentials respectively.

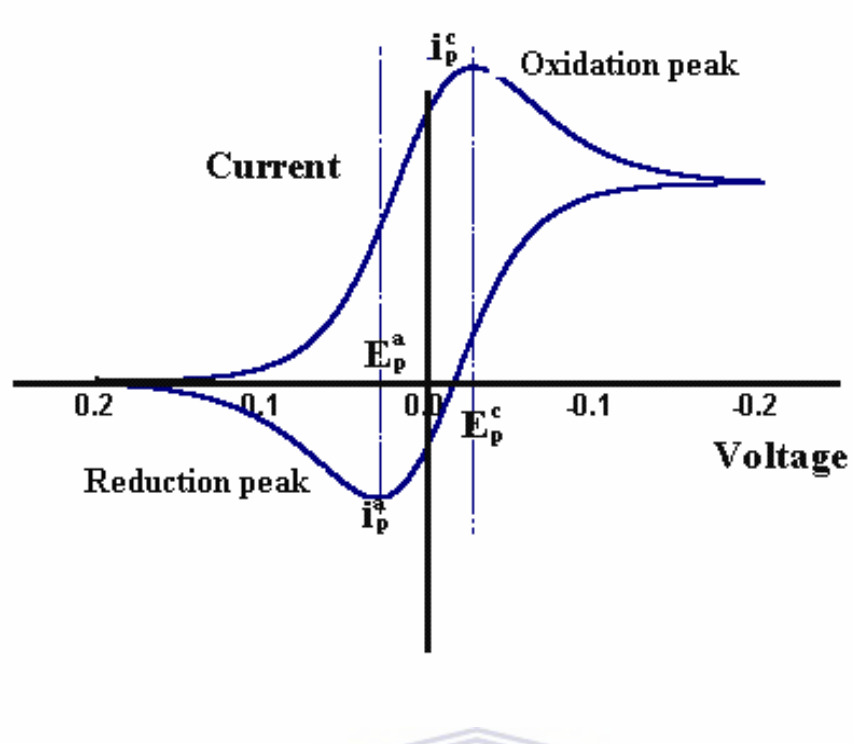

Figure 2.8: A typical cyclic voltammogram showing important parameters [114]

The electrochemically-active surface area of Pt is typically measured using cyclic voltammetry in acid electrolytes. Specifically, the area under the hydrogen adsorption/desorption peaks is determined, as shown in Figure 2.10. A larger area under the peak (per mass of Pt) indicates a larger active area. Thereforethrough the equation [2-4], can calculate the chemical-active surface area of the catalysts.

Regions of oxide formation (Q_A) and reduction (Q_C) as well as desorption of hydrogen (H_A) and its adsorption (H_C) are indicated.

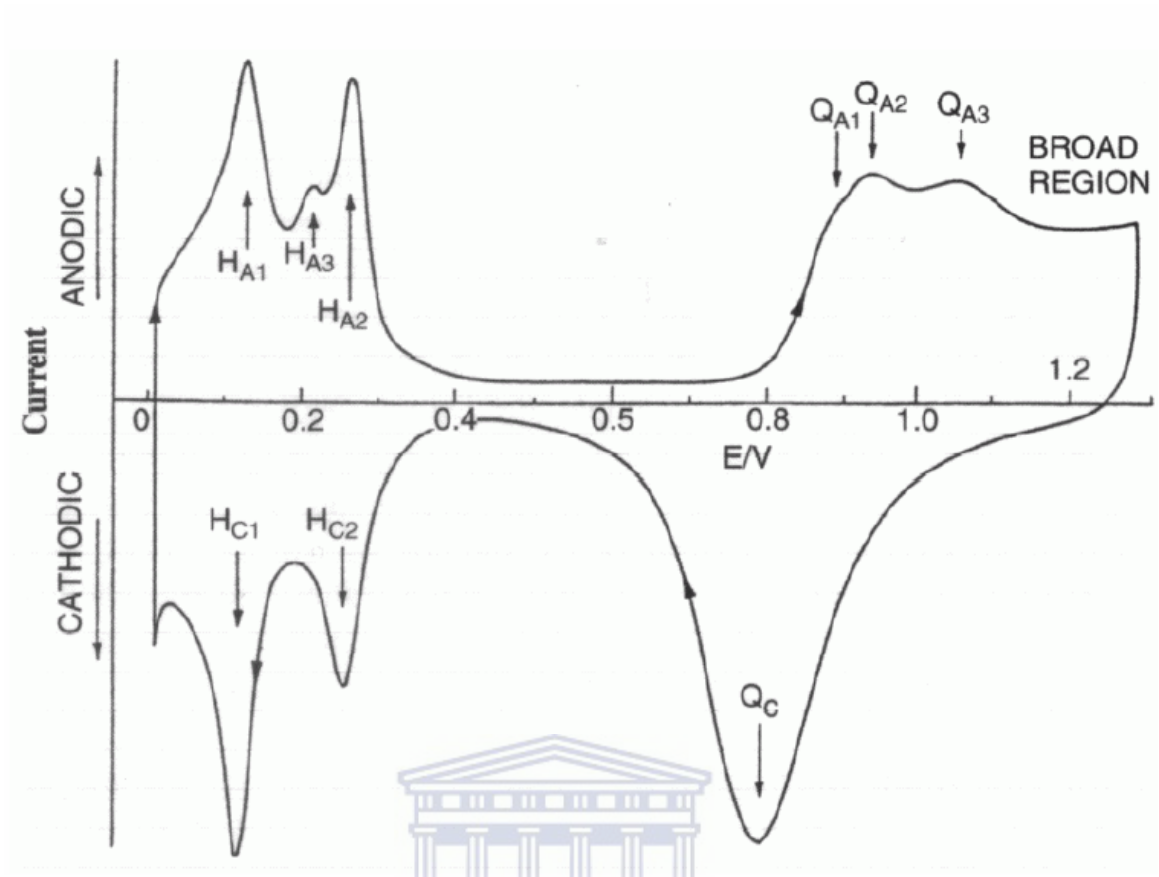

Figure 2.9: A typical current-potential curve for a platinum electrode [177]

S_e (m^2/g) = $0.1 \times Q_r/m \cdot c$ [2-14]

Where, Q_r: area of hydrogen desorption peak

m: quality of Pt loading (mg), (ICP results were chosen in this study)

c: 0.21 mC/cm^2

The chemical surface area (theoretic area) of Pt/C can be calculated by equation [2-15]

$S_c = 6000/\rho d$ [2-15]

Where, ρ: density of Pt, 21.4 g/cm^3

d: average particle size of Pt (nm), can get from XRD or TEM results

2.8 Conclusions

From the cases of nano size electrocatalysts materials under consideration, multicomponent platinum group metal electrocatalysts were identified as having the biggest practical potential for application of methanol-oxidation process. This is a result of their ability to selectively and sensitively provide a approach for tuning tuning its catalytic and electrocatalytic properties.

Platinum is a nobel metal of limited supply. The main obstacle for PGM catalysts are slow kinetics, low efficiency and high cost. To enhance catalytic performance, stability, durability and reduce operational costs of platinum electrocatalysts, advanced electro-catalyst design relying on the bi-functional mechanism, and using hybrid support carbon materials has been proposed. Currently, carbon materialshave been investigated as catalyst supports. Carbon black Vulcan XC-72 is frequently used as a catalyst support for low-temperature fuel cells. However, comparing with the carbon nanotubes, Vulcal XC-72 contains small primary pores that are inaccessible to electrolyte polymer, resulting in engulfed catalyst nanoparticles that do not contribute to electrochemical reactions.This is because the lack of a three-phase boundary of Vulcan XC-72 while carbon nanotubes are a novel class of one-dimensional nanomaterials with unique structure and electrical characteristics.

Although was firstly used for methanol electro-oxidation, however, it was easily poisoned by intermediate CO. It is necessary to enhance catalytic performance by advanced electro-catalyst design relying on the bi-functional mechanism has been proposed.Bimetallic PtRucatalysts are promising anodic catalysts forcommercial direct methanol fuel cells (DMFC). The role of Ru inPtRu catalysts for CO oxidation is commonly explained by theelectron effect or a bi-functional mechanism. According to theelectron effect, Ru alters the electronic state of Pt, causing CO tobecome more weakly adsorbed. Loss of CO binding intensityleads to a decrease in oxidation overpotential of the cell.Despite the PtRu catalyst exhibiting good methanol oxidation activity, the state-of–the–art PtRu catalyst needs further improvement of nicely higher catalytic activity and replacement of expensive nobel metals, Pt and Ru. The most successful way to achieve both these goals is to add a third metal to the PtRu catalyst, such as Fe, Cu and V.The benefit of a bi-functional nanophase containing catalyst is that the reaction mechanism involves both the metal alloy and the support. The important factors are the dispersion of the metal alloy on the support and the overall size and composition of the metal alloy.

Recently, researchers have reported that systems combining platinum, metal oxides and carbon exhibited excellent catalytic activity for electrooxidation of methanol and CO. The so-called “hypo-hyper-d-concept” is very important for the development of multi-componentplatinum group metal electrocatalysts or non-platinum electrocatalysts.TiO_2 is known for its higher value of efficiency, high catalytic activity, stability in acidic or alkaline solutions and non-toxic properties. It

has been reported that Pt or PtRu catalysts supported on TiO_2 exhibited excellent catalytic activity for methanol electro-oxidation because of the synergetic interaction between Pt and TiO_2.For this reason TiO_2 was investigated as a potential support by coating with CNTs for platinum alloy metal electrocatalysts and non-platinum electrocatalysts.

Furthermore, the deposition of precious metals either chemically or electrochemically plays an important role in the development of technologies. The greatest challenge at present is to find effective nano synthesis procedures to prepare and apply nanoscale components. Contrary to the liquid impregnation method, the proposed Organometallic Chemical Vapor Deposition (OMCVD) method is fast and the stages of impregnation, washing, drying, calcinations, activation, surface poisoning and material transformations activated during drying are avoided.The OMCVD method has been believed to allow the production of deposits in a controlled manner and on a large scale; it could be applied to the preparation of supported catalysts.

2.9 Experimental Tasks

In this study, a rapid, efficiency and simple synthesis method was improved, in which the multicomponent electrocatalysts were synthesized in nanophase form. The nanostructured catalysts were characterized by physico-chemical and electrochemical techniques. The methanol oxidation activities of the electrocatalysts were compared with that of the commercial JM catalysts.

The main concern in this research is to (1) reduce the cost of PGM electrocatalysts; (2) improve an efficient, economic synthesis technique for catalysts; (3) improve the methanol oxidationelectrocatalytic activity of the electrocatalysts; (4) study the synergy interactions of TiO_2as a support and (4) determine the relationship between catalyst and carrier

The scope of this dissertation was thus to develop new routes to prepare nanophase electrocatalysts and apply nanophase catalysts for methanol oxidation system in order to achieve high electrochemical activity at a low loading of nobel metal catalyst. Method was investigated for the preparation of nanophase electrocatalysts that can be easily scale up for industrial applications.

Based on the review of the literature, the scientific approaches (Figure 2.10) was formulated in the preparation of advanced electrocatalysts.

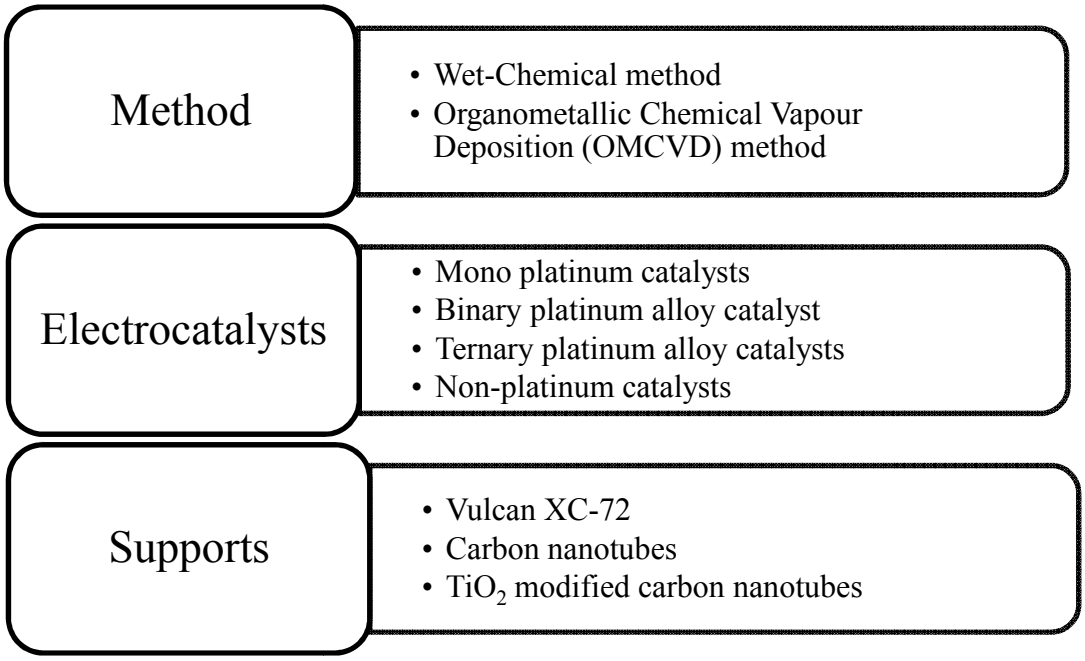

Figure 2.10: Approaches of experimental tasks

The research design and methodologies which address the set of sample characteristics of the electrocatalysts, and the experimental tasks used in their investigation, are described in detail in Chapter 4, 5 and 6. Analytical tools employed in the characterization study are discussed and reviewed in detail in Chapter 3. The principles of operation, sample preparation, and experimental parameters will also be discussed in Chapter 3.

2.10 Research Objectives

i. To synthesize Pt catalysts with OMCVD and WC methods

ii. To improve the dry-mix OMCVD method

iii. To synthesize Pt catalysts with different carbon supports, such as Vulcan and CNTs

iv. To synthesize catalysts with different Pt content

v. To synthesize metallic supported mono-, bi- and quaternary platinum based catalysts on carbon nanotubes with the CVD method

vi. To synthesize the PGM catalysts with high catalytic activity and low cost by evaluated with methanol electro-oxidation process

vii. To synthesize catalysts with similar or better electrochemical activity to JM commercial standard catalysts

viii. To modify the carbon nanotubes support with titanium oxide

ix. To characterize the structure of TiO_2 loading on CNTs

x. To synthesize PGM catalysts with TiO_2/CNT as support

xi. To improve the electro-activity of the PGM/TiO_2/CNT electrocatalysts by studying the methanol electro-oxidation process

xii. To entail the PGM/TiO_2/CNT hybrid nano-materials

xiii. To study synergy interactions between PGM nanoparticles, CNTs and titanium oxide

xiv. To characterize the effects of preparation conditions on the physical-chemical properties of the synthesized hybrid nano-materials

xv. To understand the preparation procedures and to develop a relatively simple and effective process for producing based PGM/TiO_2/CNT- hybrid nanomaterials which can be scaled up for various electro-catalytic applications, such as fuel cell, water electrolysis, or photo-voltaic application

xvi. To achieve activity of the non-platinum catalysts similar to that of Pt catalyst

2.11 Delimitation of Study

The study was limited to the following activities: improve the synthesize method; develop and characterize nanophase electrocatalysts; improve catalytic activity of catalysts by adding additional metals; improve electrochemical activities of the catalysts by deposited on TiO_2 modified CNTs; develop non-platinum catalysts by supported on TiO_2/CNT support; demonstrate methanol oxidation activities of nanostructured catalysts; optimize preparation conditions for PGM catalysts.

CHAPTER 3:

Experimental

PGM electrocatalysts are dispersed as small particles on high surface area electron conductive supports for effective use of costly Pt. Therefore, the characteristics of the metal particles play an important role in applications of catalysts.

This chapter presents the details ofthe catalysts are observed using analytical techniques, whichis similar to that of their characterizations. Sample preparation and experimental parameters used in the investigation are also described.

3.1 Physical Characterization Techniques

The following physical methods were used to characterization the catalyst:

- High-Resolution Transmission Electron Microscopy (HRTEM)
- X-ray Diffraction (XRD)
- Scanning Electron Microscopy (SEM/EDS)
- Inductively Coupled Plasma Mass Spectroscopy (ICP-MS)
- Brunauer-Emmett-Teller N_2 adsorption technique (BET)
- Fourier Transform Infrared (FTIR)
- Temperature Programmed Reduction (TPR)

3.1.1 High Resolution Transmission Electron Microscopy

High resolution transmission electron microscopy (HRTEM) is almost exclusively used in the investigation of average particle size, particle shape and particle size distribution of electrocatalysts. In this study, HRTEM was used to determine the aggregate morphology, particle size and the particle size distribution of the catalysts. All prepared samples were viewed and photographed using a Tecnai G^2 electron microscope at the University of the Western Cape. The experimental parameters are given in Table 3.1.

Sample preparation

The TEM samples were prepared by suspending the supported catalyst powder in methanol solution and depositing a drop of the suspension on a standard copper grid covered with carbon. Samples were mounted in a sample holder, which was introduced directly into the shaft of the microscope.

Table 3.1:Tecnai G^2 transmission electron microscope operational parameters

Parameter	Setting
Accelerating voltage (kV)	200
Current (μA)	20
Condenser aperture	1
Objective aperture	3
Exposure time	3

3.1.2 X-Ray Diffraction Analysis

Powder X-ray diffraction (XRD) is a powerful tool in the study of crystallinity and atomic structure of materials and forms an integral part in a comprehensive characterization study of nanophase electrocatalysts. It was used to confirm the PGM particle size and crystalline structure of the various catalysts in this study.

Average Pt particle sizes of prepared electrocatalysts were estimated from the spectral line broadening using the Scherrer equation and the analysis was done in iThemba lab.

The specifications of the Siemens D8 Advance XRD unit and operation parametersare listed in Table 3.2.

Specimen preparation

The conductive powders of the catalytic samples were dispersed upon carbon stick tabs and mounted on an aluminum stub holder. After that, the holder was loaded into the spectrometer.

Table 3.2: Hitachi X-650 SEM operational parameters

Parameter	**Setting**
Accelerating voltage	25keV
Tilt Angle	0°
Aperture	0.4mm
Resolution	3nm
Working distance	15mm
Magnification	50k

3.1.3 Energy dispersive spectroscopy (SEM-EDS)

The elemental composition of the catalysts was investigated using energy dispersive spectroscopic (EDS) emission analysis with a Hitachi X-650 SEM. Relative element concentrations were estimated using GENESIS software. Every sample was scanned five times to obtain the average wt. % of the metal. The operating parameters of the SEM are described in Table 3.3.

Specimen preparation

The conductive powders of the catalytic samples were dispersed upon the carbon stick tabs and mounted on an aluminum stub holder. After that, the holder was loaded into the spectrometer.

Table 3.3: Hitachi X-650 SEM operational parameters

Parameter	Setting
Accelerating voltage	25keV
Tilt Angle	0°
Aperture	0.4mm
Resolution	3nm
Working distance	15mm
Magnification	50k

3.1.4 Inductively Coupled Plasma Mass Spectroscopy (ICP-MS)

Inductively coupled plasma mass spectrometry (ICP-MS) is a type of mass spectrometry that is highly sensitive and capable of the determination of a range of metals and several non-metals at concentrations below one part in 10^{12} (part per trillion) [178]. Amongst these, ICP-MS is generally employed for noble metal determination in concentrates due to the poor sensitivity of the EDS technique for these elements, and has the advantage of being less subject to chemical and spectral interferences.The metals were analyzed using an Agilent 7500 ce ICP-MS and a High Matrix Introduction (HMI) accessory and He as collision gas.

Sample Preparation

An accurately weighed sample of 10.00 mg was digested gently in a 10 ml covered Pyrex beaker in 5 ml aqua regia (HCl + HNO_3 (3 + 1)) on a hot plate for 30 minutes. After cooling, the solution was filtered through two layers of filter paper with pore size of 6 µm. The filter and residue were washed with 15 ml de-ionized water. The solution along with the washings was added to a 50 ml volumetric flask and made up to volume with de-ionized water.

3.1.5 Brunauer-Emmett-Teller N_2 adsorption technique

In this study the surface area, pore volume and porosity of supports were determined through the BET technique using a Micromeritics Accelerated Surface Area and

Porosimetry (ASAP) 2010 system. The characterization was based on the physical adsorption of nitrogen at liquid nitrogen temperature.

Sample preparation

Approximately 100 mg of the sample was subjected to degassing at 100 °C for 30 minutes, followed by 120 °C for 30 minutes and then 160 °C for 1 hour to remove moisture, and then at about 260 °C under vacuum in order to free the pores of any particles. The sample was then weighed under vacuum, after which it was inserted into the analysis port and analyzed automatically at liquid nitrogen temperature (-196 °C).

3.1.6 Fourier Transform Infrared

In this study, the chemical structure of washed CNTs and Vulcan were analyzed by FTIR spectroscopy. Analysis was performed using a Perkin Elmer Paragon 1000 FTIR Spectrophotometer. The analysis of both CNTs samples used was the dried prepared powders, which were put in an oven at 110 °C overnight.

3.1.7Temperature Programmed Reduction

In this study, TPR was used to determine the active reduction species of the electrocatalysts and the interaction between the metal oxide and support in catalysis. The samples were analyzed using a Micrometrics Auto Chem and the operating parameters of the technique are described in Table 3.4.

Specimen preparation

The catalyst (0.1 g) was placed in a quartz tubular reactor. The reactor was heated in a furnace. Prior to the temperature programmed reduction measurement, the catalysts were flushed with high purity argon at 150 °C for 30 min, and then cooled down to 50 °C. Then 5% $H_{/Ar}$/Ar was switched on and the temperature was raised at a rate of C/minC/min from 50 to 800 °C (held for 1 min). The gas flow rate through the reactor was controlled by three Brooks mass flow controllers and was always 50 cm^3 min. The H_2 consumption (TCD signal) was recorded automatically by a PC.

Table 3.4: Instrumental set up conditions for TPR

Parameter	Setting
Gas flow	50 ml/min
Heating ramp	10 °C/min
Maximum temperature	800 °C
Gas	H_2/Ar

3.2 Electrochemical Measurement

Cyclic voltammetry (CV) was used to determine the most active catalyst. All the electrochemical investigation was performed with a computer connected to a BAS/50W integrated automated electrochemical workstation (Bioanalytical Systems, Lafayette, IN, USA). A conventional three electrode cell was used with an Ag/AgCl electrode as a reference, a platinum wire counter electrode and a bare modified

electrode (electrocatalyst) as working electrode. The CV operation parameters are shown in Table 3.5.

Working electrode preparation

The paste was prepared by hand mixing of ultra graphite powder and mineral oil at a ratio 70:30 (w/w) in an agate mortar until a homogenous paste was obtained. There after the home-made catalyst was added to an aliquot of the paste in a 1:10 (w/w) ratio and thoroughly blended together by grinding in an agate mortar and pestle. The paste was then tightly packed into a PVC tube (2mm internal diameter) and the electrical contact was providedby a copper wire connected to the end of the tube.

Table 3.5:Standard OperatingParametersforCV

Parameter	**Specification**
Electrolyte	0.5 M sulphuric acid to the cell. Degassed with nitrogen by saturation
Methanol	Added 3.2 ml methanol to 100 ml sulphuric acid, Stirred for 15 min.
Working electrode	Catalyst paste (see Working electrode preparation)
Counter electrode	Platinum wire
Reference electrode	Ag/AgCl
Scan rate	50 mV Base run (0.5 M sulphuric acid).
Scan range	Scanning range: -0,2 to 1.0 V

3.3 Reactor Tubing Design

Since the synthesis process needs to be completed in a sealed tube reactor, Figure 3.1 and Figure 3.2 present a reactor system was designed and built.

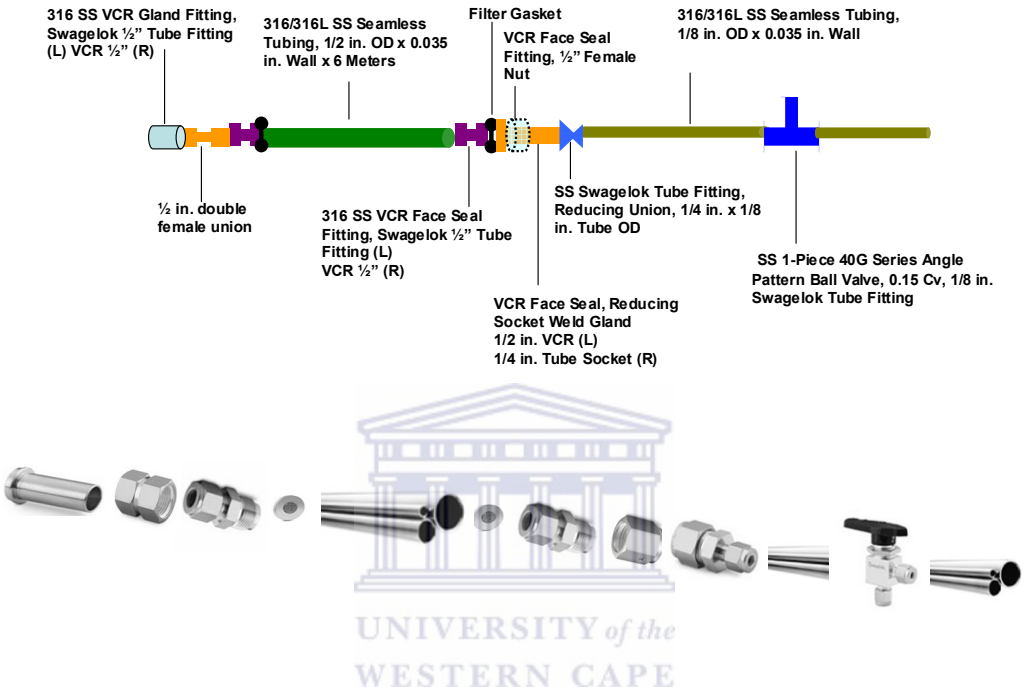

Figure 3.1: A design of reactor system

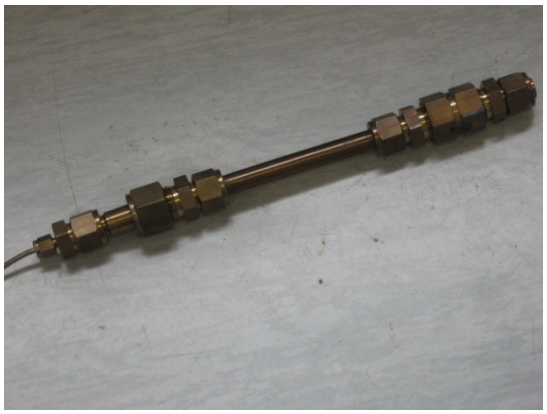

Figure 3.2: A practicality of reactor

3.4 Mechanism of precursor decomposition

Chemical Platinum acetylacetonate [$Pt(C_5H_7O_2)$] will be used as precursor for preparing PGM catalysts using OMCVD method in this study, the mechanism will be described as follows [247]:

$$Pt(C_5H_7O_2)_2 \longrightarrow Pt + 9C + CO + H_2O + 6H_2$$

Titanium acetylacetonate will be deposited on CNTs as a new support for PGM catalysts, the mechanism describes as follows [247]:

$$Ti\ (OC3H7)_4 \longrightarrow TiO_2 + CO + 13H_2 + H_2O$$

CHAPTER 4:

Platinum Group Metal Catalysts Supported On Carbon Materials Synthesize Under Different Conditions

In this chapter the results of the synthesis, characterization and interpretation of platinum group metal electrocatalysts will be presented. The investigation was initiated by synthesize methods (wet-chemical method and Organometallic Chemical Vapor Deposition method) and supports (Vulcan and multi-wall carbon nanotubes) study of four difference home-made Pt catalysts. The study of different weight loading of Pt electrocatalysts and then will be detailed. The investigation of bi- and tri-metallic Pt alloy electrocatalysts will be presented in the last section. The electrochemical characterization of electrocatalysts and their comparison to the commercial standard JM catalysts is presented in each section and the electrochemical properties will be correlated with the structural study of electrocatalysts.

4.1 Introduction

Currently, many studies have been devoted to liquid-phase methods to prepare supported catalysts. The impregnation method is a simple method to prepare supported catalysts. These methods consist in contacting a solid with a liquid

containing the components to be deposited on the surface. The type of product depends on (i) the nature of both reactants (the liquid and the solid surface), and (ii) the reaction conditions [161].The impregnation method has the advantage that metal is only deposited within the pore structure of the carbon. However, impregnation is not favored as a large-scale preparation method due to difficulties associated with dry mixing of carbon black and the poor wetting of carbons by aqueous solutions [133].Contrary to the liquid impregnation method, the proposed platinum Organometallic Chemical Vapor Deposition (OMCVD) method is fast and the stages of impregnation, washing, drying, calcinations, activation, surface poisoning and material transformations activated during drying are avoided. It is an economic and environmental friendly method to obtain controlled metallic nanoparticulate deposits of high quality.The performance of the CVD process can be affected by the choice of metallic precursors, nature of the substrate, design of the system and the system parameters, operating pressure (vacuum), deposition time and temperature, etc [180-184]. According to these criteria, it is very important to reach performance optimization by controlling synthetic procedures and conditions.

The electrical, optical and catalytic properties of nanoparticles can be tailored by changing composition, shape and size of the nanoparticles. An important factor for controlling the shape and size of the nano-particles is their dispersion stability during synthesizes. A number of techniques have been used for stabilizing the metallic nano-particles in solutions. In aqueous solution, polymeric stabilizers are very efficient dispersants, whereas long chain molecules such as alkanethiols are

most commonly used in organic media [185-187]. However, the required steps by liquid method such as adsorption, drying, calcinations and reduction would significantly alter and sinter the catalyst structure and consequently reduce the active surface area of the catalyst [188]. CVD method is a potential alternative to overcome these problems in developing stable and well-structured catalysts. Some studies have been reported of preparation of supported metal catalysts by CVD. Dossi et al. reported the study of dipostion of Pt [189-191] and Ru [192-193]. Ru [194], Rh [180], Cu [195], Co [196] and Fe [197] deposition were studied by Guerrero-Ruiz et al., respectively.

The following sections describe the preparation and outcome of the synthesis of catalysts mainly based on the use dry-mix method of OMCVD, which is specified in Section 4.2.2. These catalysts were characterized and their electrochemical (EC) activity quantified. The commercial Johnson Matthey 40% Pt/C and 40%Pt20%Ru/C was compared with home-made catalysts and this then enabled a profile for the catalysts with regards to their synthesize route, characteristics and EC activity. The most EC activity synthesize route was then used to prepare multi-metallic platinum based catalysts discussed in Section 4.3.3.

4.2 Experimental

4.2.1 Materials

The chemicals employed to prepared electrocatalysts are shown in Table 4.1.

Table 4.1 Chemicals for preparing catalysts

Chemicals	**Specifications**	**source**
Multi-wall carbon nanotubes	95 wt.%, 20 -30 diameter	Cheap Tubes Inc ©
Vulcan XC-72	-	Cabot Corporation™
Platinum acetylacetonate	97%	Sigma-Aldrich
Ruthenium acetylacetonate	97%	Sigma-Aldrich
Vanadium acetylacetonate	97%	Sigma-Aldrich
Copper acetylacetonate	97%	Sigma-Aldrich
Iron acetylacetonate	97%	Sigma-Aldrich
HNO3	55% AR	KIMIX
HCl	32% AR	KIMIX
H_2SO_4	98% AR	KIMIX
Ethylene glycol	99+%	Aldrich Chemical Corp™
Chloroplatinim acid	99.9%	Aldrich Chemical Corp™
Sodium Hydroxide	40% AR	KIMIX

4.2.2 Catalyst Synthesize

Nanophase electrocatalysts supported on Vulcan XC-72 and multi-wall carbon nanotubes synthesized by using the wet-chemical (WC) andorganometallic chemical vapor deposition (OMCVD) methods given in the following subsections. Eleven catalysts were synthesized under the different conditions and tabulated in Table 4.2.

Table 4.2: Summary of prepared PGM electrocatalysts

Catalyst identifier	Metal	Support	Metal theoretic Loading (wt. %)	Synthesize Method
A1	Pt	Vulcan XC-72	10	WC
A2	Pt	MCNTs	10	WC
A3	Pt	Vulcan XC-72	10	OMCVD
A4	Pt	MCNTs	10	OMCVD
A5	Pt	MCNTs	20	OMCVD
A6	Pt	MCNTs	40	OMCVD
A7	Pt	MCNTs	60	OMCVD
A8	Pt:Ru	MCNTs	20:20	OMCVD
A9	Pt:Ru:Fe	MCNTs	20:10:10	OMCVD
A10	Pt:Ru:Cu	MCNTs	20:10:10	OMCVD
A11	Pt:Ru:V	MCNTs	20:10:10	OMCVD

4.2.2.1 Pre-treatment of Vulcan® XC-72

Vulcan® XC-72 was washed with a 2N HCl solution for 3 hours under reflux at room temperature with the aim of removing contaminants such as sulfur and ash. This HCl ─ washed and activated carbon was directly oxidized in 5N HNO_3 solution for 3 hours under reflux at room temperature and then washed with boiling distilled water until the pH of the rinsed solution reached 5.5. Overnight drying in an oven at 110°C followed these treatments.

4.2.2.2 Modification of Multil-wall carbon nanotubes

Exposing the carbon nanotubes to an oxidizing agent leads to their partial oxidation and the generation on their surface of oxygen-containing groups, such as phenol, carbonyl, carboxyl, quinine and lactone groups [198].With this aim, commercial MCNTs were washed with a boiling solution of 98% H_2SO_4 and 55% HNO_3 (volume ratio of 2:3) for 1 hour under reflux, and then washed with distilled water until the pH of the rinsed solution reached 6-7. Overnight drying in an oven at 80^{o}C followed these treatments.

4.2.2.3 Synthesizeof 10% Pt supported on Vulcan XC-72 with wet-chemical method (A1)

500 mg Vulcan support was mixed with 50 ml ethylene glycol (EG) and sonicated for 20 minutes to get a suspension. 16.45 ml 7.4 mg/ml chlorplatinic acid, which used EG as solvent, was gradually added to the Vulcan suspension with burette and stirred for 4 hours. After the stirring, the solution was titrated with 1M NaOH until the pH=8 and then keep the solution at 130°C in an oil bath for 3 hours. Finally, the solution was left to cool at room temperature before being filtered. The precipitate was dried under vacuum at 80 °Cfor 8 hours. The nominal loading of Pt in the catalyst was 10%.

4.2.2.4 Synthesize of 10% Pt supported on MCNTs with wet-chemical method (A2)

Following the synthesize procedure as specified in Section 4.2.2.3 and replaces the Vulcan XR-72 with MCNTs as support for the catalyst to produce 10% Pt/CNT.

4.2.2.5 Synthesizeof 10% Pt supported on Vulcan XC-72 with OMCVD method

(A3)

112.05 mg Platinum acetylacetonate[Pt $(acac)_2$)] and 500.00 mg modified Vulcan XC-72 carbon support (Section 4.2.2.1) were physically mixed and ground with a mortar and pestle before the mixture was loaded into a reactor tube. The reactor tube was sealed and firstly evacuated for 1hour to a pressure of 7.7 x 10^{-1} mbar at room temperature. The catalyst was then slowly ramped to 100 °C and kept for another 1 hour to remove traces of water, at which temperature the pressure decreased substantially to 2.8x 10^{-1}mbar. After sublimation, the reactor tube was ramped to 400 °C in a tube furnace and held for 30 min to decompose the platinum precursor properly. The reactor tube was cooled to room temperature, and the sample was removed. This catalyst was denoted A3.

4.2.2.6 Synthesizeof 10%, 20%, 40% and 60% Pt catalysts supported on multi-wall carbon nanotubes (A4-A7)

In order to synthesize Pt/CNT catalysts with different Pt wt. % loadings, 112.05 mg, 250.00 mg, 627.00 mg and 1151.00 mg Platinum acetylacetonate[Pt $(acac)_2$)] were separately weighedon an analytical balance and mixed with500.00 mgacid washed and modified CNTs by ground with a mortar and pestle, and the solid mixture was loaded into a reactor tube. The reactor tube was then sealed and firstly evacuated for 1hour to a pressure of 7.7 x 10^{-1} mbar at room temperature. The catalyst was then slowly ramped to 100 °Cin a tube furnace and kept for another 1 hour to remove the trace of water and water, at which temperature the pressure decreased substantially to 2.8x 10^{-1}mbar. After sublimation, the catalyst temperature was ramped to 400 °C

and held for 30 min to decompose the platinum precursor properly. The reactor tube was cooled naturally to room temperature, and the sample was removed. These series of catalysts was denoted A4-A7 (see Table 4.2)

4.2.2.7 Synthesizeof 20:20 (w/w) PtRu supported on MCNTs (A8)

335.00 mg Platinum acetylacetonate[$Pt(acac)_2$)] and 654.78 mgRuthenium acetylacetonate [$Ru(acac)_3$] well mixed with 500 mg acid washed and modified CNTs (as specified in Section 4.2.2.2) by ground with a mortar and pestle and then following the synthesize procedure specified in Section 4.2.2.6 to produce catalyst PtRu/CNT (Table 4.2).

4.2.2.8 Synthesize of 20:10:10 (w/w) PtRuFe supported on MCNTs (A9)

335.00 mg Platinum acetylacetonate[$Pt(acac)_2$)], 327.16 mgRuthenium acetylacetonate [$Ru(acac)_3$] and 524.85 mg Ironacetylacetonate [$Fe(acac)_3$] were physically well mixed with 500 mg acid washed and modified CNTs (as specified in Section 4.2.2.2) by ground with a mortar and pestle and then following the synthesize procedure specified in Section 4.2.2.6 to produce catalyst PtRuFe/CNT (see Table 4.2).

4.2.2.9 Synthesize of 20:10:10 (w/w) PtRuCu supported on MCNTs (A10)

335.00 mg Platinum acetylacetonate[$Pt(acac)_2$)], 327.16 mgRuthenium acetylacetonate [$Ru(acac)_3$] and 341.87 mg Copper acetylacetonate [$Cu(acac)_2$] were physically well mixed with 500 mg acid washed and modified CNTs (as specified in Section 4.2.2.2) by ground with a mortar and pestle and then following the synthesize procedure specified in Section 4.2.2.6 to produce catalyst PtRuCu/CNT (see Table 4.2).

4.2.2.10 Synthesize of 20:10:10 (w/w) PtRuV supported on MCNTs (A11)

335.00 mg Platinum acetylacetonate[$Pt(acac)_2$)], 327.16 mgRuthenium acetylacetonate [$Ru(acac)_3$] and 567.46 mg Vanadium acetylacetonate [$V(acac)_3$] were physically well mixed with 500 mg acid washed and modified CNTs (as specified in Section 4.2.2.2) by ground with a mortar and pestle and then following the synthesize procedure specified in Section 4.2.2.6 to produce catalyst PtRuV/CNT(see Table 4.2).

4.2.3 Characterization Techniques

In this study, various techniques were employed to characterize the electrocatalysts which may include the followingmethods. N_2 adsorption/desorption (N_2BET) gives the information of total surface area, pore size distribution andporosity of support. Particle size, particle size distribution,metal surface area, and metal dispersion/agglomeration are established byhigh resolution transmission electron microscopy (HRTEM) and the histograms of electrocatalysts were described from

the analysis of 200 Pt particles in each case. X-ray diffractometry (XRD) gaveinformation about crystal/atomic structure and phase identity and purity. Composition was quantitatively determined by Ion Coupled Plasma (ICP), or qualitatively by using energy dispersive analysis(SEM/EDS).Electrochemical activities of the catalysts are determined using cyclic voltammetry (CV). Characterization techniques were employed as described in Chapter 3.

4.3 Results and Discussion

4.3.1 Effect of different methods and supports for Pt catalysts

A heterogeneous catalyst consists of a solid support and an active phase each presenting their own physical and chemical properties, which can evolve during the preparation. The study of the surface reaction between a catalyst precursor and a support is a key point in the design of a supported catalyst. The Pt-based catalyst has been supported on some high-surface-area materials, such as activated carbon and CNTs in this study, in order to achieve high dispersion and maximum utilization, as well as to avoid catalyst agglomeration during the chemical process operation.

Carbon nanotubes, due to their unique structural and electrical characteristics, have been used as catalysts support. In comparison with Vulcan XC-72, they have higher chemical and mechanical stability, higher electrical conductivity and more appropriate surface area [136]. In this section, 10% Pt supported on either Vulcan

XC-72 or CNTs (as prepared in Section 4.2.2.1 and 4.2.2.2), which were synthesized by wet-chemical and OMCVD methods, respectively, are characterized in this section, and comparison drawn as prepared in Section 4.3.1.

4.3.1.1 Surface area and pore size volume study of MCNTs and Vulcan XC-72

The surface area and pore volume were investigated by N_2BET as described in Section 3.1.5. The N_2BET parameters of the treated MCNTs and Vulcan XC-72 (Section 4.2.2.1 and 4.2.2.2) are listed in Table 4.3.

Table 4.3: Porous characteristics of MCNTs and Vulcan XC-72

Sample	**BET surface area (m^2/g)**	**Micropore surface area (m^2/g)**	**Micropore ration (%)**
MCNTs	157	0.0889	0.057
Vulcan XC-72	269	77.20	28.7

It can be seen that the BET surface of MCNTs was 157 m^2/g and the micropore surface area was 0.057 m^2/g, while Vulcan XCN had higher surface and much bigger micropore surface areas, which were 269 m^2/g and 77.20 m^2/g, respectively.

MCNTs are made up of graphite sheets, and the majority of nanotubes are closed and blocked. The N_2 does not penetrate into the pores of MCNTs during analysis. Therefore, it can be seen that there is a much smaller micropore surface area in carbon nanotubes than in Vulcan carbon black which is about 500 times higher.

The large surface area of carbon can provide the necessary three-phase zone for

electrocatalysis, which includes the reactant gas, solid catalyst surface and ions from the electrolyte (solid or liquid), and electrical pathways for efficient current distribution [199]. However, the electrolyte (such as Nafion), which provides pathways for ions, cannot enter into the micropores of Vulcan black so that Pt particles in micropores do not have catalytic functions for the electrodes' performance [200]. Therefore, too many micropores will affect the transfer of reactants and products, as well as the dispersion of platinum particles in a negative way.

4.3.1.2 X-ray diffraction study of MCNTs and Vulcan XC-72

Comparison of XRD patterns obtained forMCNTs and Vulcan XC-72 (XCN) are shown in Figure 4.1.

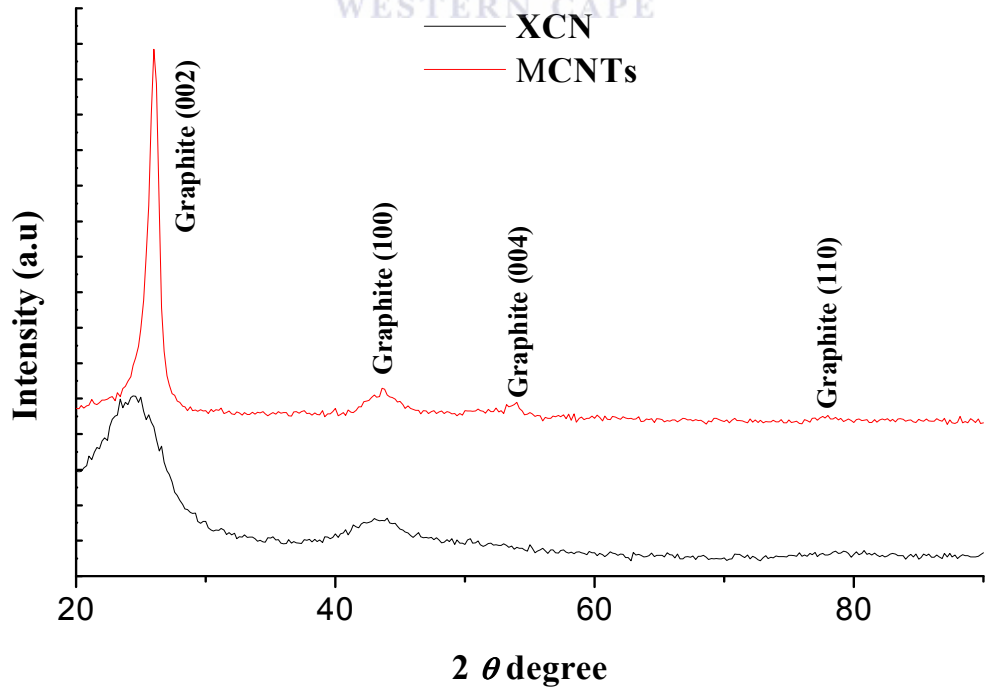

Figure 4.1: XRD patterns of MCTNs and Vulcan XCN.

From the XRD patterns it can be seen that there are obvious differences between the structures of these two carbon materials. The pattern for MCNTsexhibited the four characteristic diffraction peaks, which are at26.8, 42.4, 53.7 and 78.4° 2θdegrees. These peaks can be attributed to the hexagonal graphite structures (220), (100), (004) and (110) of the multi-wall CNT [201]. The first peak at 26.8º is particularly pronounced. XCN has two broad peaks, which are centred at 25 and 42° 2θ degrees, that are the (002) and (100)diffraction peaks respectively. The diffraction peaks of MCNTs are comparatively stronger. It can be concluded that the structure of the Vulcan support (XCN) is mostly amorphous carbon black mixed with some crystalline graphite while MCNTs has a distinctly crystalline structure, which is clearly graphitic. Thusit corresponds that the electronic conductivity of MCNTs supports would be better than that of the Vulcan carbon support (XCN).

4.3.1.3 Elemental composition study of 10% Pt catalysts

The elemental composition of platinum supported on either Vulcan XC-72 (sample A1 and A3) orCNTs (sample A2 and A4) electrocatalysts, which were prepared by wet-chemical (WC) and OMCVD methods, were determined by EDS and ICP, following the procedure given in Section 3.1.3 and 3.1.4. The Pt wt. % loading obtained from these twotechniques was accordant. The results are listed in Table 4.4.

Table 4.4: Pt loading of catalysts obtained by EDS and ICP

Catalyst	*Initial theoretical Pt content (wt. %)	Pt content from EDS (wt. %)	Pt content from ICP (wt. %)	Synthesized Method
A1: Pt/C	10	9.2	9.4	WC
A2: Pt/CNT	10	9.5	9.3	WC
A3: Pt/C	10	9.9	9.8	OMCVD
A4: Pt/CNT	10	9.8	9.8	OMCVD

* Refer to APPENDIX A for initial theoretical Pt content calculation

It is well known that EDS results are mainly quantitative as it giving loading on specific sites while ICP results represent the bulk sample in general. According to the Table 4.4, it can be seen that OMCVD method produced higher Pt wt.% loading on both Vulcan and CNTs supports (A3 and A4), which are 9.8% and 9.8%, respectively, when WC method only produced 9.4% and 9.3% Pt wt.% loading on the supports (A1 and A2), respectively. This is because in WC method the Pt precursor was not reduced completely as it significantly altered by the steps of adsorption, drying, calcinations and reduction while OMCVD method overcomes these problems in synthesizing procedures.

It also can be seen that the elemental composition results of EDS and ICP analyses correlated fairly well with the for initial theoretical platinum wt. % loading. The results have shown that the CVD method can be successfully applied for producing the specified platinum catalyst loading on the different carbon supports.

4.3.1.4 Particle size and distribution of 10% Pt electrocatalysts

HRTEM analysis was conducted on the four catalysts (A1 – A4) to investigate the morphology, metal particle size and particle size distribution, using the procedure given in Section 3.1.1. The TEM images for Pt nanoparticles deposited on Vulcan and CNTs are presented in Figure 4.2.

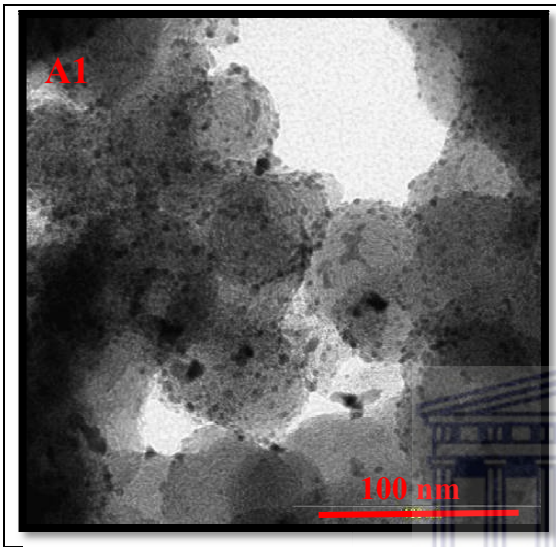

A1: Pt/C (WC Method)

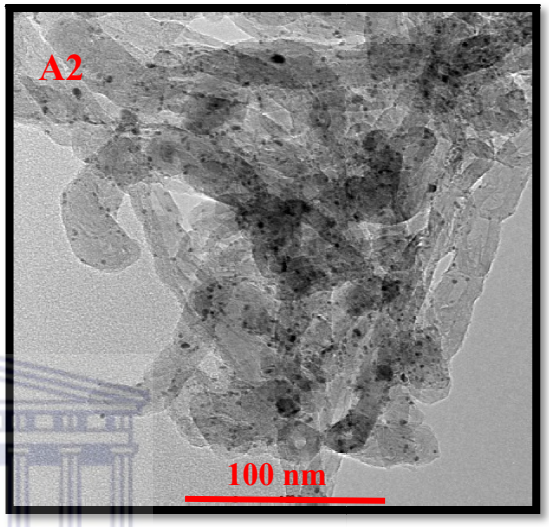

A2: Pt/CNT (WC Method)

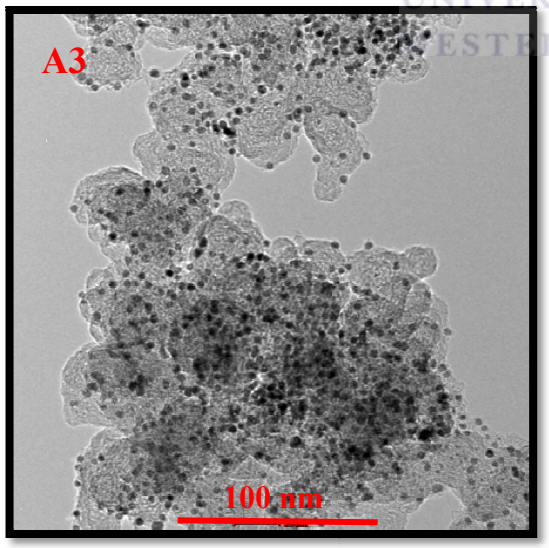

A3: Pt/C (OMCVD Method)

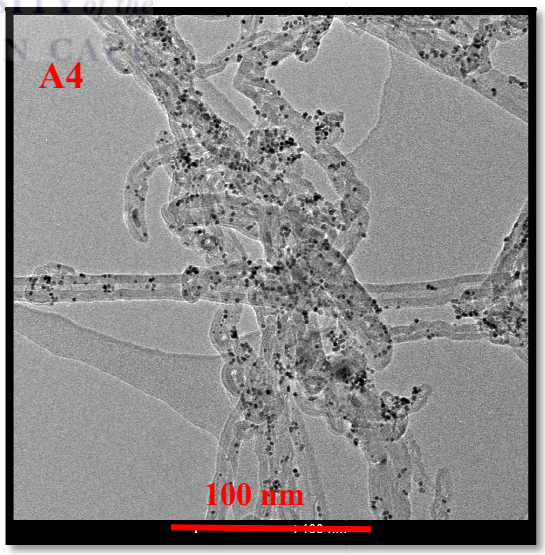

A4: Pt/CNT (OMCVD Method)

Figure 4.2: HRTEM images for samples A1- A4

From the initial TEM observations, the clear carbon support is visible in the case of samples A1 and A3 as large grey particles of 50 – 70 nm decorated with the small black Pt particles and CNTs (samples A2 and A4) have an average outer diameter of 20 – 30 nm and a wall thickness of ~ 10 nm decorated small black Pt particles.

It can be observed that well-dispersed Pt nanoparticles, which were made by CVD method (specified in Section 4.2.2.5 and Section 4.2.2.6), were dispersed uniformly either on the Vulcan or CNTs supports and there was no aggregation of Pt that could be seen in the images (A3 and A4) and the average Pt particle sizes are 2.31 and 2.50 nm for Pt/C and Pt/CNT, respectively. It was apparent that the particle sizes of Pt deposited on both supports were quite small and homogenous. The Pt/C (sample A3) and Pt/CNT (sample A4) have similar Pt particle size, and this is consistent with the fact that both catalysts were prepared by the same method.

However, as can be seen from Figure 4.2, the severe aggregation and growth of Pt particle occur when WC method was used as synthesizing method (samples A1 and A2).The particle size of Pt/C (sample A1) and Pt/CNT (sample A2) are 2.89 and 2.94 nm, respectively. This is due to the poor wetting of carbons by aqueous solutions and alsoethylene glycol is not a highly volatile solvent and the nanosized metal particles could have clustered together during the slow drying procedure.

The particle size distribution histograms of the Pt catalysts are presented in Figure 4.3.The histograms were described from the analysis of 200 Pt particles in each case and measured by hand on the HRTEM images.

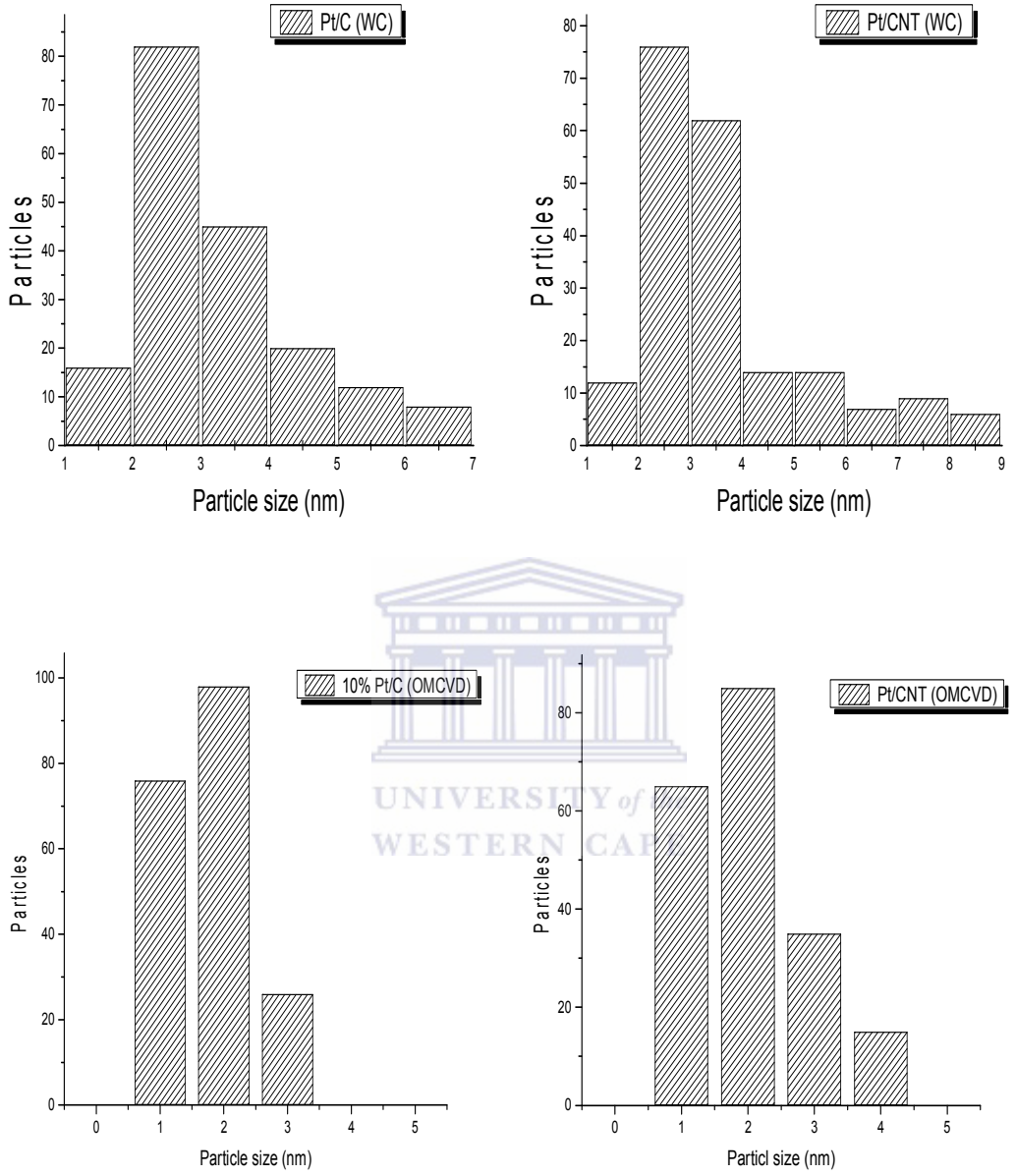

Figure 4.3: Particle size distributions histogram of samples A1 – A4

From the histogram it is apparent thatthe catalysts Pt/C (sample A1) and P/CNT (sample A4), which were produced by wet-chemical method, had wider range particle size distribution – from 1-7 nm and 1-9 nm, respectively, while the catalysts (samples A3 and A4) made by OMCVD method obtained particle size distribution

range are 0.5 – 3.5 nm and 0.5 – 4.5 nm, respectively. It is obvious that OMCVD method can produce smaller Pt particle sizes with narrower particle size distribution than that of WC method.

It also can be seen that for the catalysts of Pt supported on Vulcan showed the better particle size range than that Pt supported on CNTs in both applied methods. This may be related to the bigger surface area of Vulcan (Section 4.3.1.1). In terms of the HRTEM investigation, it can be emphasized that the use of CVD method produced uniform Pt particles upon either carbon black or carbon nanotubes supports.

4.3.1.5 Particle size and crystallinity study of 10% Pt catalysts

The crystallinity and particle size of 10% Pt electrocatalysts (samples A1 – A4) were determined using XRD, following the procedure given in Section 3.1.2. The corresponding patterns of the four catalysts are shown in Figure 4.4.

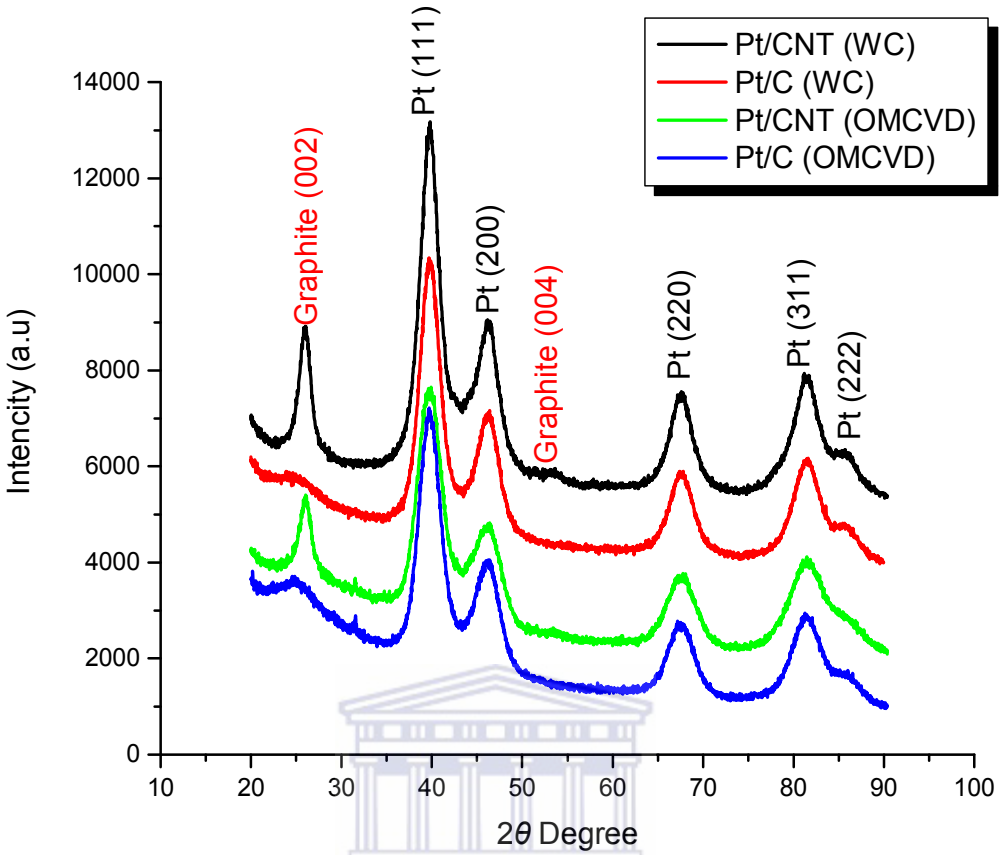

Figure 4.4: X-Ray diffraction patterns of the samples A1 – A4

It can be seen that all catalysts exhibited face-centered cubic (*fcc*) structure. The characteristic diffraction peaks at ca. 2θ = 26° of the Pt supported on CNTs catalysts indicate the crystalline nature of graphite, which is attributed here to the graphitic structure of CNTs. The XRD pattern clearly shows the five characteristic Pt diffraction peaks are around 39, 45, 68, 82º 2Θ degree, corresponding to Pt (111), (200), (220), (311) and (222) in all the cases. This indicates that the catalysts made by CVD and WC methods process a Pt (*fcc*) crystal structure [202-206] on both supported types used.

By use of the Scherrer equation (Equation [2-1]), it was confirmed that the catalysts made by WC method obtained bigger particle size, which are 2.65 and 2.78 nm for Pt/C (sample A1) and Pt/CNT (sample A2), respectively, which confirms the particle distribution size obtained by TEM. In the case of Pt produced by OMCVD method, the particle size of Pt/C (sample A3) and Pt/CNT (sample A4) catalysts 2.12 and 2.42 nm, respectively. It should be noted that as the crystallite size is related to the area of coherent diffraction, the particle size obtained from XRD can be smaller than the true particle size in general [207]. These results are in agreement with particle sizes obtained from TEM images based upon the histograms patterns of the catalysts (Figure 4.3).

4.3.1.6 Chemical-activity surface of 10% Pt electrocatalysts

The electrochemical (EC) activityand active surface area of the catalysts were evaluated by cyclic voltammetric (CV) using a three-electrode system and setup conditions as specified in Section 3.2. 0.50 M H_2SO_4 was used as the electrolyte during electrochemical evaluation and followed by the addition of 0.50 M methanol, which undergoes oxidation on the platinum surface. The methodogy was specified in Section 3.2. The measured potential range was from -0.2 to 1.0V (vs. Ag/AgCl) at a sweep rate of 50 mV/s. The objective and application of the EC activity is mainly to determine the activity of the catalyst synthesize by different supports, and give an indication as to which support produces a catalyst with the higher EC activity.

The EC active surface area for the Pt catalysts is presented in Figure 4.5.

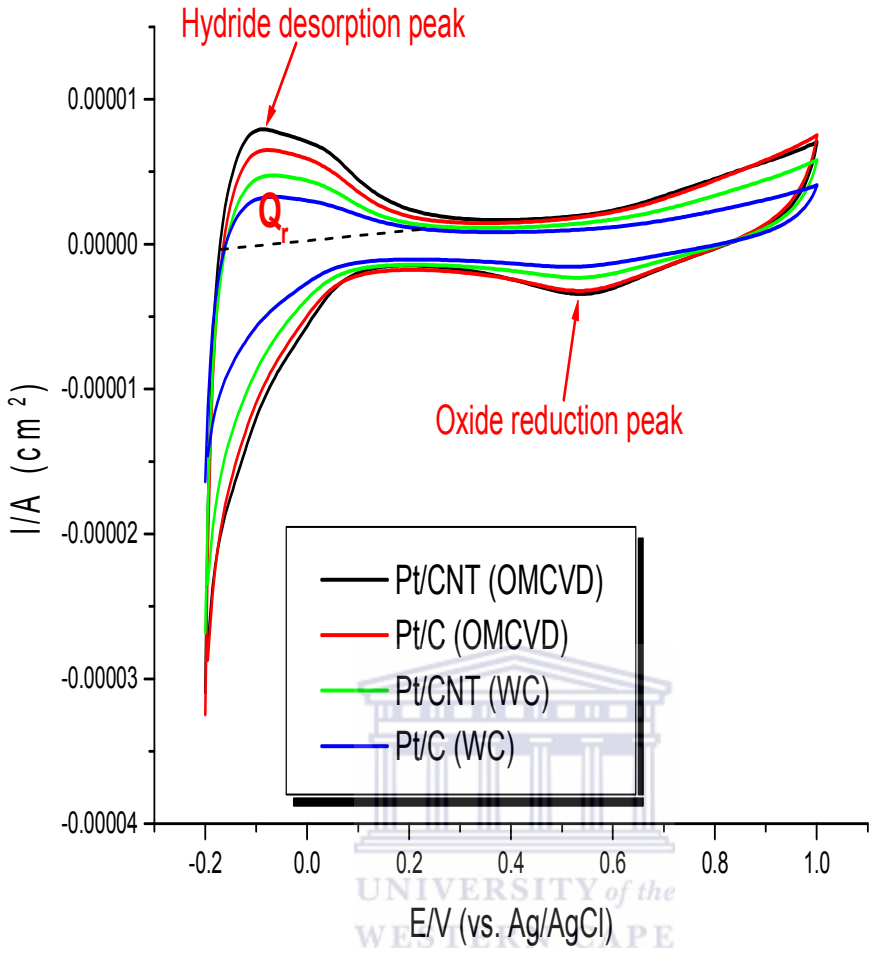

Figure 4.5: Cyclic voltammograms of 10% Pt electrocatalysts

It can be seen from Figure 4.5 and Table 4.5 that all catalysts showed the Pt-Hydride desorption peak around potential -0.21 to 0.10 V and the Pt-Oxide reduction peak from potential 0.30 to 0.80 V. These results show that all catalysts are active for hydrogen and oxygen according to the areas of the reaction peaks.

The columbic charge for hydride desorption Q_r and consumed wt. % Pt loading was used to calculate the active platinum surface of the electrodes and followed the

equation [2-4], which was described in Section 2.7.5. The resulting parameters for the Pt catalysts are summarized in Table 4.5.

Table 4.5: Electrochemical-active surface area parameters of electrocatalysts

Sample	**[Pt] (mg/cm^2)**	**Q_r (μC)**	**S_e (m^2/g)**	**Particle size by TEM (nm)**
A1: Pt/C	0.00094	18	91	2.89
A2: Pt/CNT	0.00093	21	107	2.94
A3: Pt/C	0.00098	26	138	2.31
A4: Pt/CNT	0.00098	30	153	2.50

[Pt]: consumed wt. % Pt loading for the CV test from the working electrode of each catalyst (see Section 3.2)

It is well known that the larger active surface results to the higher reaction area for methanol and water to produce electrons and protons [208-209]. Comparing the electrochemical-active surface area of the four catalysts, it can be seen that the catalysts (samples A3 and A4) made by CVD method showed the bigger active surface area than that of catalysts (samples A1 and A2) produced by WC method. This is because the catalysts made by CVD method obtained relatively higher Pt amount, uniform particles and smaller particle sizes of the catalysts (see discussion in Sections 4.3.1.3 and 4.3.1.4). It also displayed that the catalysts of Pt supported on Vulcan (samples A1 and A3) displayed smaller chemical-active surface area than that of Pt supported on CNTs catalysts (samples A2 and A4) in both applied methods. This is related to the unique structure and electrical characteristics of

CNTs. The high chemical-active surface area allows high diffusivity and good reactant flux. Thus, Pt catalystssupported on CNT materials show higher catalytic activitythan the same Pt catalysts supported on carbon black. Furthermore, CNTs provide not only a higher chemical and mechanical stability, and higher electrical conductivity, but also a relatively large surface area.

4.3.1.7 Oxidation of methanol on the 10% Pt electrocatalysts

The methanol oxidation reaction can be used to study the activities of the platinum electrocatalysts as well.

Methanol oxidation activity of the Pt catalysts was measured by cyclic voltameotry in 0.5 M H_2SO_4 +0.5 M MeOH solution as specified in Section 3.2 is shown in Figure 4.7.

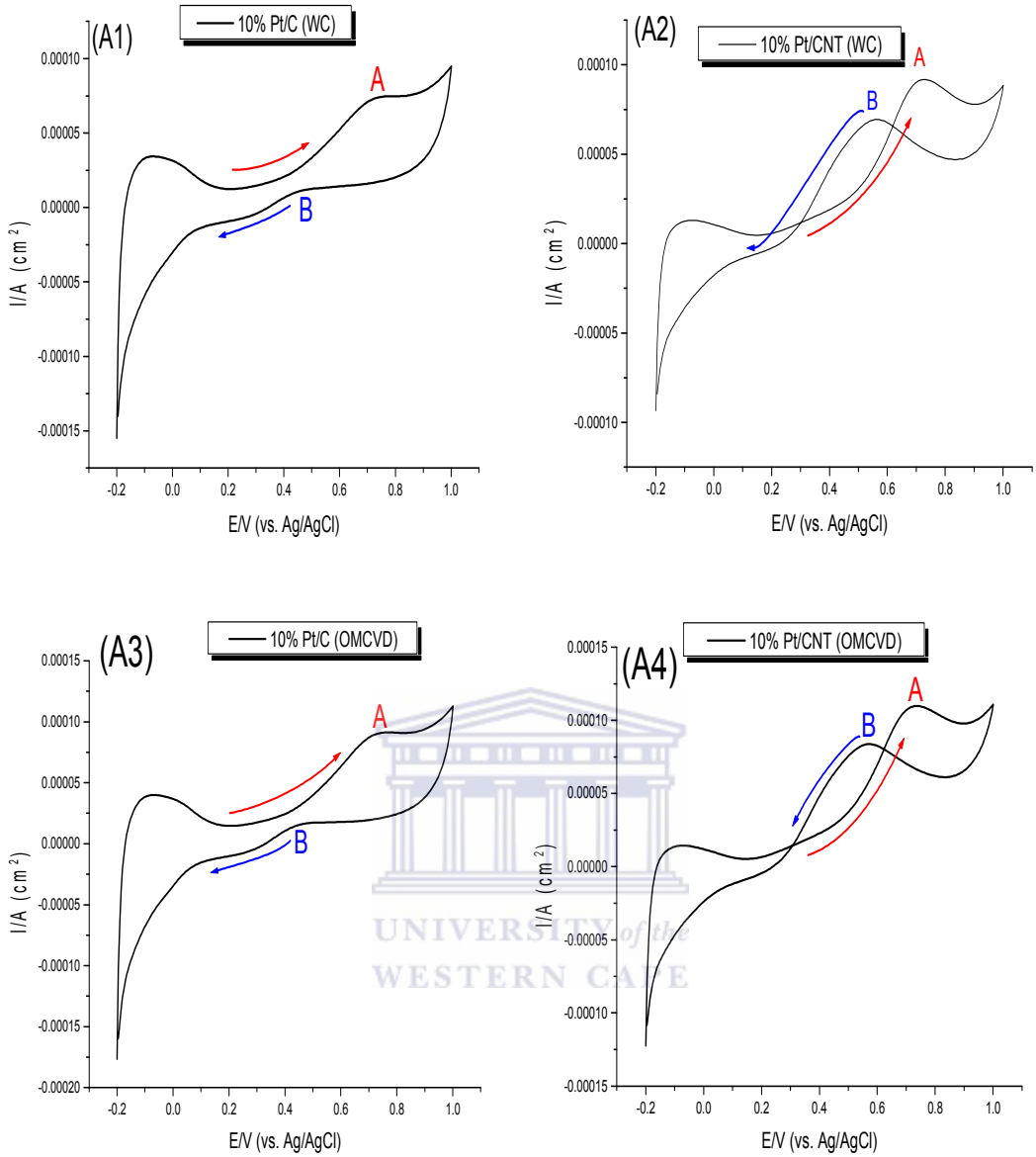

Figure 4.7: Oxidation of methanol voltammograms of the Pt electrocatalysts in 0.5 MH_2SO_4 + 0.5 M MeOH: (sample A1) Pt/C (WC), (sample A2) Pt/CNT (WC), (sample A3) Pt/C (OMCVD) and (sample A4) Pt/CNT (OMCVD)

Figure 4.7 show the voltammograms of methanol oxidation with the Pt catalysts. In all the voltammograms there are observed the direct oxidation peaks (A) and a methanol reoxidation peaks (B). It can be seen that all the onset of the methanol oxidation reaction of the catalsyts occurred in the same potential window, which

begins at about 0.38 V after almost complete desorption of adsorbed hydrogen. The oxidation currents increase considerably with increasing potential until the current peaks are seen at about 0.75 V. This means all the catalysts showed methanol oxidation activities. It is also normally observed that a Pt surface at +0.8V versus Ag/AgClshould be largely oxidized [210-211] and in the present studywith the Pt loaded either on the Vulcan and CNTs, the same behaviours wereobserved.

Table 4.6 shows that currents and potentials for the oxidation and re-oxidation of methanol for the catalysts.

Table 4.6: Currents and potential for the oxidation and re-oxidation of methanol for the catalysts

Catalyst	**Direct Potential (V)**	**Direct Current (I_A) (mA cm^{-2})**	**Inverse Current (I_B) (mA cm^{-2})**	**I_B/I_A*100%**
A1: Pt/C	0.75	70	19	27.1
A2: Pt/CNT	0.73	99	68	68.7
A3: Pt/C	0.73	82	20	24.4
A4: Pt/CNT	0.73	115	78	67.8

It is clear that the catalysts (samples A3 and A4) produced by OMCVD method showed higher positive peak current than that of the catalysts (samples A1 and A2) synthesized by WC method, while in the case of the catalysts of Pt supported on CNTs (samples A2 and A4) exhibited higher current than that of Pt supported on Vulcan catalysts (samples A1 and A3). The positive peak current densities for samples A1 – A4 are 79, 99, 82 and 115 mA/cm^2, respectively. This conclusion is

related with the chemical-active surface area of the catalysts, the larger active surface area, and the higher oxidation reaction activity.

Another feature of these catalysts is the variable broadening of the methanol oxidation peaks. The catalysts supported on Vulcan present broader peaks than that of Pt supported on CNTs catalysts. It is broadly known that the direct scan peak current (I_A) display the methanol oxidation and the reverse scan peak current (I_B) points to the methanol re-oxidation. The difference between the forward and the reverse current also indicates the methanol oxidation activities of the catalysts. The bigger ratio of I_B/I_A suggests the lower poisoning effect and the better tolerance of the electrode towards strongly adsorbed intermediates [212].

Table 4.6 shows that for the catalysts of Pt supported on CNTs (A2 and A4), the ratio (I_B/I_A) contribute with 68.7 % and 67.8 %, respectively, while the ratio of Pt supported on Vulcan are only 27.1% and 24.4 %, respectively. This is a significant difference of the two supports. This feature is indicated to the much higher tolerance of the Pt/CNT catalysts. This is because the unique structural and electrical characteristics of CNTs.This structure not only provides high conductivity, surface area and porosity, resulting in exceptional diffusivity but also have a positive effect on catalyst structure, yielding higher catalystic activity and stability than carbon black. Carbon black contains small primary pores that are inaccessible to electrolyte polymer, resulting in engulfed catalyst nanoparticles that do not contribute to electrochemical reactions due to the lack of a three-phase boundary [2].

It also can be seen that the bigger particle size contributed to the better re-oxidation current. This fact can be associated to smaller particles present on the surface of catalyst, which favours the surface poisoning by CO [213]. It indicates that the oxidation of methanol to CO_2 is performed in more selective way on the catalyst with bigger particle size than on the catalyst with smaller particles.

4.3.1.8 Summary of investigation of the methods and supports

In this section, four 10 wt. % Pt loading samples (A1 – A4) were produced by WC and OMCVD methods. EDS and ICP results indicate that the platinum was reduced entirely by the developed CVD method. From TEM results, it could be seen that the catalysts (samples A3 and A4) produced by OMCVD method obtained better Pt nanoparticles distribution range and smaller particle sizes of 2.31 and 2.50 nm, respectively, while the WC method produced Pt catalysts (samples A1 and A2) with particle size around 2.89 and 2.94 nm, respectively. XRD analysis confirmed that particle sizes of the catalysts are consisted with TEM results and all the Pt catalysts are with *fcc* structures. Electrochemical activities of the catalysts were measured by CV. According to the results, all the electrocatalysts are active for hydrogen and oxygen according to the areas of the reaction peak. The catalysts prepared by OMCVD method displayedlarger chemical-active surface area than that of the catalysts preparedby WC method.These larger surface area leads to the higher methanol oxidation activity of the Pt catalysts.On the other side, the platinum

catalysts supported on CNTs also showed a better methanol oxidation activity than that of the Pt supported on Vulcan due to the highly crystalline structure of CNTs.

According to these results, OMCVD method and CNTs will be applied in further studies.

4.3.2 Effect of Pt content

In order to increase catalytic activity, it is necessary to increase catalyst utilization. This will not only increase performance but also lead to an optimum Pt loading. If a low platinum loading is desired it is necessary that all of the platinum present is utilized efficiently and that the platinum is evenly dispersed over the entire active area. Normally, increasing metal loading leads to larger Pt particles and lower specific metal surface area on a given carbon support. Therefore, increasing the loading of metal on a carbon support might be expected to lead to lower activity.

On the other hand, although lower loading may achieve smaller Pt particle sizes and result in a bigger surface area, however, a too small amount of catalyst does not uniformly cover the electrode geometric area and would result in a poor electrochemical activity.

For the above reasons, an optimal Pt loading with the highest electrochemical activity of the catalyst needs to be investigated. Pt supported on MCNTs with different loading 20%, 40% and 60% were produced according to the method set out in Section 4.2.2.6 and JM 40% Pt/C catalyst was compared as a standard.

4.3.2.1 Elemental composition

The elemental composition of a series of different electrocatalystsPt loading with between 20 – 40 wt. % and commercial 40% JM Pt/C was determined by EDS and ICP, following the procedure given in Section 3.1.3 and 3.1.4, respectively. The results are listed in Table 4.7.

Table 4.7: Pt loading of different catalysts obtained by EDS and ICP

Catalyst	*Initial theoretical Ptcontent (wt. %)	Pt Content from EDS (wt. %)	Pt Content from ICP (wt. %)
JM 40% Pt/C	40	39	42
A5:Pt/CNT	20	22	20
A6:Pt/CNT	40	31	39
A7:Pt/CNT	60	50	59

* Refer to APPENDIX A for initial theoretical Pt content calculation

Table 4.7 shows that the elemental composition results of EDS and ICP analyses correlatedfairly wellcompared to the wt. %platinum loading.It is well known that EDS results are mainly quantitative as it giving loading on specific sites while ICP results represent the bulk sample in general. It can be seen from Table 4.7 that ICP analyses results correlate well with initial theoretical elemental loading of different wt. % loading catalysts.These results showed that the CVD method could be used to prepare a relatively well-defined atomic ratio of electrocatalysts.

4.3.2.2 Particle size and particle distribution study

The particle size and particle size distribution of catalysts 20%, 40% and 60% Pt/CNT were analyzed by HRTEM. The CNTs are visible in the TEM pictures as grey tubes. The dark spots correspond to Pt nanoparticles.

Figure 4.8, 4.9 and 4.10 present the HRTEM graphs and histograms of 20 % Pt/CNT, 40 % Pt/CNT and 60 % Pt/CNT catalysts, respectively.The histograms were described from the analysis of 200 Pt particles in each case and measured by hand on the HRTEM images.

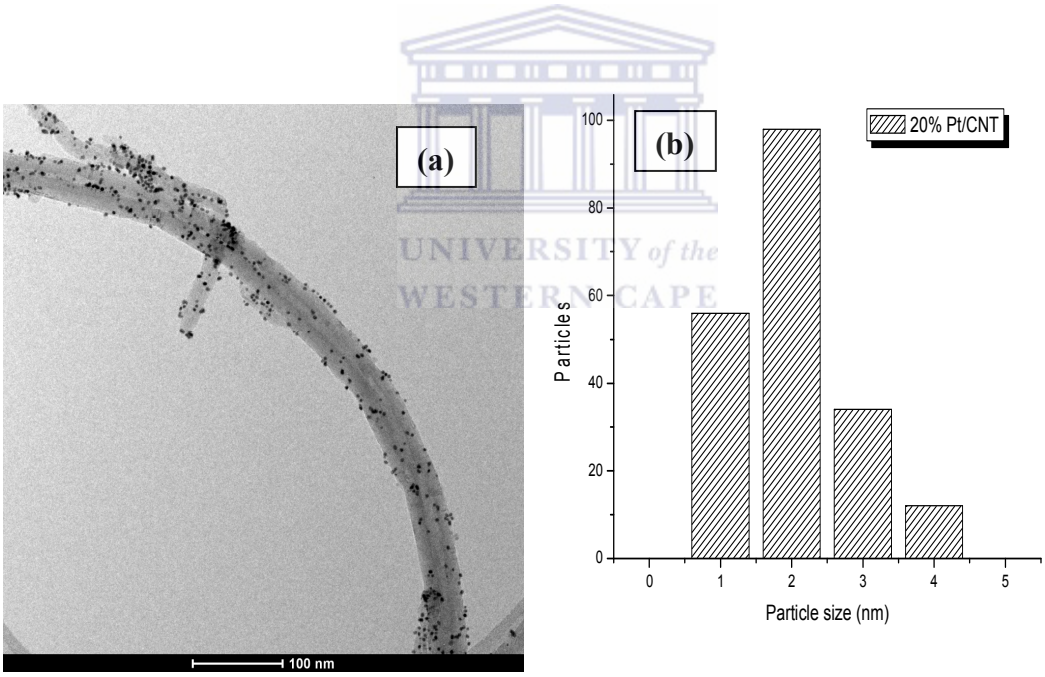

Figure 4.8: HRTEM graph (a) and particle size distribution histogram (b) of 20% Pt/CNT catalyst

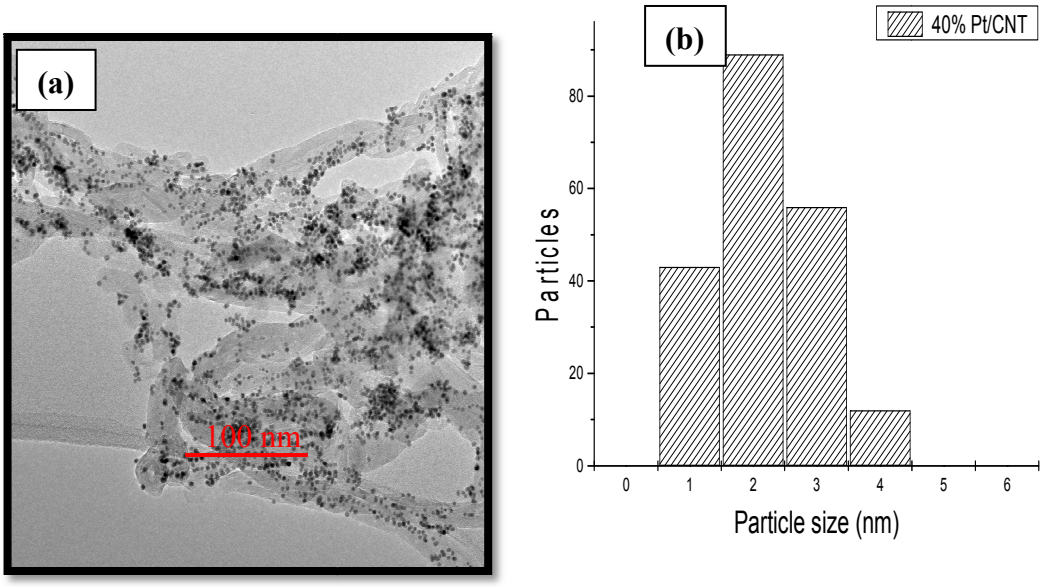

Figure 4.9: HRTEM graph (a) and particlesize distribution histogram (b) of 40% Pt/CNT

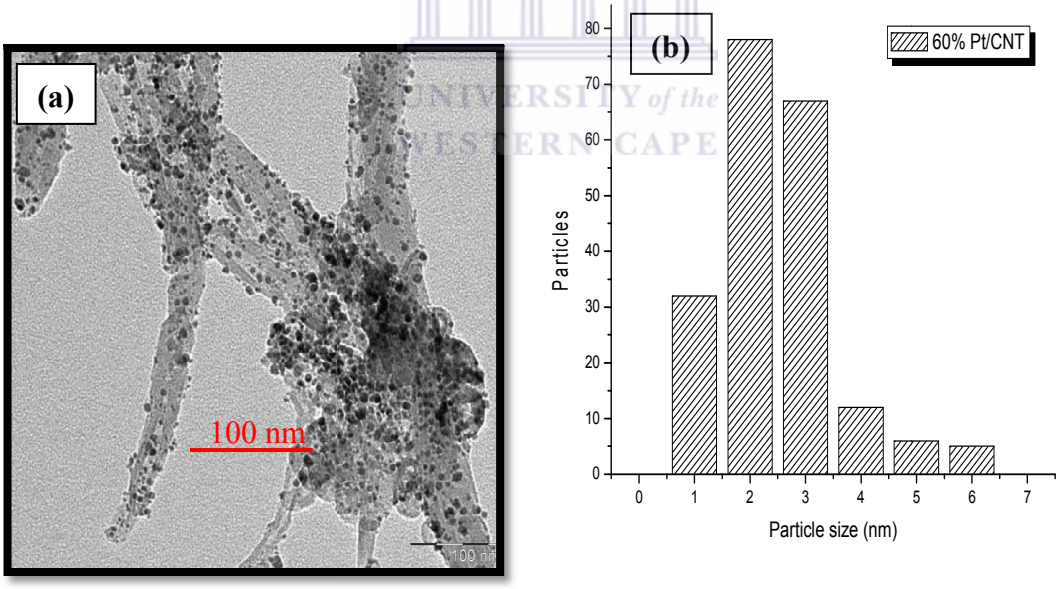

Figure 4.10: HRTEM graph (a) and particle size distribution histogram (b) of 60% Pt/CNT

The images show that the Pt nanoparticles dispersed uniformly either on the 20 or 40 wt. % Pt loading catalysts while there are some Pt aggregations were observed on 60 wt. % Pt loading catalyst. The average Pt particle sizes are 2.61, 2.77 and 3.82 nm for the different loading catalysts, respectively. It is obvious that the particles of Pt in 20 wt. % and 40 wt. % catalysts loaded were small and homogenous dispersed on the CNT supports compared to the 60 wt. % loaded Pt/CNT catalyst. It was found that agglomeration occurred more easily when the Pt content is higher than 40 wt. %.

From the histograms it is apparent thatthe particle size distribution ranges of Pt on the CNT support was increased with the increasing loading. Specifically, for the 20 wt. %and 40 wt. % Pt/CNT catalysts, the Pt nanoparticles showed a narrower distribution range between 0.5 to 4.5 nm (Figure 4.8 and 4.9), which is the same as 10 wt. % Pt/CNT (Figure 4.3) while 60 wt. % Pt/CNT (Figure 4.10) catalysts had particle size ranges from 0.5 to 6.5 nm.

In terms of the HRTEM investigation, it can be seen that the particles size range of Pt/CNT is related to the Pt contents of the catalysts. The less owner the content Pt, the more uniform the particles. Compared with the catalysts which were produced by wet-chemical (WC) method [133], the catalysts made by CVD method obtained a narrower particle size distribution. The uniform Pt particles and Pt content both play important roles in the activities of catalysts. Further studies will be pareented in the section on cyclic voltammetry test (see Section 4.3.2.4).

4.3.2.3 Particle size and crystallinity study

The crystallinity and particle size of Pt/CNT electrocatalysts were determined using XRD (see Section 3.1.2 for experimental details). The corresponding patterns of catalysts are shown in Figure 4.11 and a commercial standard catalyst JM 40 % is also presented for comparison.

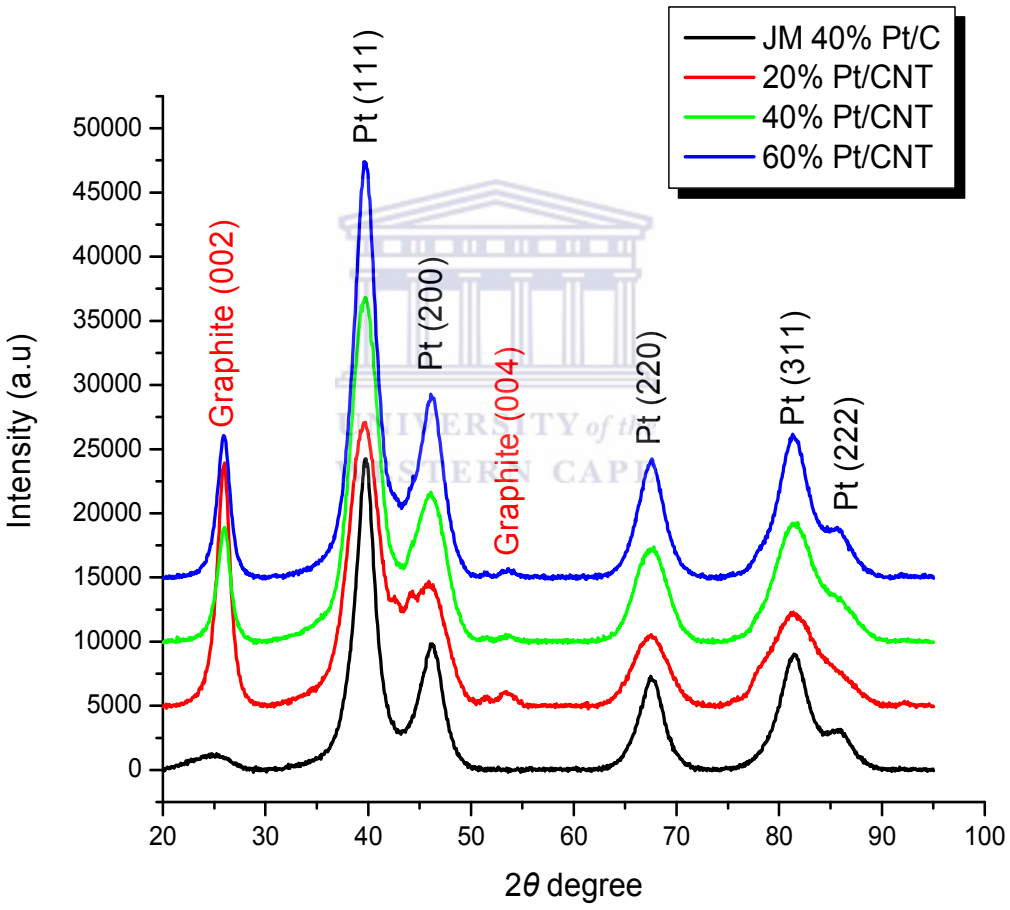

Figure 4.11: X-Ray diffraction patterns of Pt/CNT catalysts with different wt.% loading

As mentioned previously section 4.3.1.5, the characteristic diffraction peaks of the face centered cubic (*fcc*) Pt demonstrate that successful reduction of the Pt precursor

to the metallic form has been achieved. The diffraction peaks at around 39° 2θ and 46° 2$\theta$are due to the Pt (111) and (200) plane, respectively, which represents the typical character of a crystalline Pt face. This indicates that the in-house Pt/CNT catalysts are Pt (*fcc*) crystal structure.

It is known that the higher peak intensity shows higher Pt crystallite and indicates the bigger particle size. By use of the Scherrer equation (Equation [2-1]), it was confirmed that the 60 wt. % Pt/CNT catalyst had the biggest crystallite particle size, which was 3.43 nm, and 20 wt. % and 40 wt. % Pt/CNT catalysts had particle sizes are 2.72 and 2.89 nm, respectively, while in the case of the JM Pt/C catalyst, the Pt particle size was 3.25 nm. It can be seen that the peak intensities of Pt/CNT catalysts were increased by increasing the Pt content of the catalyst. These results corresponded to the TEM results (Section 4.3.2.2). Since Pt loading on all three CNT supported catalysts was produced by the same method, it was confirmed that the wt.% loading Pt content plays an important role in tailoring the particle size.

The intensity of the carbon graphite diffraction peaks (002) of all of the Pt/CNT catalysts is obviously stronger than in the case of the commercial JM Pt/C. It can be concluded that the structure of Vulcan is mostly amorphous carbon black mixed with some crystalline carbon graphite while carbon nanotubes have distinctly crystalline structure, which is clearly graphitic.

4.3.2.4 Electrochemical activity of electrocatalysts

The electrochemical (EC) activity and active surface area of the catalysts were determined by cyclic voltammetric (CV) and compared to that of the commercial JM Pt/C catalyst.

The EC active surface area graph for the JM Pt/C and home-made Pt/CNT catalysts, which were produced by CVD method, is presented in Figure 4.12.

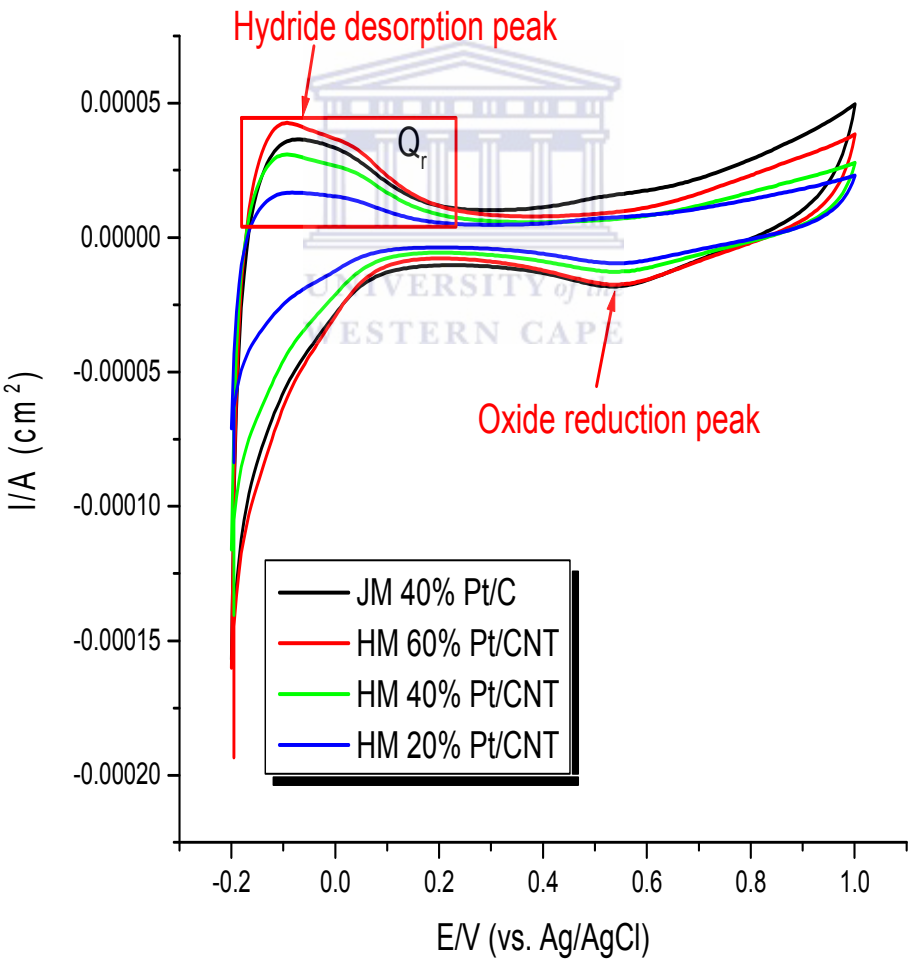

Figure 4.12: Cyclic voltammograms of Pt/CNT and JM Pt/C electrocatalysts

It can be seen from Figure 4.12 that all catalysts showed the Pt-Hydride desorption peak around a potential of -0.21 to 0.10 V and the Pt-Oxide reduction peak from a potential of 0.30 to 0.80 V. From these results it can be concluded that all catalysts synthesized here are active for hydrogen and oxygen redox reactions as indicated by the relative peak areas.

The columbic charge for hydride desorption Q_r and consumed wt. % Pt loading was used to calculate the active platinum surface of the electrodes and followed the equation [2-4], which was described in Section 2.7.5. The resulting parameters for the Pt catalysts are summarized in Table 4.8.

Table 4.8: Electrochemical-active surface area parameters of electrocatalysts

Sample	**[Pt] (mg/cm^2)**	**Q_r (µC)**	**S_e (m^2/g)**	**Particle size by TEM (nm)**
JM 40% Pt/C	0.0042	168	190	3.28
A5: Pt/CNT	0.0017	61	170	2.61
A6: Pt/CNT	0.0036	152	201	2.77
A7: Pt/CNT	0.0055	175	151	3.22

[Pt]: consumed wt. % Pt loading for the CV test from the working electrode of each catalyst (see Section 3.2)

It isgenerally recognized that the active surface coverageS_e is an important indication in determiningelectrochemical activity of a catalyst. The higher the surfacecoverage, the greater the electrochemical activity can beobtained. Table 4.8 shows that 40 wt. % Pt/CNT presented the promising results during active surface

area investigation, which compared better than that of the commercial standard JM 40% Pt/C catalyst. 60 wt. % Pt/CNT catalysts exhibited the smallest electrochemical-active surface area when compared to the other catalysts. This is because as the platinum loading increased, the agglomeration occurred more easily in high Pt content catalyst and leads to the decrease of the active surface area. 20 wt. % Pt/CNT catalyst showed the better chemical-active surface area than that of the 60 wt. % Pt/CNT due to its smaller particle size.

The methanol oxidation reaction was used as activity probe for testing the catalytic activity of thedifferent wt. % loading Pt/CNT catalysts and were measured by cyclic voltammotary in 0.5 M H_2SO_4 +0.5 M MeOH solution. The Methanol oxidation paragraphs of each catalyst were shown individually in Figure 4.13 and a comparison graph for all the catalysts together was displayed in Figure 4.14, the commercial JM Pt/C catalyst was presented for comparing as well.

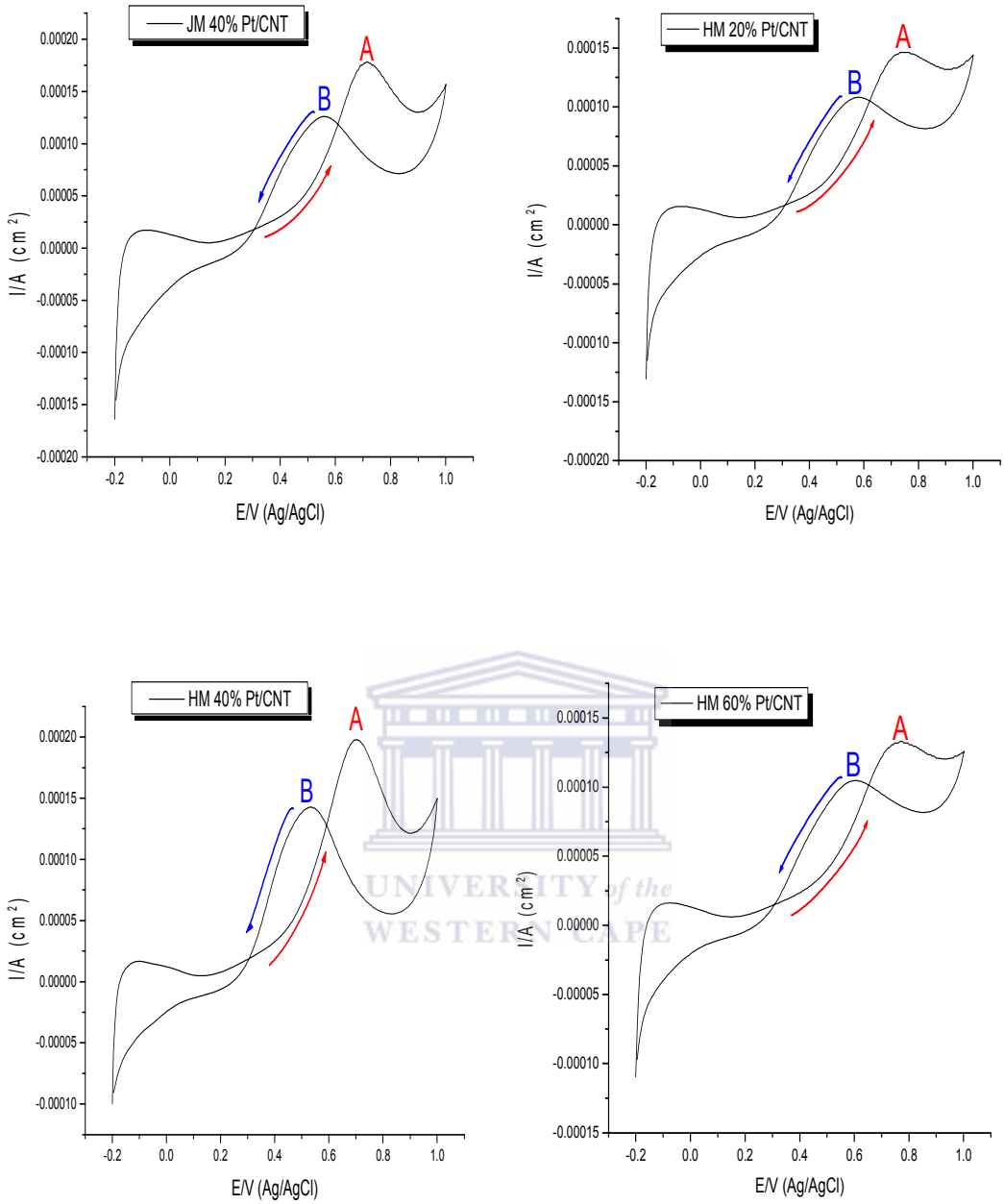

Figure 4.13: The individual methanol oxidation paragraphs for catalysts of JM Pt/C, HM 20 % Pt/CNT, HM 40 % Pt/CNT and HM 60 % Pt/CNT in 0.5 MH_2SO_4 + 0.5 M MeOH

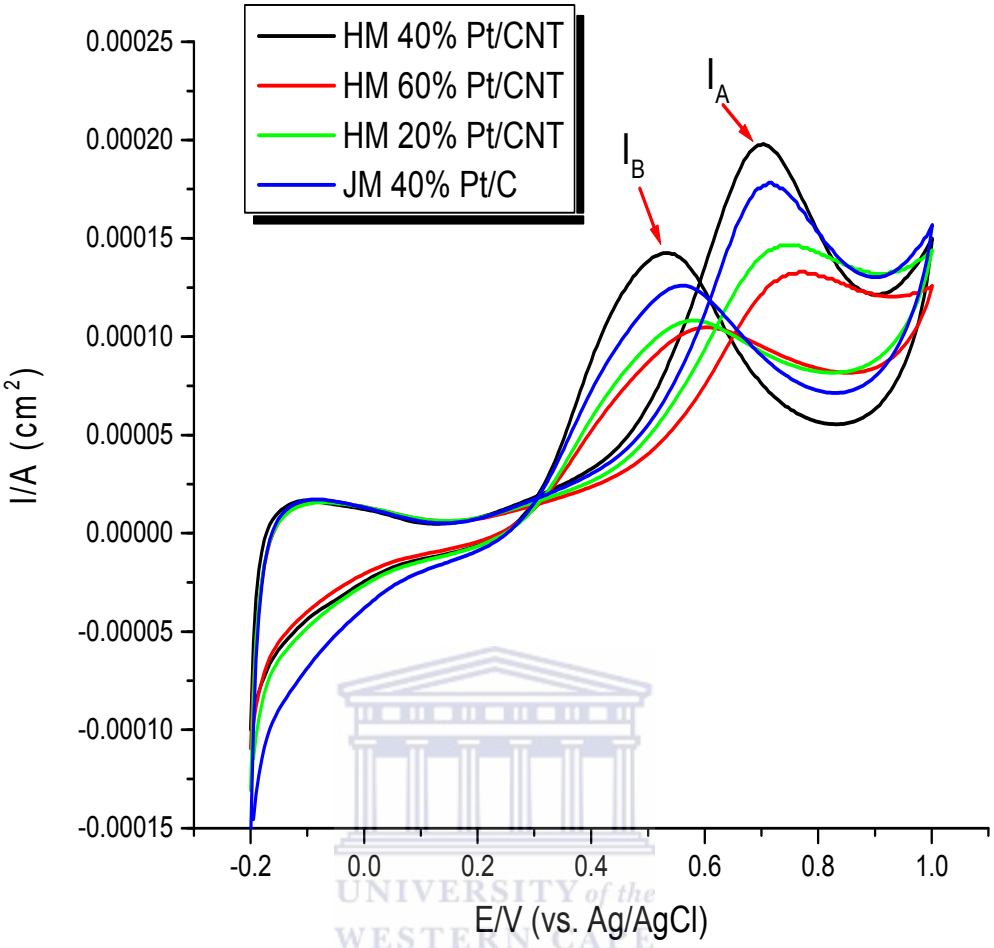

Figure 4.14: Cyclic voltammograms of JM 40% Pt/C catalyst and home-made 20%, 40% and 60% Pt/CNT electrocatalysts in 0.5 MH_2SO_4 + 0.5 M MeOH

Figure 4.13 and 4.14displayed a comparison of methanol oxidation activitiy for JM 40 % Pt/C and in-house PGM/CNT catalysts. It can be seen that in all the voltammograms there are observed the direct oxidation peaks current (I_A) and a methanol reoxidation peaks current (I_B). All the catalysts showed voltamperograms of methanol oxidation. The onset potential for methanol oxidation is very similar for all the catalysts (0.36-0.38 V), which correspond well with the results shown in Figure 4.7 for the onset potential for 10 wt. % Pt/C and Pt/CNT.

Table 4.9 shows that currents and potentials for the oxidation and re-oxidation of methanol for the catalysts.

Table 4.9: Currents and potential for the oxidation and re-oxidation of methanol for the catalysts

catalyst	**Direct Potential (V)**	**Direct Current (I_A) (mA cm^{-2})**	**Inverse Current (I_B) (mA cm^{-2})**	**I_B/I_A *100%**
JM 40% Pt/C	0.72	182	122	67.0
A5: Pt/CNT	0.72	149	103	69.1
A6: Pt/CNT	0.70	200	140	70.0
A7: Pt/CNT	0.76	137	103	75.1

The highest current (200 mA/cm^2) was obtained in the case of 40 wt. % Pt/CNT catalyst, which was larger than that of the commercial JM Pt/C (182 mA/cm^2), although its wt. % Pt loading (36 %) as lower than that of standard JM Pt/C catalyst (42 %). The catalysts 20 wt. % and 60 wt. % Pt/CNT obtained currents of 149mA/cm^2 and 137 mA/cm^2, respectively. This result confirmed the finding that is the larger active surface area (see Table 4.8) that leads to a higher methanol oxidation activity.

Furthermore, it is well known that the direct scan peak current (I_A) display the methanol oxidation and the reverse scan peak current (I_B) points to the methanol re-oxidation (Figure 4.14). The bigger ratio of I_B/I_A suggests the lower poisoning effect and the better tolerance of the electrode towards strongly adsorbed intermediates [212]. For the home-made 20 wt. %, 40 wt. % and 60 wt. % Pt/CNT

catalysts, the re-oxidation current contribute 69.1 %, 70.0 % and 75.1 % of I_B/I_A ratio, respectively; whereas the JM 40% Pt/C catalyst had the lowest I_B/I_A ratio of 67.0 %. This feature is indicative of the higher tolerance of the 60 wt. % Pt/CNT and lower tolerance of 20 wt. % Pt/CNT of the home-made catalysts. It can be seen that the higher Pt loading produces the better tolerance of catalysts. This fact can also be associated to smaller particles present on the surface of catalyst, which favours the surface poisoning by CO [213]. These results indicate that the oxidation of methanol to CO_2 is performed in more selective way on the catalyst with bigger particle size than on the catalyst with smaller particles. Nevertheless, it can be seen from Table 4.9 that all the home-made catalysts presented better ratio than that of the commercial JM catalyst. This may indicate the role of the different supports as home-made catalysts supported on CNTs while commercial catalyst supported on Vulcan.

Hence, it can be seen that the direct oxidation peak (A) potentials for methanol oxidation of catalysts are slightly reduced with increasing current (Table 4.9). Since the lower the peak potential, the better the electro-catalytic activity, these results indicate that the 40 wt. % Pt/CNT is the most active catalyst of the different Pt loaded in-house catalysts.

4.3.2.5 Summary of investigation of Pt content

Different Pt wt.% loading catalysts were successfully produced byOMCVD method and studied in this section. EDS and ICP results indicate that the platinum was

reduced fairly by the developed OMCVD method with different Pt contents. HRTEM results showed that Pt nanoparticleswere dispersed uniformly either on the 20 wt. % or 40 wt. % catalysts while there are some aggregations observed on 60 wt. % Pt catalysts. The average Pt particle sizes are 2.61, 2.77 and 3.22 nm for 20 wt. %, 40 wt. % and 60 wt. % catalysts, respectively. XRD analysis confirmed the Pt all catalysts had *fcc*structures and the particle sizes of Pt obtained from Scherrer equation corresponded with the HRTEM results. Electrochemical activities were measured by CV, and all electrocatalysts were active for hydrogen and oxygen reactions according to the areas of reaction peaks, and the methanol oxidation reaction. 40 wt. % Pt/CNT catalyst showed the largest electrochemical surface area (201 m^2/g) and the highest methanol oxidation activity (200 mA/cm^2), which is compared better to that of the commercial standard JM Pt/C catalyst (190 m^2/g and 182 mA/cm^2). Nevertheless, in the CO_2tolerance study, 60 wt. % Pt/CNT showed the best result (75.1 %) as it contained the highest Pt loading while compared to the other catalysts. However, due to the cost of Pt and the electrochemical activities were presented, the 40 wt. % Pt/CNT is seen as the best relatively catalyst in this study.

According to the results, 40 wt. % Pt metal contentshowed the best activity and will be used for further studies.

4.3.3 Effect of different metal alloys

As platinum is a noble metal of limited supply and can easily be poisoned by adsorbed CO in the methanol oxidation reaction, it is necessary to enhance catalytic performance by advanced electro-catalyst design relying on the bi-functional mechanism has been proposed. It has been found that the methanol electro-oxidation activity of PtRu/C is the highest among the binary Pt-based alloy, which is attributed to the ability of the Ru in the alloys to form active oxygen species (-OH) at low electrode potential (~0.2V) that can remove poisonous carbon monoxide on the Pt sites [214]. Through the "bi-functional mechanism", Ru significantly reduces the CO poisoning when incorporated into the Pt catalyst [215].

Despite the PtRu catalyst exhibiting good methanol oxidation activity, the state-of –the –art PtRu catalyst needs further improvement nicely higher catalytic activity and replacement of expensive nobel metals, Pt and Ru. The most successful way to achieve both these goals is to add a third metal to the PtRu catalyst. Ternary catalysts PtRuFe, PtRuNi, PtRuCo, PtRuW and PtRuIr [60-61] were found to have high activities in methanol oxidation reaction. Demirci used theoretical calculations and agreed that incorporation of a third metal might be the best way to improve the methanol oxidation activity [215]. The mixing of Pt with the third metal leads to weakly adsorbed CO on Pt sites and OH strongly adsorbed only on the third metal sites. Such tri-metallic catalysts favour the formation of OH_{ads} species which assist in the oxidation of CO_{ads} [216].

In this section, the catalysts PtRu/CNT was produced by using the CVD method as described in Section 4.2.2.7 and Fe, Cu and V were selected as a third member of the PtRu catalyst to lower the activation energy of reaction [4-10]. The effects of bi- and tri-metallic catalysts on the metal particle size, crystal structure and the electrocatalytic activity was studied and the commercial JM PtRu/C catalyst is also shown as the baseline comparison for the bi-metallic system.

4.3.3.1 Elemental composition study

EDS and ICP were used to investigate the elemental compositions of the catalysts. The results of alloy loading and element analysis on the PGM/CNT composites are given in Table 4.10.

Table 4.10: Pt loading of different catalysts obtained by EDS and ICP

Catalyst	Metal	*Initial theoretical metal content (wt. %)	Metal Content from EDS (wt. %)	Metal Content from ICP (wt. %)
JM PtRu/C/C (JM)	Pt:Ru	40:20	36:18	41:22
A8: PtRu/CNT	Pt:Ru	20:20	17:15	19:20
A9: PtRuFe/CNT	Pt:Ru:Fe	20:10:10	17:7:8	20:9:10
A10: PtRuCu/CNT	Pt:Ru:Cu	20:10:10	17:8:9	19:10:10
A11: PtRuV/CNT	Pt:Ru:V	20:10:10	19:7:7	19:9:10

* Refer to APPENDIX A for initial theoretical PGM content calculation

It can be seen that the Pt alloys' loading obtained from the EDS and ICP techniques, which were used to determine elemental composition, were accordant. Table 4.10 shows that the elemental composition results of EDS and ICP analyses correlate relatively well with initial theoretical platinum alloys loading. These results presented that the CVD method enable to prepare a well-defined atomic ratio of electrocatalysts.

4.3.3.2 Particle size and particle distribution study

The particle size and particle size distribution of catalysts PtRu/CNT, PtRuFe/CNT, PtRuCu/CNT and PtRuV/CNT were analyzed by HRTEM as specified in Section 3.1.1. The images of catalysts are shown in Figure 4.15.

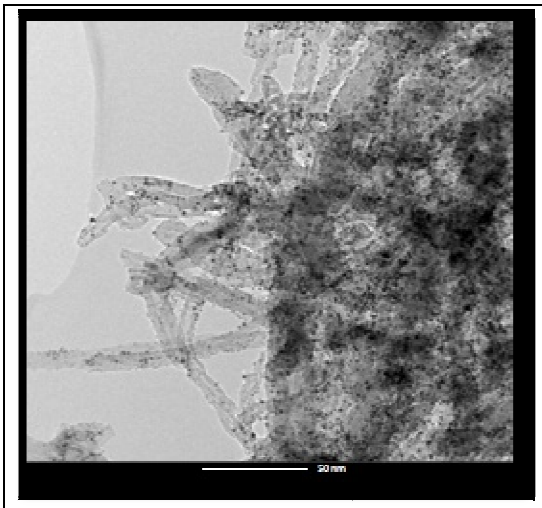

PtRu/CNT (a)

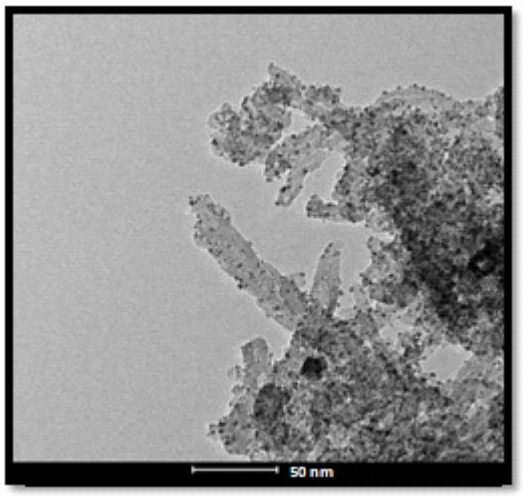

PtRuCu/CNT (b)

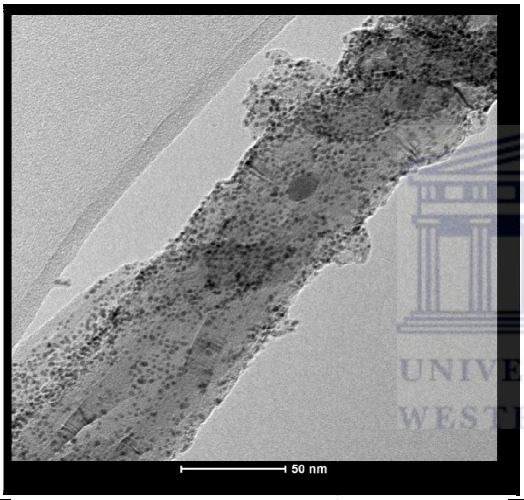

PtRuFe/CNT (c)

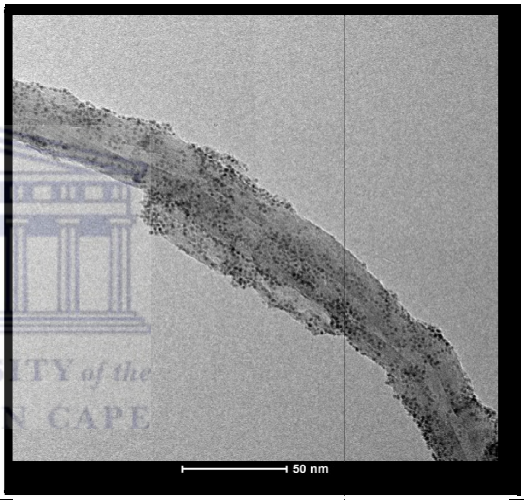

PtRuV/CNT (d)

Figure 4.15: HRTEM graphs of (a) 20:20 PtRu/CNT, (b) 20:10:10 PtRuCu/CNT, (c) 20:10:10 PtRuFe/CNT and (d) 20:10:10 PtRuV/CNT

As can be seen from Figure 4.15, all catalystswere dispersed uniformly upon CNT supports and no agglomeration was observed. When PtRu and PtRuM (M = Fe, Cu and V) catalysts compared with the 40 wt. % Pt/CNT catalyst (Figure 4.8), smaller particles were obtained and well-separated nanoparticles were observed by the combination of the extra metals with Pt. When PtRuM/CNT catalysts (Figure 4.14 (b), (c) and (d)) were compared with the PtRu/CNT (Figure 4.14 (a)), PtRuFe/CNT

and PtRuV/CNT showed smaller particle sizes and better nanoparticles dispersion while PtRuCu/CNT obtained bigger particles. The average particle sizes are 1.75, 2.31, 1.66, and 1.58 nm for PtRu/CNT, PtRuCu/CNT, PtRuFe/CNT and PtRuV/CNT, respectively. These results are agreement with particle sizes obtained from application of the Scherrer equation based upon the X-ray diffraction pattern of the catalysts (Figure 4.17 – 4.20), which will be presented in Section 4.4.3.3.

The particles size distribution histograms of the catalysts are presented in Figure 4.16. the histograms were discribed from the analysis of 200 particles in each case.

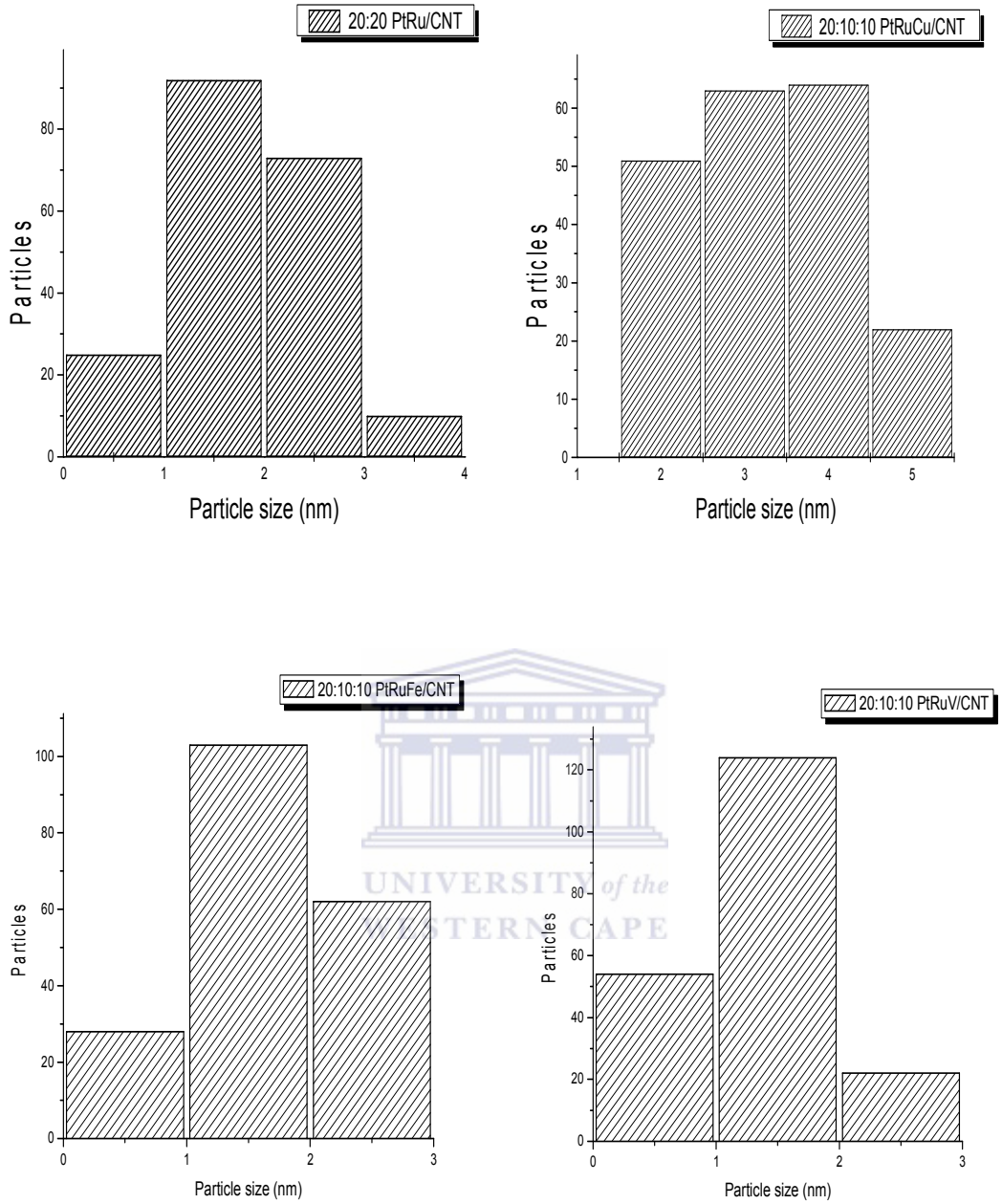

Figure 4.16: Particle size distribution histograms of PGM/CNT catalysts

From the histograms it is apparent that the distribution range of PtRu/CNT is 0 to 4 nm. PtRuCu/CNT catalyst had a somewhat bigger particle size distribution – from 1.5 to 5.5 nm, while the other two tri-metallic combinations of PtRuFe/CNT and PtRuV/CNT, was relatively uniform with the particle range between 0 to 3 nm.

In terms of the HRTEM investigation, it can be seen thatthe combination with additional metals during preparation did cause a particle size difference. The particle sizes of tri-metallic PGM catalysts systems are all smaller than that of the Pt/CNT catalyst. This may because the Ru, Fe, Cu and V atoms are smaller than Pt and incorporated with Pt. Further investigation will be reported in the Section 4.3.3.4 of the cyclic voltammetry test.

4.3.3.3 Particle size and crystallinity study

The crystallinity and particle size of PGM/CNT electrocatalysts were also determined using XRD. The corresponding XRD patterns of bi- and tri-metallic catalysts are shown in Figure 4.17 – 4.20 and the commercial catalyst 40%Pt20%Ru/C and home-made 40 wt. % Pt/CNT catalysts were also presented for comparison.

The Figure 4.17 – 4.20 show the characteristic diffraction peaks at ca. 2θ = 26°, which indicate the crystalline nature of graphite, which is attributed here to the graphitic structure of CNTs. The diffraction peaks in all the diffractograms indicate the presence of the face centered cubic (fcc) structure of the Pt represented by the planes (111), (200), (220), (311) and (222), which are around 39, 45, 68, 82° 2θ degree, respectively. This indicates that the in-house PGM catalysts all have the Pt (*fcc*) crystal structure, similar to the JM commercial catalyst.

Figure 4.17 shows the XRD patterns for the home-made catalysts, Pt/CNT, PtRu/CNT and commercial JM PtRu/C.

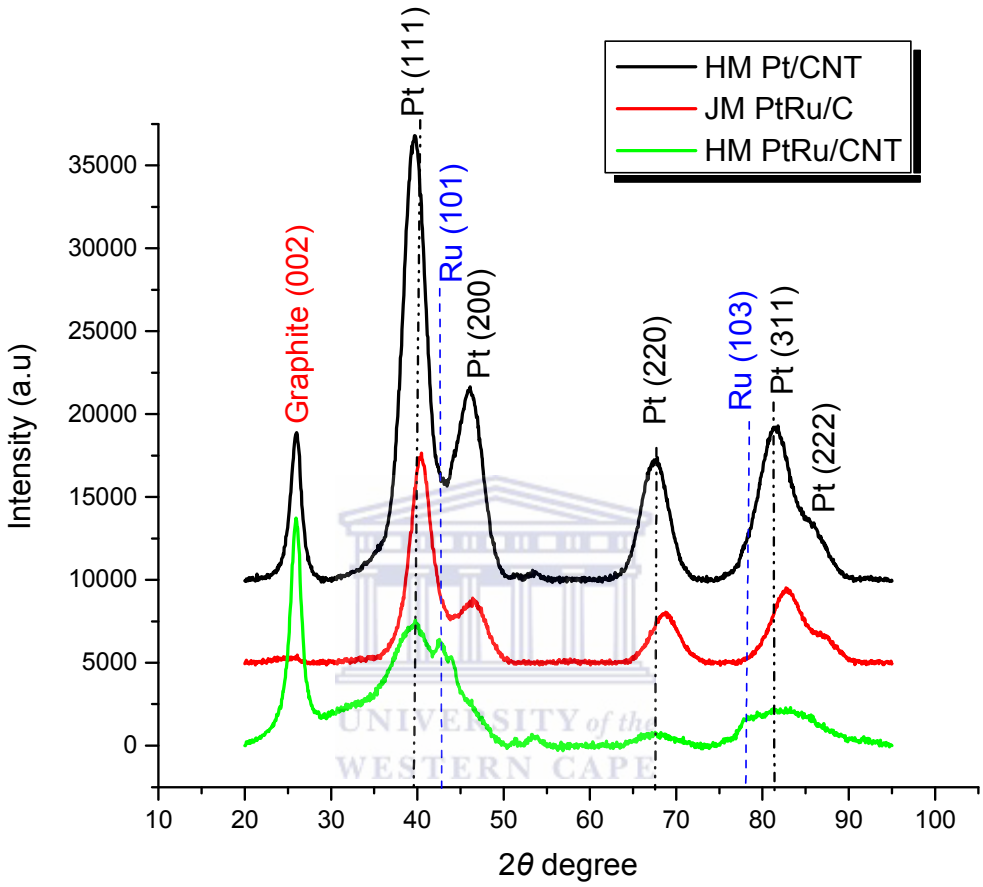

Figure 4.17: X-Ray diffraction patterns of JM Pt/C, JM PtRu/C and HM PtRu/CNT

Figure 4.17 showsthat both commercial and home-made Pt-Ru catalysts obtained the same diffraction peaks.In the case of home-made Pt/CNT, the diffraction peaks for Pt (111) and Pt (220) are observed at 2θ values, 39.0° and 67.5°, respectively, where as for the commercial and home-made Pt-Ru catalysts these peaks are seen displaced to higher angles are at 41.0° and 69.0°. This displacement of the peaks indicates the formation of Pt-Ru in an alloyed phase [217]. However, in case of in-house

PtRu/CNT small diffraction peaks were observed at 43.5° (101) and 78.5° (103), which peaks are shown as the dashed line in the figurethose were assigned to the hcp structure of Ru while there is no diffraction peaks corresponding to the characteristic hexago-nal-closest-packing structure of Ru was observed in the case of commercial PtRu/C catalyst.This results indicate that the commercial JM PtRu/C catalyst obtained complete alloying of Ru into the face-centered cubic lattice of Pt [217] while there may exist the separate phases of Pt and Ru [214] of home-made PtRu/CNT catalyst. It also can be seen that for the PtRu/CNT catalyst, the Pt (222) peak is not easy to identify while compared with Pt/CNT and commercial PtRu/C. It is because of the very small platinum particle sizes in the catalyst PtRu/CNT that the peak of the facet is broadened significantly[217].

The lattice parameters α_{fcc} (Equation [2-2]) of catalysts Pt/CNT, PtRu/CNT and PtRu/C are 3.92, 3.89 and 3.89 Å, respectively. It can be seen that for the Pt-Ru alloy there exists a decrease in α_{fcc}value due to the smaller size of Ru incorporated in the fcc structure of Pt. The value of $\alpha_{fcc}$for PtRu/CNT and PtRu/C also indicates the formation of Pt-Ru alloy. By use of the Scherrer equation (Equation [2-1]), it was confirmed that the Pt/CNT and PtRu/CNT catalysts had particle sizes of 2.89 and 1.57 nm, respectively, while in the case of the JM PtRu/C catalyst, the Pt particle size was of 1.88 nm. These results corresponded to the TEM results (Section 4.3.3.2).

Figure 4.18 shows the XRD pattern for PtRuCu/CNT and JM PtRu/C catalysts.

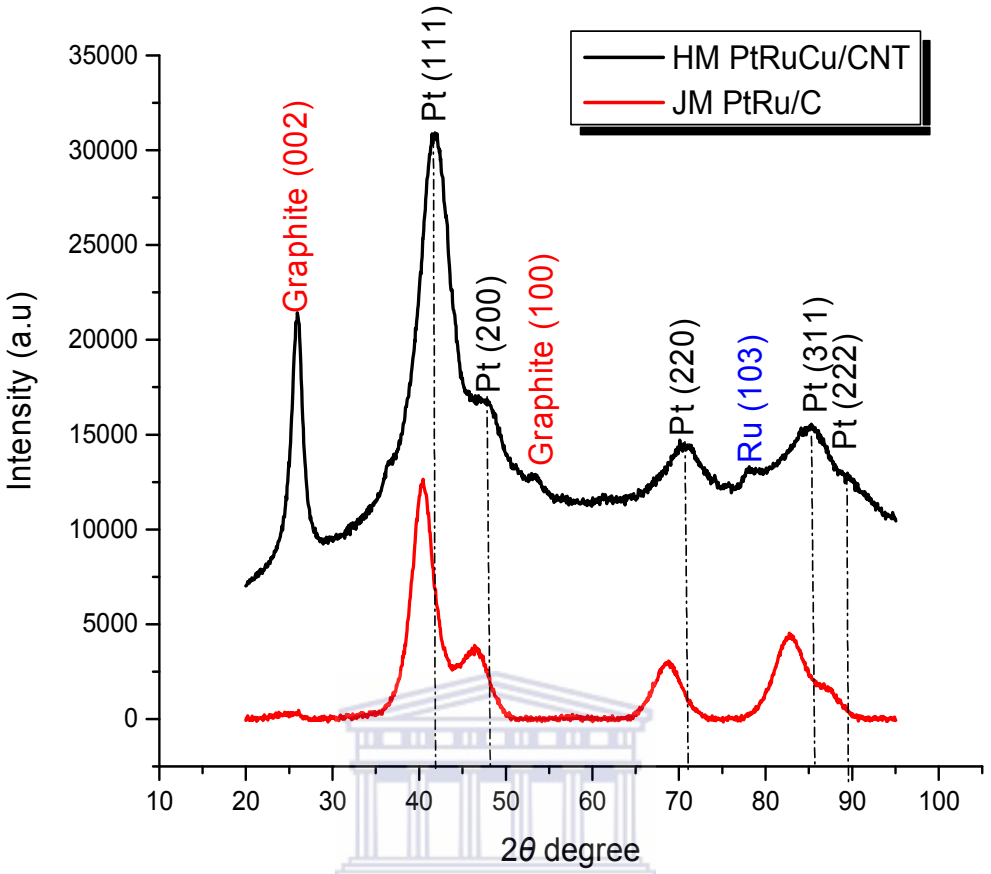

Figure 4.18: X-Ray diffraction patterns of HM PtRuCu/CNT and commcial JM PtRu/C

It can be seen from Figure 4.18 that Cu or Cu oxide diffraction peaks of PtRuCu/CNT are not observed, indicateing that alloying was relatively complete [217]. Nevertheless, the diffraction peak of Ru (103) is seen at 78.5° 2θdegree in the diffractgram. In the PtRuCu/CNT catalyst, all peaks were shifted to higher 2θ values than that of the commercial PtRu/C catalyst which is ascribed to the incorporation of Cu. The (220) peak moved from 67.5° in PtRu/C to 71.0° in PtRuCu/CNT. This is because the Cu atom is smaller than Pt, thus the interaction of Cu would cause

shrinkage of the lattice parameter, which results in the peak shift to the higher 2θ values [218].

The lattice parameters of catalysts PtRuCu/CNT is 3.86 Å. With PtRuCu/CNT catalyst there may also exist separate phases of Pt and Ru, as seen in the diffraction peak of Ru (103) in the gram. By use of the Scherrer equation (see Equation [2-1]), it was confirmed that the particle size of PtRuCu/CNT is 2.12 nm. This result corresponded to the TEM result (Section 4.3.3.2).

Figure 4.19 shows the XRD patterns for the catalysts PtRuFe/CNT and commercial PtRu/C as comparison.

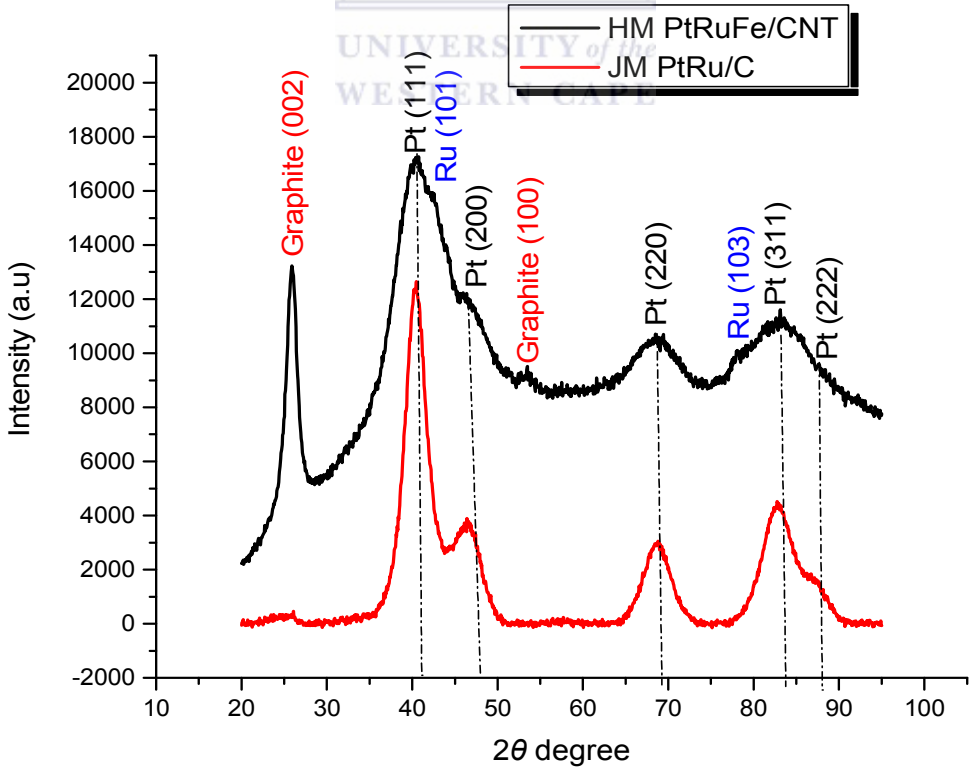

Figure 4.19: X-Ray diffraction patterns of HM PtRuFe/CNT and JM PtRu/C

It can be seen from Figure 4.19 that in the case of home-made PtRuFe/CNT, Fe or Fe oxide diffraction peaks are not observed and the diffraction peaks for Pt (111) and Pt (220) are observed at 2θ values, 41.0° and 69.5°, respectively, where as for the commercial PtRu/C catalysts these peaks are seen at lower angles, being at 40.5° and 69.0°. This slightly shift of the peaks is due to the lattic incorporation of Fe and shows that alloying was relatively complete [218]. In addition, there are small diffraction peaks that were observed at 43°and 78° of PtRuFe/CNT, which were assigned to hcp structure of Ru (101) and (103). These results indicate thatthere may exist separate phases of Pt and Ru for PtRuFe/CNT catalyst [214].It also can be seen that for the PtRuFe/CNT catalyst, the Pt (222) peak is not easy to identify while compared with commercial JM PtRu/C. It is because of the very small platinum particle sizes in the catalyst PtRuFe/CNT that the peak of the facet is broadened significantly [217].

The lattice parameters of catalysts PtRuFe/CNT is 3.89 Å. By use of the Scherrer equation (see Equation [2-1]), it was confirmed that the particle size of PtRuFe/CNT is 1.42 nm. This result corresponded to the TEM result (Section 4.3.3.2).

The XRD patterns for the catalysts PtRuV/CNT and commercial PtRu/C is shown in Figure 4.20.

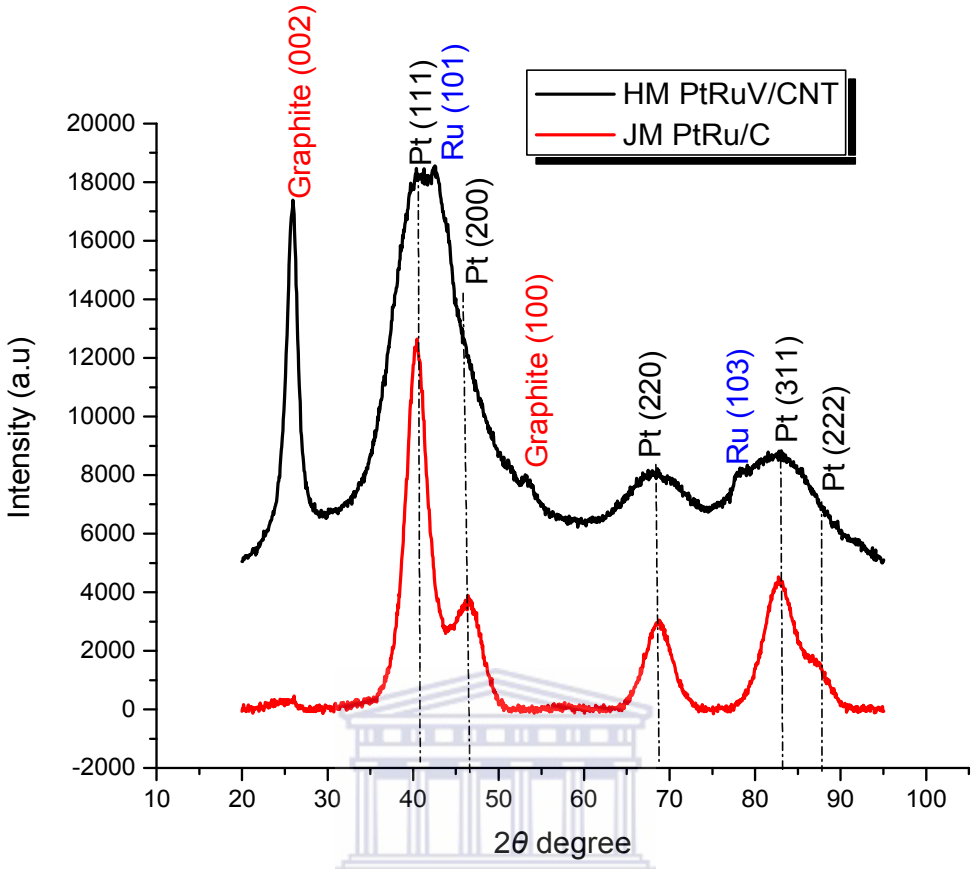

Figure 4.20: X-Ray diffraction patterns of HM PtRuV/CNT and JM PtRu/C

It can be seen that V or V oxide diffraction peaks of PtRuV/CNT are not observed, which indicates that alloying was relatively complete [218]. Nevertheless, the diffraction peaks of Ru (101) and (103) are seen in the diffraction gram. These results indicate thatthere may exist separate phases of Pt and Ru for PtRuV/CNT catalyst [214]. In the PtRuV/CNT catalyst, there are slight shifts in peaks to higher 2θ values compared to that of the commercial PtRu/C catalyst, due to the incorporation of V. It also can be seen that for the PtRuV/CNT catalyst, the Pt (222) peak is not easy to identify while compared with commercial JM PtRu/C. It is because of the very small platinum particle sizes in the catalyst PtRuFe/CNT that the

peak of the facet is broadened significantly [217]. By use of the Scherrer equation (Equation [2-1]), it was confirmed that the particle size of PtRuV/CNT was 1.30 nm. This result corresponded to the TEM result (Section 4.3.3.2).

4.3.3.4 Electrochemical activity of catalysts

The electrochemical (EC) activity and active surface area of the home-made catalysts were determined by cyclic voltammetric (CV) as described in Secion3.2 and compared to that of commercial JM PtRu/C catalyst.

The EC active surface area graphs for the JM PtRu/C and home-made bi- and tri-metallic Pt catalysts are presented in Figure 4.21.The integrated peak areas of the catalysts, whice are based on the area of the hydrogen desorption peak ($Q_{r)}$, were well defined by the Autolab software, and the electrochemical-active surface areas were calculated by the equation [2-4], which was described in Section 2.7.5.

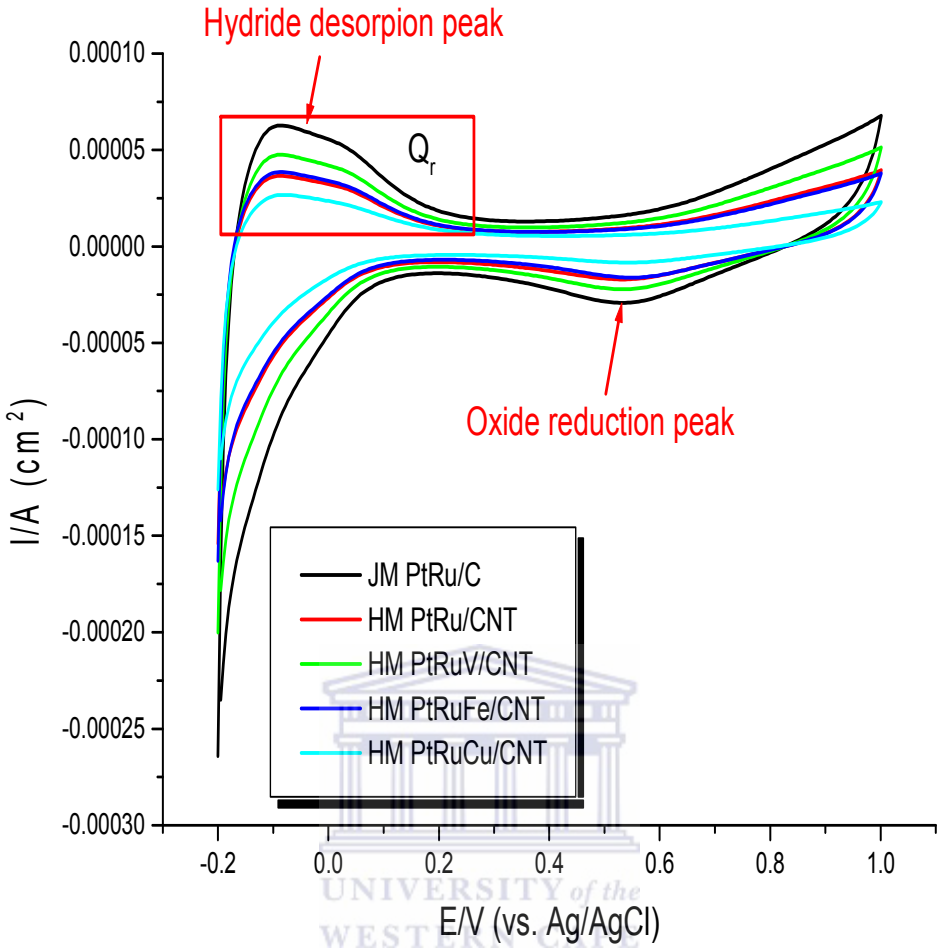

Figure 4.21: Cyclic voltammograms of PGM/CNT and JM PtRu/C electrocatalysts

It can be seen from Figure 4.21 that all catalysts showed the Pt-Hydride desorption peak around potential -0.21 to 0.10 V and the Pt-Oxide reduction peak from potential 0.30 to 0.80 V. from these results it can be concluded that all catalysts were active for hydrogen and oxygen reactions according to the areas of the reaction peaks.

Table 4.11 summarize the respective charges (Q_r)and electrochemical active surface area of the catalysts.

Table 4.11: Electrochemical-active surface area parameters of electrocatalysts

Sample	[Metal loading] (mg/cm^2)	Q_r (µC)	S_e (m^2/g)	Particle size by TEM (nm)
JM Pt Ru/C	0.0058	194	159	2.01
A8: PtRu/CNT	0.0035	158	215	2.77
A9: PtRuCu/CNT	0.0033	139	200	2.31
A10: PtRuFe/CNT	0.0033	154	222	1.75
A11: PtRuV/CNT	0.0032	160	238	1.66

[Metal loading]: Consumed wt. % metal loadings for the CV test from the working electrode of each catalyst (see Section 3.2)

It shows that all home-made catalysts showed larger chemical-active surface areas than that of the JM PtRu/C catalyst. This may because the high metal loading of the commercial catalyst (60 wt. %) causes the agglomeration of Pt and leads to the decrease of the active surface area which was shown in Table 4.11. PtRuV/CNT presented the best active surface area compared to other catalysts. This may be attributed to the smallest particle size (1.66 nm) and a higher amount of Pt content obtained (Table 4.10) of the catalyst. Catalyst PtRuCu/CNT displayed the smallest active surface area when compared with the other home-made catalysts as it obtained the biggest particle size than those other catalysts (Table 4.11).

It can be seen from Table 4.11 that smaller particle size leads to the bigger active surface area of catalysts when the catalysts contain the similar metal weight

loading.It also can be concluded that for the home-made catalysts, PtRu/CNT showed a bigger chemical active surface area than that of Pt/CNT (Table 4.8) and the tri-metallic catalysts also displayed relatively better results when compared with PtRu/CNT.These results proved that the addition metals incorporated with Pt can reduce the particle size and increase the active surface area of the catalysts. The interaction of the second or third metal can cause the positive electrochemical activity of the catalysts. This conclusion also accorded with the TEM results.

The methanol oxidation analyse is for thePGM/CNT catalysts and JM PtRu/C were measured by cyclic voltammotry in 0.5 M H_2SO_4 +0.5 M MeOH solution as described in Section 3.2 is shown in Figure 4.22.

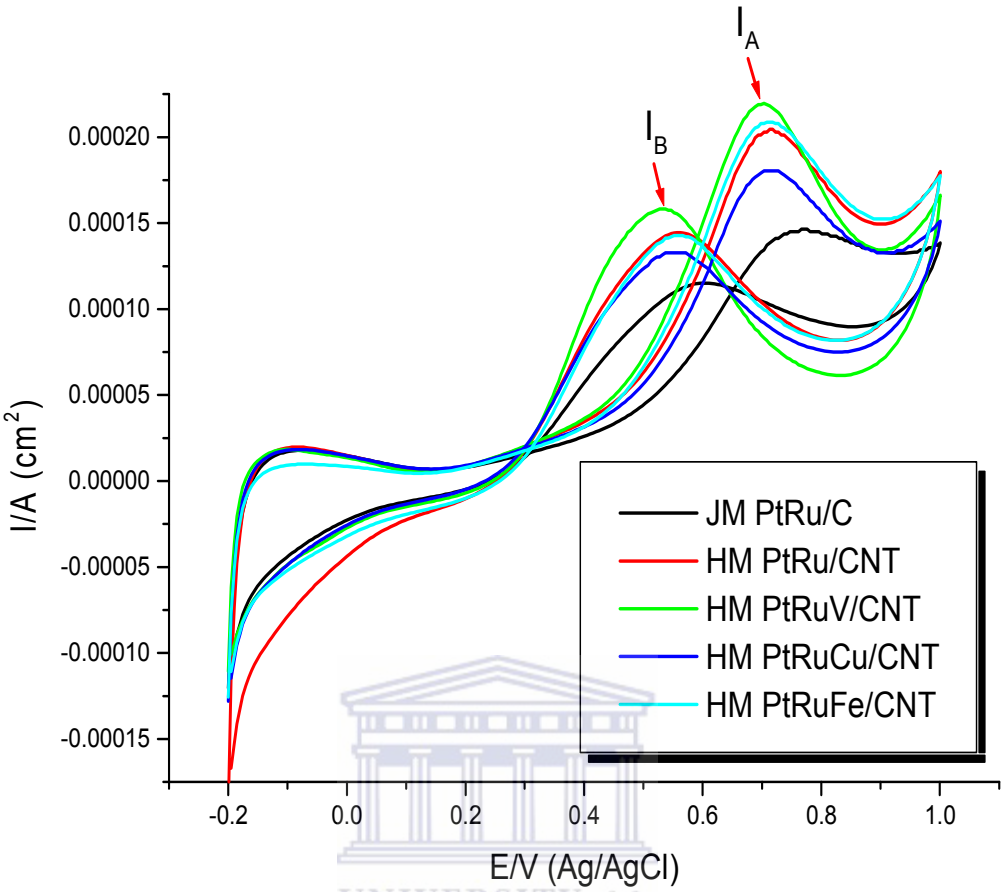

Figure 4.22: Cyclic voltammograms of JM PtRu/C catalyst and home-made PGM/CNT electrocatalysts in 0.5 MH_2SO_4 + 0.5 M MeOH

Figure 4.22displays a comparison of methanol oxidation activity for JM PtRu/C and in-house PGM/CNT catalysts. It can be seen that in all the voltammograms there are observed the direct oxidation peaks current (I_A) and a methanol reoxidation peaks current (I_B). All the catalysts showed voltamperograms of methanol oxidation. The onset potential for methanol oxidation was very similar for all the catalysts (0.36-0.38 V), which correspond well with the results which were shown in the previous section (Figure 4.13 and Figure 4.7).

Table 4.12 summarizes the results obtained for the oxidation of methanol on the catalysts.

Table 4.12: Currents and potential for the oxidation and re-oxidation of methanol for the catalysts

catalyst	**Direct Potential (V)**	**Direct Current (I_A) ($mAcm^{-2}$)**	**Inverse Current (I_B) ($mAcm^{-2}$)**	**I_B/I_A *100%**
JM Pt Ru/C	0.78	140	105	75.0
A8: PtRu/CNT	0.72	205	148	72.2
A9: PtRuCu/CNT	0.72	185	138	74.6
A10: PtRuFe/CNT	0.74	210	150	71.4
A11: PtRuV/CNT	0.71	228	159	70.6

The highest direct current (228 mA/cm^2) of the PtRuV/CNT catalyst was observed in Table 4.12. Catalysts JM PtRu/C, home-made PtRu/CNT, PtRuCu/CNT and PtRuFe/CNT catalysts displayed direct currents of 140mA/cm^2, 205 mA/cm^2, 185mA/cm^2 and 210 mA/cm^2, respectively. The order of the current amplitude corresponded to that of the chemical active surface area of the catalysts (Table 4.11). It can be seen that the direct oxidation peak (A) potentials for methanol oxidation of catalysts are slightly reduced with increasing current (Table 4.11). The lower the peak potential, the better the electro-catalytic activity, thus these results indicate that the PtRuV/CNT is the best catalyst in all the catalysts were studied in this section.

Furthermore, it is well known that the direct scan peak current (I_A) (Figure 4.21) displays the methanol oxidation and the reverse scan peak current (I_B) shows to the

methanol re-oxidation. The higher ratio of I_B/I_A suggests the lower poisoning effect and the better tolerance of the electrode towards strongly adsorbed intermediates [234].

Table 4.12 also lists the oxidation potentials for the direct conversion of methanol to CO_2, as well as the corresponding current intensities when the scan is switched towards cathodic potentials. For the catalysts PtRu/CNT, PtRuCu/CNT, PtRuFe/CNT and PtRuV/CNT, the ratio of I_B/I_A contributed with 72.2 %, 74.6 % and 71.4 % and 70.6 %, respectively; whereas in the case of the JM PtRu/C catalyst, the ration contributed with 75.0 %. The feature points to the highest poisoning tolerance of PtRuCu/CNT and the lowest tolerance of PtRuV/CNT compared to the commercial catalysts. This fact could be associated with smaller particles present on the carbon surface of catalyst, which would favour the surface poisoning by CO [213]. It indicates that the oxidation of methanol to CO_2 is performed in a more selective way on the catalyst with bigger particle size than on the catalyst with smaller particles. It also can be seen that all bi- and tri-metallic catalysts showed better poisoning tolerance than that of 40 wt. % Pt mono-metallic catalysts (Table 4.9). This is because the second and third metals added to Pt enhanced CO removal from the surface, since the addition metals promote a weakening of the Pt-CO bond producing easily the CO oxidation reaction to CO_2 via a bi-functional mechanism.

4.3.3.5 Summary of investigation of Pt alloys

Bi- and tri-metallic Platinum group metal catalysts and commercial PtRu/C catalyst were studied in this section. EDS and ICP results indicate that PGM metals were reduced relatively completely by the chemical vapour deposition method. HRTEM results presented that all catalysts obtained uniform nanoparticles. The average particle sizes are 1.75 nm, 2.31 nm, 1.66 nm and 1.58 nm for catalysts PtRu/CNT, PtRuCu/CNT, PtRuFe/CNT and PtRuV/CNT, respectively. The XRD analysis confirmed the all catalysts had Pt *fcc* structures and the particle sizes of catalysts obtained from Scherrer equation corresponded with HRTEM results. All the catalysts showed relatively complete alloy phases by XRD though there may exist separate phases of Pt and Ru. Electrochemical activities were measured by CV, all electrocatalysts were active for hydrogen and oxygen according to the areas of the hydride desorption and oxide reaction peaks, as well as for the methanol oxidation reaction. Catalyst PtRuV/CNT displayed the highest electrochemical surface area (238 m^2/g)and methanol oxidation activity (228 mA/cm^2). In the case of the CO_2tolerance study, all PGM/CNT showed better results than monometallic catalysts due to bi-functionality of the additional metal. However, PtRuV/CNT obtained the lowest tolerance (70.6 %) while PtRuCu/CNT showed the best poison tolerance (74.6 %) of home-made catalysts. This is associated with the particle size of the catalyst.

It should be emphasized that the CVD method can not only produce the different contents of catalysts but also different metals combination catalysts in one step.

4.4 Conclusions

In this chapter platinum group metal catalysts have been synthesized under preparation conditions. In the investigation of being used different synthesis methods and supports for Pt catalysts, Physio-chemical analyses showed that the OMCVD can produce the platinum catalysts in very simple synthesis procedure and producing consistent results that resulted in uniform particle size, high dispersion and high electrochemical activity when compared to the wet-chemical method.Carbon nanotubes showed significantly improved characteristics than that of the Vulcan as the support for the platinum catalysts due to their circular graphite structure and better electroconductivity.

In the study of the different Pt contents of the electrocatalysts, which were produced by OMCVD method and supported on carbon nanotubes, 40 wt. % of Pt catalyst showed as the best loading for Pt/CNT catalysts when compared with the 20 and 60 wt. % Pt loading catalysts as well as the commercial JM 40 % Pt/C catalyst. 40 wt. % Pt/CNT catalyst showed the highest electrochemical surface area (201 m^2/g) and the methanol oxidation activity (200 mA/cm^2). The electrochemical investigation presented that the methanol oxidation activity was directly related to the electrochemical-active surface area of the catalysts where the chemical activity of electrocatalysts was increased by an increased active surface area.

In the investigation of platinum alloy electrocatalysts study, the results of the bi- and tri-metallic catalysts showed that the added additional metals of platinum alloys could reduce the particle sizes and resulted in a larger chemical-active surface area and higher methanol oxidation activity of the catalysts. The home-made bi- and tri-metallic catalysts exhibited much better results than that of the commercial JM PtRu/C catalyst. It also could be concluded that the bi-metallic catalyst showed higher electrochemical activity than that of the monocatalysts and the tri-metallic catalysts displayed better electrochemical activity than that of the bi- catalyst. A significantly higher catalytic activity for PtRuV/CNT catalyst was found in this study. PtRuV/CNT displayed the highest electrochemical surface area (238 m^2/g) and methanol oxidation activity (228 mA/cm^2).

In a conclusion, the use of the OMCVD method resulted in the successful presentation of the PGM electrocatalysts with different supports, metal contents and combination metal alloys in very simple synthesis procedure. The advantage to this method is that the stages of impregnation, washing, drying, calcinations, activation, surface poisoning and material transformations activated during drying are avoided. It is an economic and environmental friendly method to obtain controlled metallic nanoparticulate deposits of high quality.

Since the best results with suitably synthesize method and prepared conditions were observed for PGM/CNT samples, further catalyst synthesis will be done using OMCVD method at 40 wt. % metal loading.

CHAPTER 5:

Titanium Oxide Modified Carbon Nanotutes as Support for Platinum Group Metal Catalyst

In this chapter, comparison between the characteristics of pre-treated CNTs and TiO_2 coating on CNTs (TiO_2/CNT) are made. Thereafter, the properties of nanophase PGM electrocatalysts supported on TiO_2/CNT are presented and compared with those of Pt supported on CNTs and commercial JM catalysts.

5.1 Introduction

Recently, organic-inorganic hybrid nanocomposite materials have attracted considerable research interests in fundamental and application studies. TiO_2 is a well-known substrate material due to the superior properties such as large specific surface area, high uniformity, and excellent biocompatibility and has been applied in a variety of fields including highly efficient photocatalysis [219-220], fuel cells [221-222], biosensors [223], hydrogen sensor [224-225] and hydrogen evolution [226].

Fuel cells received much attention due to their high theoretical fuel efficiency and low environmental impact and the direct methanol fuel cell (DMFC) has been developed with a simplified structural system among them. However, the main problem in the DMFCs is the poisoning of Pt surface by CO like species produced

during methanol electro-oxidation.Recently, researchers have reported that systems combining platinum, metal oxides and carbon exhibited excellent catalytic activity for electrooxidation of methanol and CO. Metal oxides, such as Pt/WO_2[227], Pt/ZrO_2[228] and Pt/MoO_2 [229] have been used to increase the activity and CO toleranceof the catalysts, based on a bifunctional mechanism oran electronic effect.It has been demonstrated that the metal oxides can be good surface promoters for improving Pt activity towards methanol oxidation due to their special "spillover" effect [230]. First, metal oxides stabilize Pt particle dispersion, being in favour of the increase of active surface per weight of the catalyst. Second, they possess a good capacity for storing and releasing oxygen, which plays an important role in CO_{ads} electro-oxidation. In addition, the low price and the abundance of metal oxides can help reduce the cost of DMFC [231].

TiO_2known for its high catalytic activity and stability in acidicor alkaline solutions has been widely studied for its specialproperties. It has beenreported that Pt [232] or PtRu [233] catalysts supported onTiO_2 exhibited excellent catalytic activity for methanol electro-oxidationbecause of the synergetic interaction between Pt andTiO_2.He *et al* [234] also found that a TiO_2/CNT/Pt electrode by electrodepositing Pt nanaoparticles on CNT-modefied TiO_2 displayed a higher and more stable electrocatalytic activity for methanol oxidation compared with a graphite/CNT/Pt electrode.

The section below describes the outcome of the synthesis of Pt monometallic, binary and ternarycatalysts supported on TiO_2/CNT andbased on the use dry-mix method of OMCVD. These multicomponent catalysts were investigated and compared with commercial Johnson Matthey 40 % Pt/C catalyst. The results then enabled a profile for the catalysts with regards to their synthesis route, characteristics and EC activity.

5.2 Experimental Work

5.2.1 Materials

The chemicals employed to prepare the series of electrocatalysts are shown in Table 5.1.

Table 5.1 Chemicals for preparing catalysts

Chemicals	**Specifications**	**Source**
Multi-wall carbon nanotubes	95 wt.%, 20 -30 OD	Cheap Tubes Inc ©
Titanium acetylacetonate	97%	Sigma-Aldrich
Platinum acetylacetonate	97%	Sigma-Aldrich
Ruthenium acetylacetonate	97%	Sigma-Aldrich
Vanadium acetylacetonate	97%	Sigma-Aldrich
Copper acetylacetonate	97%	Sigma-Aldrich
Iron acetylacetonate	97%	Sigma-Aldrich
HNO_3	55% AR	KIMIX
HCl	32% AR	KIMIX
H_2SO_4	98% AR	KIMIX

5.2.2 Catalyst Synthesis

Nanophase electrocatalysts supported on TiO_2/CNT and synthesized by using the methodologies given in the following subsections are tabulated in Table 5.2. The theoretical molar ratio of TiO_2:Pt is 1:1 in this study as it was described as the optimal molar ratio for TiO_2/Pt by H.Q. Song *et al* [235].

Table 5.2: Summary of prepared PGM/TiO_2/CNT electrocatalysts

catalyst	Metal	Metal Theoretical Loading(wt. %)	Support
A12	Pt	40	TiO_2/CNT
A13	Pt:Ru	20:20	TiO_2/CNT
A14	Pt:Ru:Fe	20:10:10	TiO_2/CNT
A15	Pt:Ru:Cu	20:10:10	TiO_2/CNT
A16	Pt:Ru:V	20:10:10	TiO_2/CNT

5.2.2.1 Synthesis of TiO_2/CNT support

418.12 mg $TiO(acac)_2$ and 500 mg modified Multiwall Carbon Nanotubes (modified procedure specified in Section 4.2.2.2) were weighed separately on an analytical balance, and then $TiO(acac)_2$ and MWCNTs were mixed and ground with a mortar and pestle. Thereafter, the mixed powers were placed into a reactor. The reactor was then evacuated for 30 min to a pressure of 7.7 x 10^{-1} mbar and kept evacuating for another 1 hour with the same pressure at 120 °C. Following the evacuation, the reactor was then put into a tube furnace and the temperature was increased to 400 °C,

at a heating rate of 20 °C/min and kept for another 30 min at 400 °C to form the TiO_2/CNT composite substrate.

5.2.2.2 Synthesis of 40 wt. % Pt /TiO_2/CNT catalyst (A10)

627.00 mg Platinum acetylacetonate[Pt $(acac)_2$)] was weighedon an analytical balance and was then ground with a mortar and pestle nicely with500.00 mgprepared TiO_2/CNTsupport, and the solid mixture was loaded into a reactor tube. The reactor tube was sealed under vacuum and then was firstly evacuated for 1hour to a pressure of 7.7 x 10^{-1} mbar at room temperature. The catalyst was then slowly ramped to 100 °Cat a heating rate of 20 °C/min and kept for another 1 hour to remove traces of water, at which temperature the pressure decreased substantially to 2.8x 10^{-1}mbar. After sublimation, the catalyst was ramped to 400 °C a heating rate of 20 °C/min and held for 30 min to decompose the platinum precursor properly and form catalyst Pt/TiO_2/CNT (A10). The reactor tube was cooled to room temperature, and the sample was removed.

5.2.2.3 Synthesis of 20:20 (w/w) PtRu supported on TiO_2/CNT (A11)

335.00 mg Platinum acetylacetonate[Pt$(acac)_2$)] and 654.78 mgRuthenium acetylacetonate [Ru$(acac)_3$] were well mixed with 500 mg prepared TiO_2/CNT and then the CVD synthesis procedure specified in Section 5.2.2.2 was followed to produce catalyst PtRu/TiO_2/CNT (A11).

5.2.2.4 Synthesis of 20:10:10 (w/w) PtRuFe supported on TiO_2/CNT (A12)

335.00 mg Platinum acetylacetonate[$Pt(acac)_2$)], 327.16 mgRuthenium acetylacetonate [$Ru(acac)_3$] and 524.85 mg Ironacetylacetonate [$Fe(acac)_3$] were physically well mixed with 500 mg TiO_2/CNT support and then the synthesis procedure specified in Section 5.2.2.2 was followed to produce PtRuFe/TiO_2/CNT catalyst (A12).

5.2.2.5 Synthesis of 20:10:10 (w/w) PtRuCu/TiO_2/CNT catalyst (A13)

335.00 mg Platinum acetylacetonate[$Pt(acac)_2$)], 327.16 mgRuthenium acetylacetonate [$Ru(acac)_3$] and 341.87 mg Copper acetylacetonate [$Cu(acac)_2$] were physically well mixed with 500 mg TiO_2/CNT support and then the synthesis procedure specified in Section 5.2.2.2 was followed to produce PtRuCu/TiO_2/CNT catalyst (A13).

5.2.2.6 Synthesis of 20:10:10 (w/w) PtRuV/TiO_2/CNT (A14)

335.00 mg Platinum acetylacetonate[$Pt(acac)_2$)], 327.16 mgRuthenium acetylacetonate [$Ru(acac)_3$] and 567.46 mg Vanadium acetylacetonate [$V(acac)_3$] were physically well mixed with 500 mg TiO_2/CNT support and then the synthesis procedure specified in Section 5.2.2.2 was followed to produce catalyst PtRuV/TiO_2/CNT catalyst (A14).

5.2.3 Characterization Techniques

In this study, various techniques were employed to characterize the electrocatalysts which may include the following methods. The structural configuration of TiO_2/CNT was determined by Fourier Transform Infra red (FTIR). N_2 adsorption/desorption (N_2BET) provided the information of total surface area, pore size distribution andporosity of support. Particle size, particle size distribution,metal surface area, and metal dispersion/agglomeration were established byhigh resolution transmission electron microscopy (HRTEM) and the histograms of particle sizes of electrocatalysts were described from the measurement of 200 Pt particles in each case. X-ray diffractometry (XRD) was used to obtain theinformation on crystal/atomic structure and phase identity and purity. Composition was quantitatively determined by Ion Coupled Plasma (ICP), or qualitatively by using energy dispersive analysis(SEM/EDS).Electrochemical activities of the catalysts were determined using cyclic voltammetry (CV).

5.3 Results and Discussion

5.3.1 Characteristics of TiO_2/CNT support

Titanium dioxide (TiO_2) owns excellent physical and chemical properties and is easily prepared from hydrolysis of titanium organic or inorganic salt. However, TiO_2 has a drawback, the low electrical conductivity, which affects the catalytic activity of Pt. In order to overcome the drawback, deposits of TiO_2 on some porous materials

have been studied [236-237]. Carbon nanotubes have increasingly attracted great interest because of its unique structure and exceptional properties. Recently, the combination of TiO_2 with CNTs as support for PGM catalysts has been studied [238-239]. CNTs can provide a large network for collecting electrons from the oxidation process, thereby assisting efficient current generation [231].

In this chapter, TiO_2 supported on modified CNTs was prepared by a CVD method. The characteristics of the TiO_2/CNT composite support was investigated by ICP, FTIR, BET, TEM and XRD techniques as specified in Section 3.1 and modified TiO_2/CNTs was compared to the CNTs. The results of the characteristics of the TiO_2/CNT composites using each specific technique are presented and discussed below.

5.3.1.1 Elemental composition of TiO_2/CNT and CNTs

ICP as specified in Section 3.1.4 was used to investigate the elemental compositions of TiO_2/CNT. The results are listed in Table 5.3.

Table 5.3 Composition of TiO_2/CNT and CNTs

Element	***Initial theoretical loading of TiO_2 (wt. %)**	**Ti (wt. %) loading**
TiO_2/CNT	20	16.3

* Refer to APPENDIX A for initial theoretical TiO_2 content calculation

The ICP results showed that TiO_2/CNT was composed of 16.3 wt. % Ti. The analysis indicates that the CVD method was successfully used to reduce Ti on the CNTs. These functional groups may react with Pt^{4+} and form the nucleation sites. The nucleation sites could enhance the process of Pt deposition on the carbon materials and could promote the stabilization of Pt particles [133].

5.3.1.2 IR spectra analysis of the TiO_2/CNT composites

The structures of TiO_2/CNT and CNTs were investigated by FTIR spectra as specified in Secion 3.1.6 and shown in Figure 5.1.

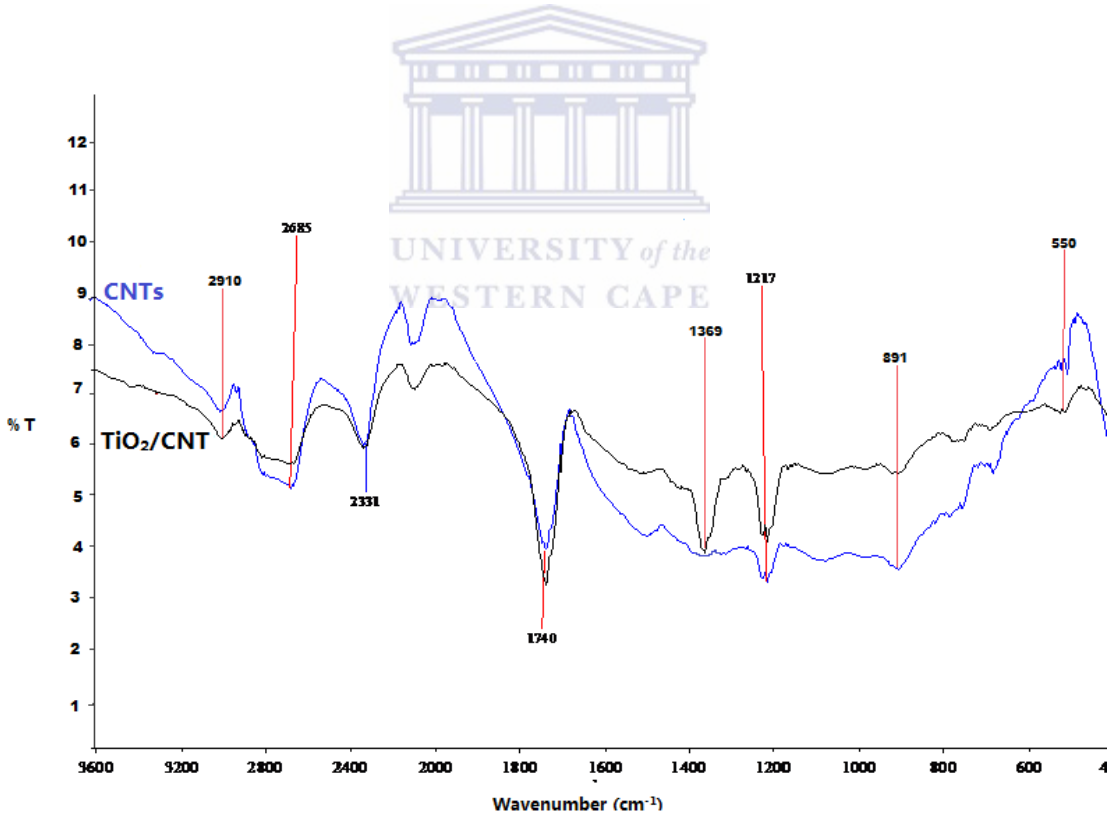

Figure 5.1 FTIR spectra for modified CNTs and TiO_2/CNT

It can be seen from Figure 5.1 that both curves show various types of functional group as CNTs have been oxidized by a strong acid (Section 4.3.2.2). The bands at 2910 and 891 cm^{-1} were assigned to the C-H stretching vibration. The signature of C=O functional groups appears at about 1740 cm^{-1} and the band assigned to –OH functional groups is evident at about 2331 cm^{-1}, respectively. The band in the 1217 cm^{-1} region demonstrates the presence of C-O groups. These functional groups can increase the number of active sites on the CNTs surface [240] and thus are beneficial for the coating of TiO_2 on the CNTs [241].

FTIR spectra of TiO_2/CNT composite support shows the two obvious peaks compare of TiO_2 with CNTs by itself. The band near 550 cm^{-1} corresponded to Ti-O [242] and the C-H band centered at 1369 cm^{-1} might come from intermolecular condensation of TiO_2, respectively [243]. Thus, it can be concluded that TiO_2 was formed on the surface of CNTs by the CVD process.

5.3.1.3 Surface area and pore structure for TiO_2/CNT

The surface area and pore volume of the TiO_2/CNT composite were investigated by N_2 BET as described in Section 3.1.5 and compared to the CNTs by itself. Figure 5.2 shows the N_2 adsorption isotherms for the TiO_2/CNT and CNTs.

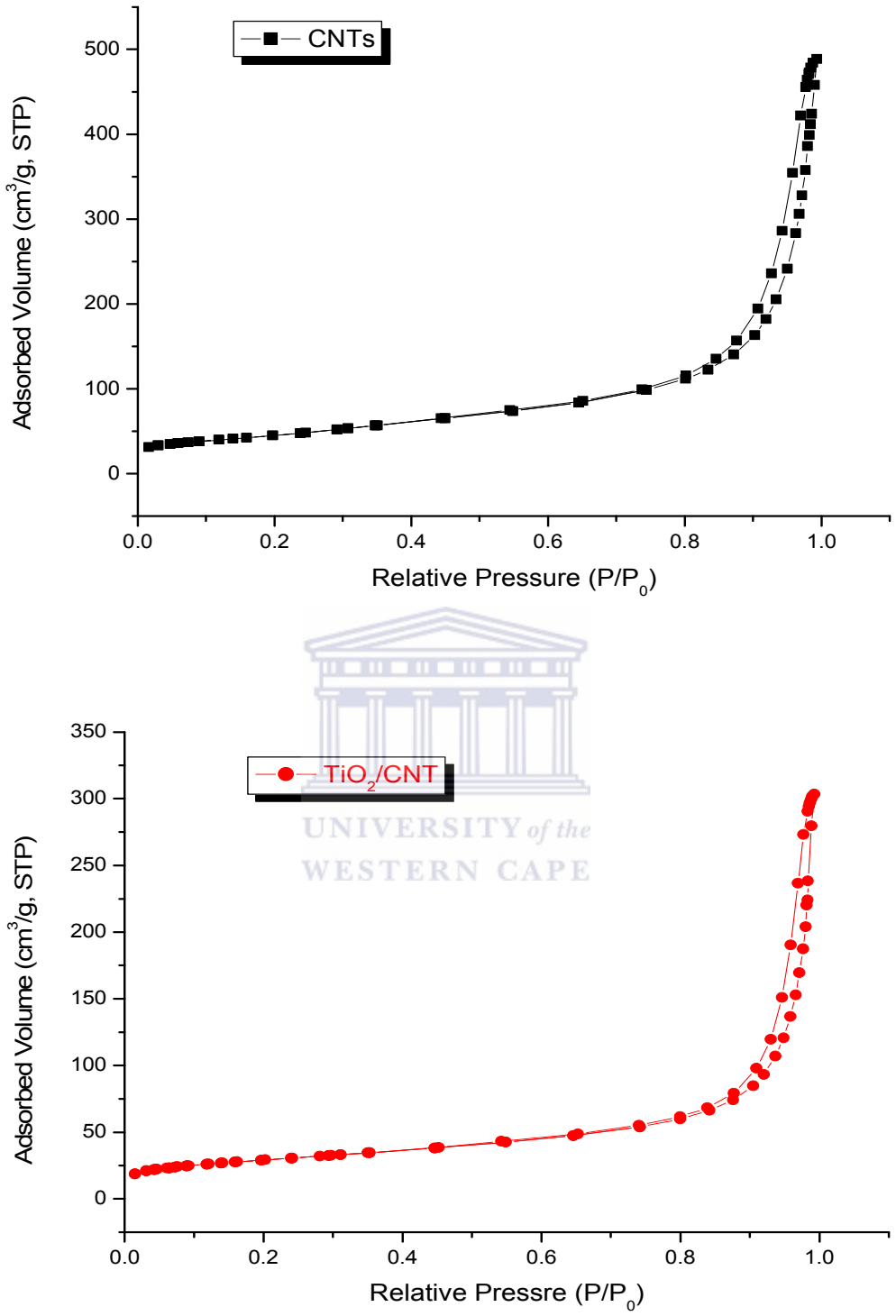

Figure 5.2: Nitrogen adsorption isotherms obtained for the CNTs and TiO_2/CNT

Figure 5.2 shows that at very low relative pressures, both curves of CNTs and TiO_2/CNT exhibit a very small hysteresis loop, indicating the presence of small

amounts of micropores (type I). At high relative pressures, the monolayer is filled and the isotherm reaches a plateau, which indicates the presence of mesoporous (type IV). Both isotherms were type II classified according to IUPAC, which is normally given by a nonporous or macroporous adsorbent on which unrestricted monolayer-multilayer adsorption can occur [244]. It also can be seen that the curve of CNTs shows the total adsorption is more than that of TiO_2/CNT, which suggests that TiO_2 is introduced into CNTs [243].

The N_2BET analysis also showed that the surface area of CNTs and TiO_2/CNT are 157 and 104 cm^2/g, respectively. It can be observed that introducing TiO_2 into CNTs decreased the surface area. This may indicate that the TiO_2 dispersed on the surface and occluded the pores of CNTs [245].

5.3.1.4 Structural study of TiO_2/CNT

The XRD patterns of the TiO_2/CNT and CNTs are shown in Figure 5.3, a pattern of the anatase form of TiO_2 is presented as comparison in Figure 5.4.

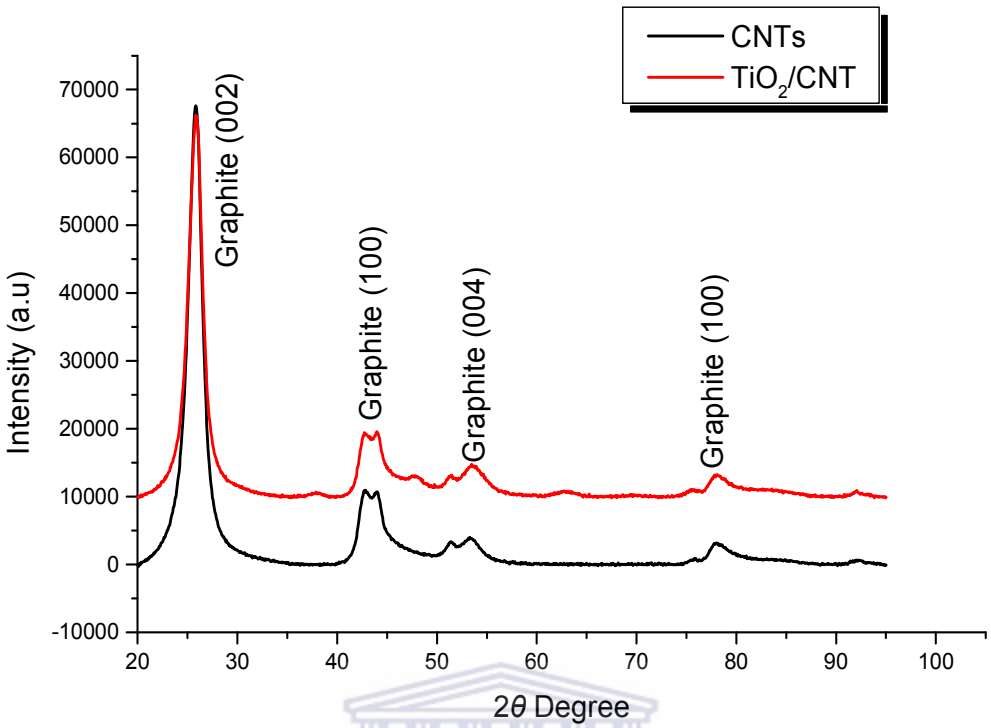

Figure 5.3 XRD patterns of CNTs and TiO_2/CNT

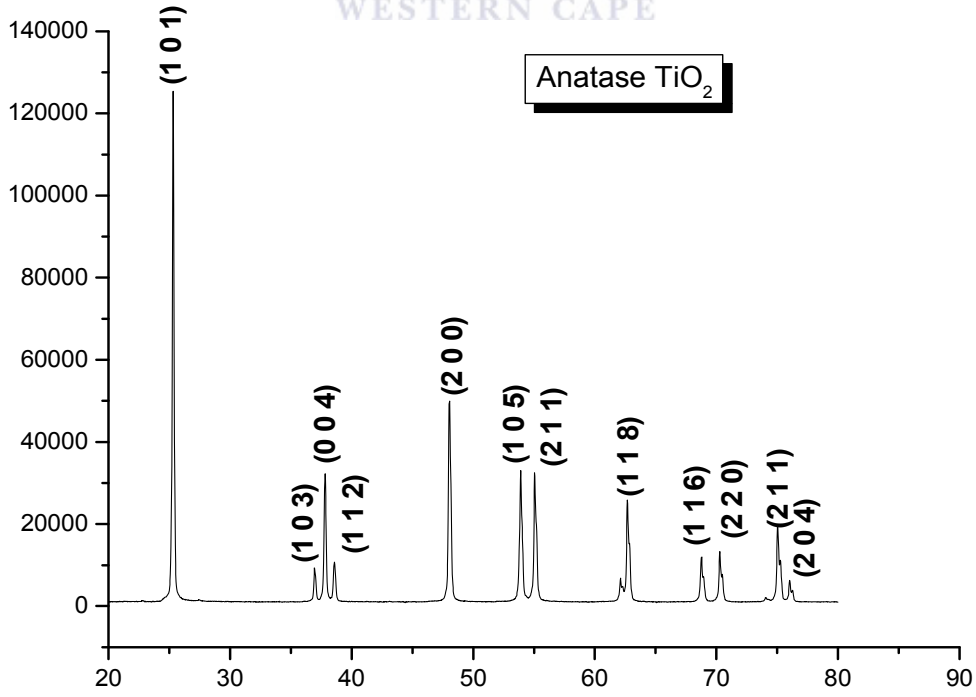

Figure 5.4: XRD pattern of anatase TiO_2

It can be seen from Figure 5.3 that the pattern for CNTs exhibited four characteristic diffraction peaks, which were around 26.8, 42.4, 53.7 and 78.4° 2θ degrees. These peaks can be attributed to the hexagonal graphite structures (220), (100), (004) and (110) of the multi-wall CNT. In Figure 5.4, XRD patterns of anatase TiO_2 exhibited strong diffraction peaks at 25, 38, 48, 54 and 55° 2θ degrees, which indicating TiO_2 in the anatase phase. All peaks of anatase TiO_2 are in good agreement with the standard spectrum (JCPDS no.: 84 – 1286) [238]. Comparing the XRD patterns of TiO_2/CNT and CNTs, it is observed that there was no any shift in the diffraction peaks of CNTs indicating that the addition of TiO_2 had no effect on the crystalline lattice of CNTs. It wasalso be found that there is no diffraction peak of TiO_2 in the XRD patterns of TiO_2/CNT, which means that the prepared TiO_2 is amorphous [235]. This conclusion can be confirmed from high-resolution electro-microscopy (HRTEM) in further part of this study.

5.3.1.5 Morphological analysis of TiO_2/CNT

The morphology of TiO_2/CNT was studied by SEM and HRTEM as specified in Sections 3.1.3 and 3.1.1. The images are shown in Figure 5.5.

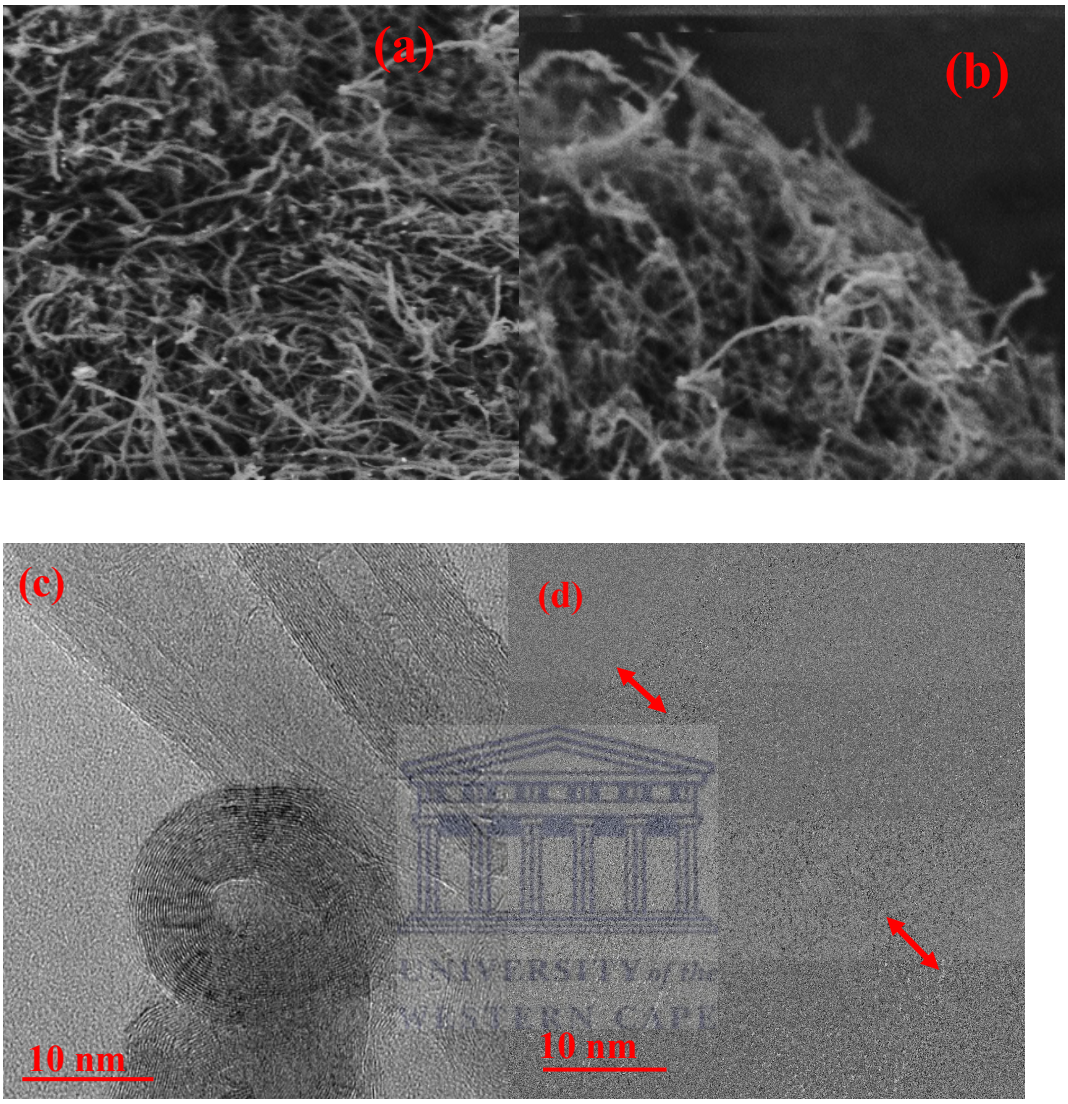

Figure 5.5: SEM images of (a) CNTs, (b) TiO_2/CNT and HRTEM imagesof (c) CNT, (d) TiO_2/CNT

It can be seen from Figure 5.5 (a) that before $TiO_2$was deposited on CNTs, CNTs were very clean and intertwined with each other while in Figure 5.5 (b) the CNTs were observed to have an external coating and some agglomerations were found as TiO_2 was coated on CNTs. The HRTEM image of Figure 5.5 (d) confirms that there is a layer of amorphous TiO_2 on CNTs which can be clearly seen and the thickness of the TiO_2 is about 3-4 nm [160] while Figure 5.5 (c) shows the clean surface of CNTs before TiO_2coating.

From XRD and HRTEM analysis, it appears that the amorphous TiO_2 layer on CNTs may play an important role in synergetic interaction between platinum group metal and TiO_2/CNT support.

5.3.2Physico-chemical characterizations of PGM/TiO_2/CNT electrocatalysts

The electrocatalysts of the platinum group metals supported on TiO_2/CNT were synthesized and details of their characteristics were investigated in this chapter. The home-made 40 wt. % Pt/CNT and 20%Pt20%Ru/CNT catalysts described in Section 4.3.2 and 4.3.3 were used as representative of the Pt supported on CNTs for comparison with the TiO_2 containing series as these catalysts were prepared by the same method except for the difference in the supports.

The results of characterization by ICP, EDS, XRD, TEM and CV are presented in the next section.

5.3.2.1 Elemental composition

ICP as specified in Section 3.1.4 was performed to determine the Ti and metal levels as major elements for catalysts. The results of the elemental composition of the PGM/TiO_2/CNT composites are given in Table 5.4.

Table 5.4: Pt loading of different catalysts obtained by ICP

Catalyst	Element (wt. %)					
	Ti	Pt	Ru	Fe	Cu	V
A12: Pt/TiO_2/CNT	16.3	39.2	-	-	-	-
A13: PtRu/TiO_2/CNT	16.3	19.5	19.2	-	-	-
A14: PtRuFe/TiO_2/CNT	16.2	19.4	9.6	9.5	-	-
A15: PtRuCu/TiO_2/CNT	16.2	19.7	9.3	-	9.2	-
A16: PtRuV/TiO_2/CNT	16.3	19.7	9.4	-	-	9.5

It can be seen from Table 5.4 that ICP analyses results correlate relatively well with initial theoretical elemental loading of the PGM/TiO_2/CNT catalysts. These results showed that the CVD method could be usedto prepare a relatively well-defined atomic ratio of electrocatalysts.

5.3.2.2 Particle size and particle distribution

HRTEM analysis was conducted on the catalysts to investigate the morphology, metal particle size and particle size distribution, using the procedure given in Section 3.1.1. The TEM images for well-dispersed catalysts Pt/TiO_2/CNT, PtRu/TiO_2/CNT, PtRuFe/TiO_2/CNT, PtRuCu/TiO_2/CNT and PtRuV/TiO_2/CNT are shown in Figure 5.6.

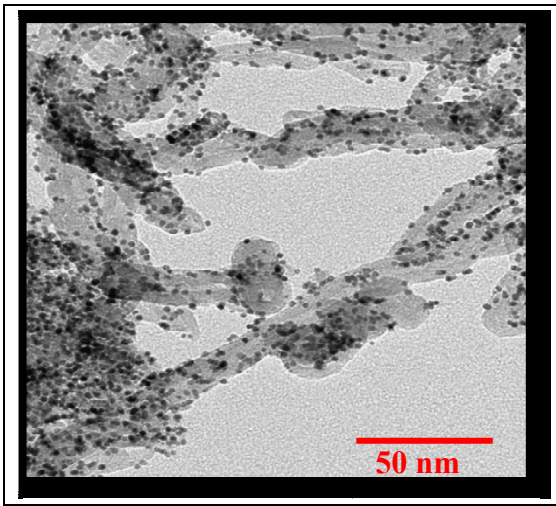

A12: Pt/TiO_2/CNT (a)

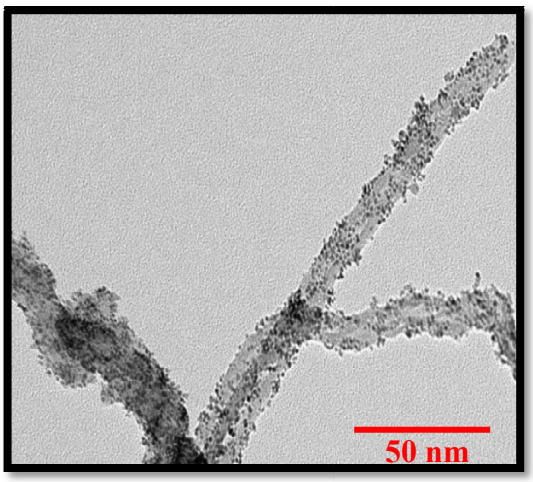

A13: PtRu/TiO_2/CNT (b)

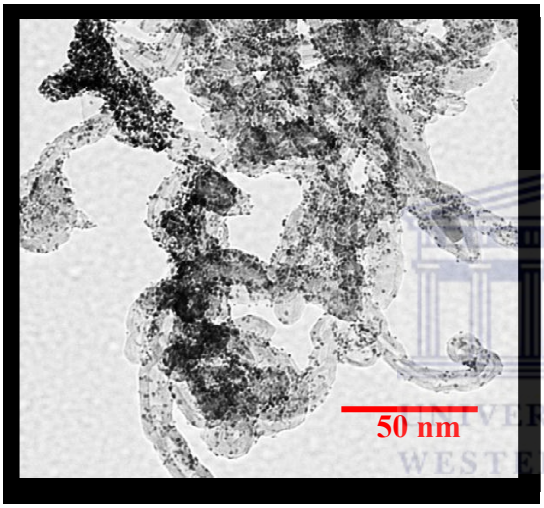

A14: PtRuFe/TiO_2/CNT (c)

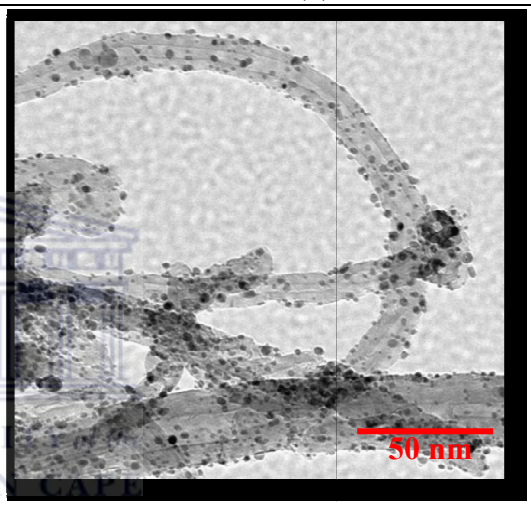

A15: PtRuCu/TiO_2/CNT (d)

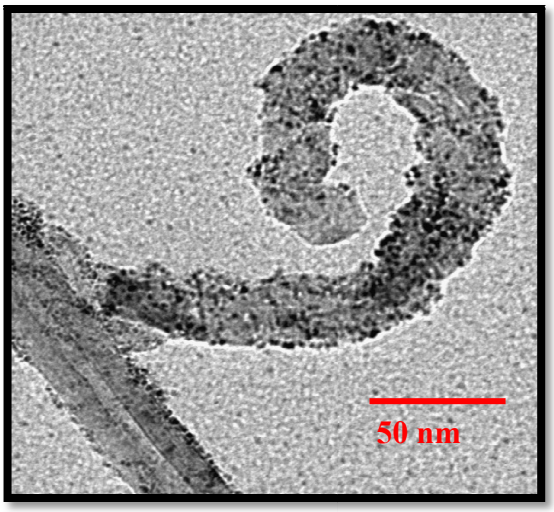

A16: PtRuV/TiO_2/CNT (e)

Figure 5.6: HRTEM graphs of (a) Pt/TiO_2/CNT, (b) PtRu/TiO_2/CNT, (c) PtRuFe/TiO_2/CNT, (d) PtRuCu/TiO_2/CNT and (e) PtRuV/TiO_2/CNT

As can be seen from Figure 5.6, all the catalysts were dispersed uniformly and without agglomeration upon TiO_2/CNT support. When PtRu/TiO_2/CNT (Figure 5.6 (b)) and PtRuM/TiO_2/CNT (M = Fe, Cu and V) (Figure 5.6 (c), (d) and (e)) catalysts are compared with the Pt/TiO_2/CNT catalyst (Figure 5.6 (a)), smaller particles were obtained and well-separated nanoparticles were observed by the combination of the additional metals with Pt. In addition, catalysts PtRuFe/TiO_2/CNT and PtRuV/TiO_2/CNT showed smaller particle sizes and better nanoparticle dispersion than catalyst PtRu/TiO_2/CNT while in the case of PtRuCu/TiO_2/CNT bigger particles were obtained. This result is the same as that observed for the series of PGM metals supported only on CNTs. The average particle sizes obtained from TEM are 2.63, 1.81, 1.52, 1.66, and 1.39 nm for Pt/TiO_2/CNT, PtRu/TiO_2/CNT, PtRuFe/TiO_2/CNT, PtRuCu/TiO_2/CNT and PtRuV/TiO_2/CNT, respectively.The particles size of PGM/TiO_2/CNT and PGM/CNTs catalysts obtained by TEM were listed in Table 5.5 for comparison.

The histograms were discribed from the analysis of 200 particles, which were measured by hand on the HRTEM images in each case.

Table 5.5: Particle size for PGM/TiO_2/CNT and PGM/CNT catalysts

Sample	Particle size of PGM/TiO_2/CNT(nm)		Particle size of PGM/CNT (nm)		Sample
	By TEM	By XRD	By TEM	By XRD	
A12: Pt/TiO_2/CNT	2.63	2.95	2.77	2.89	**A6: Pt/CNT**
A13: PtRu/TiO_2/CNT	1.66	1.40	1.75	1.57	**A8: PtRu/CNT**
A14: PtRuFe/TiO_2/CNT	1.52	1.31	1.66	1.42	**A9: PtRuFe/CNT**
A15: PtRuCu/TiO_2/CNT	1.98	1.98	2.31	2.12	**A10: PtRuCu/CNT**
A16: PtRuV/TiO_2/CNT	1.39	1.30	1.58	1.30	**A11: PtRuV/CNT**

It can be easily seen from Table 5.5 that the metal catalysts supported on TiO_2/CNT generally formed smaller particle sizes than in the case of catalysts that were supported only on CNTs. The smaller particle size leads to a bigger surface area and may produce better electrocatalytic activity of the catalyst. From the results, it seems that addition of TiO_2 showed as a good surface promoterfor the PGM catalysts. This will be further confirmed by electrochemical-activity analysis (see Section 5.3.2.4).

The particles size distribution histograms of the catalysts are presented in Figure 5.7.

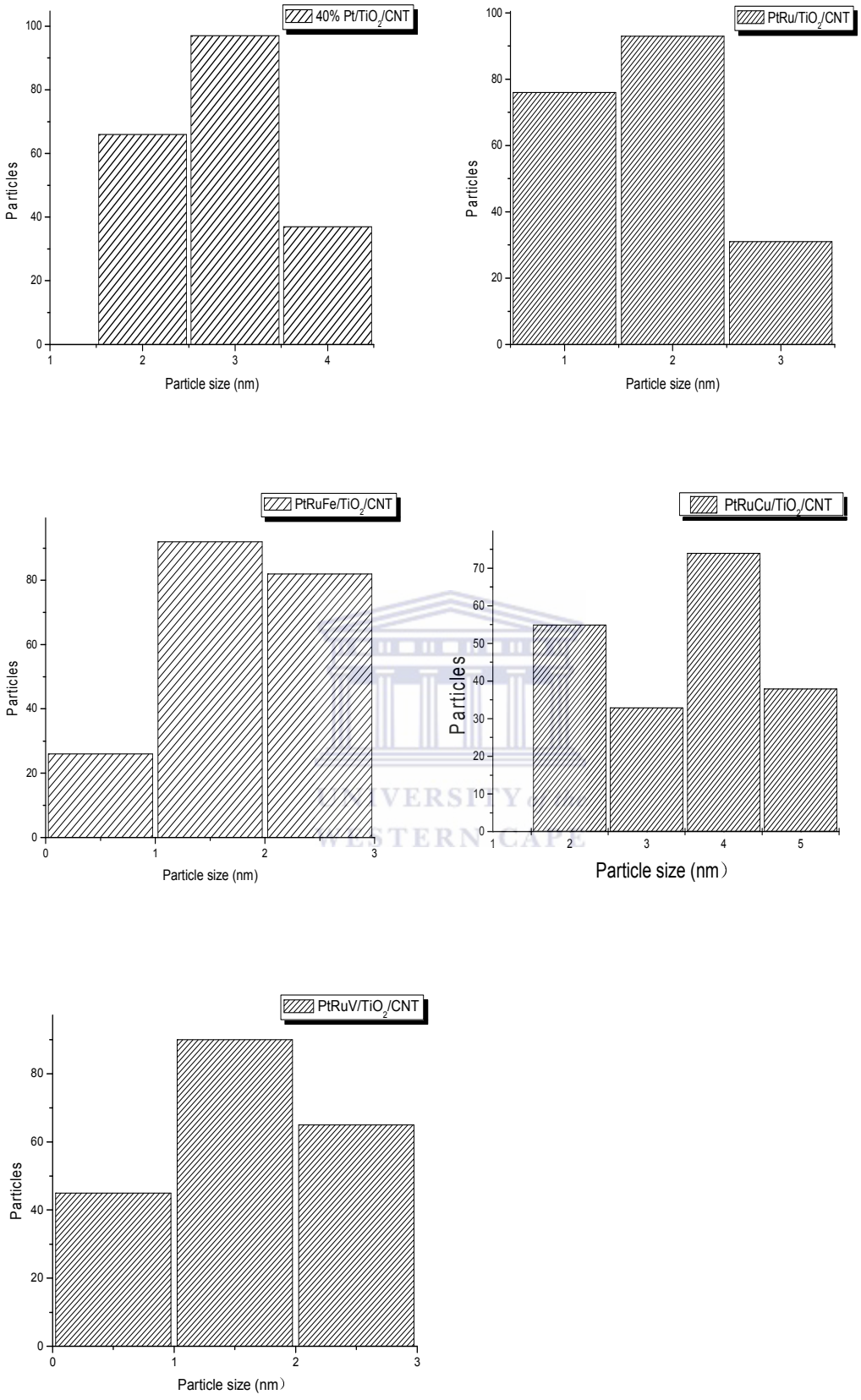

Figure 5.7: Histograms of PGM/TiO_2/CNT catalysts

From the histograms it is apparent that the distribution range of Pt/TiO_2/CNT and PtRu/TiO_2/CNT are 1.5 to 4.5 and 0.5 to 3.5 nm, respectively. PtRuCu/TiO_2/CNT catalyst had the widest particle size distribution – from 1.5 to 5.5 nm while the particle sizes of the tri-metallic systems comprised of PtRuFe/TiO_2/CNT and PtRuV/TiO_2/CNT were relatively uniform, with the particle size range from 0 to 3 nm. The distribution ranges of PGM supported on TiO_2/CNT are similar to the PGM supported on CNTs catalysts (Figure 4.14).

In terms of the HRTEM investigation, it can be seen thatthe additional TiO_2 during preparation did not cause a negative results of the catalysts. This may be because of the synergetic interaction between PGM metals andTiO_2 as has beenreported by K.W. Park et al. [232-233]. Further studies will be carried out in the section of cyclic voltammetry test.

5.3.2.3 Particle size and crystallinity

The crystallinity and particle size of PGM/TiO_2/CNT electrocatalysts were also determined using XRD as described in Section 3.1.2. The corresponding patterns of catalysts are shown in Figure 5.8 – 5.12 and the JM commercial catalysts of Pt/C and PtRu/C and home-made PGM/CNT catalysts were also presented for comparison.

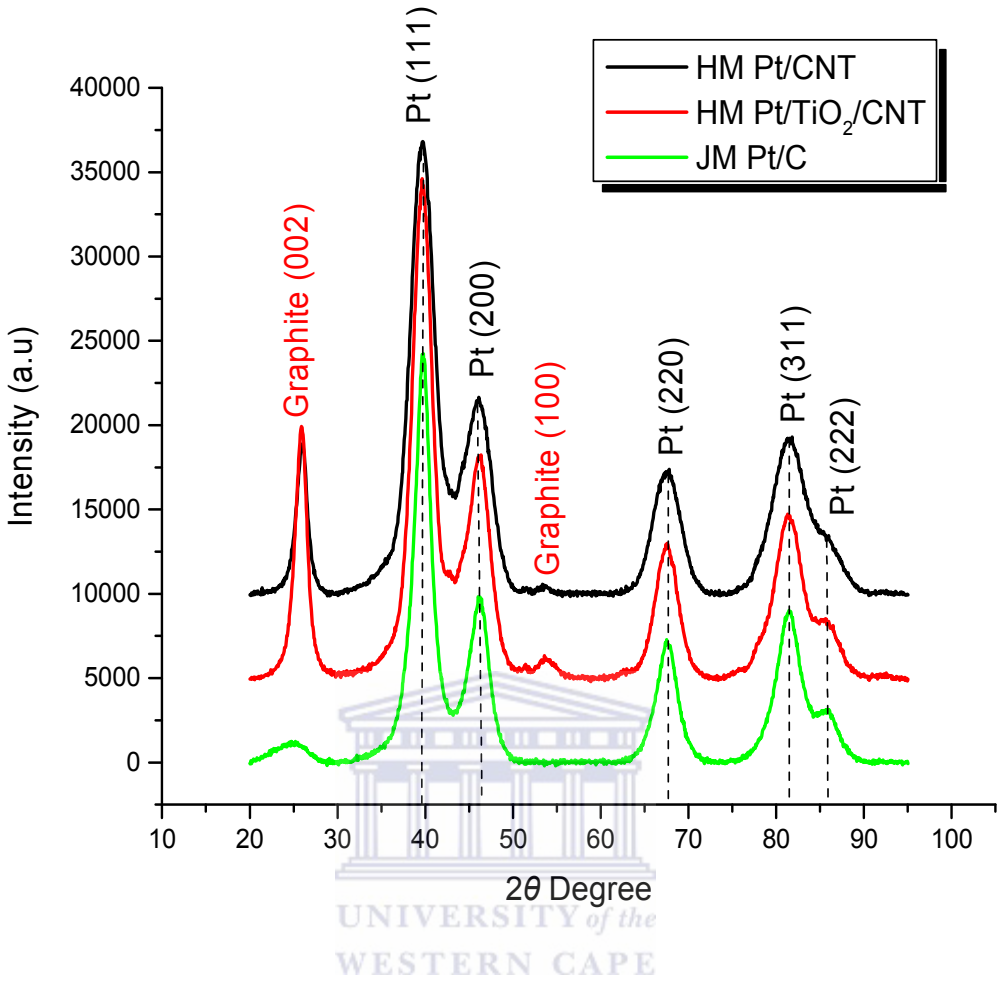

Figure 5.8: X-Ray diffraction patterns of JM Pt/C, HM Pt/CNT and Pt/TiO_2/CNT

Figure 5.8 shows the characteristic diffraction peaks at ca. 2θ = 26° indicateing the crystalline nature of graphite, which is attributed here to the graphitic structure of the CNTs. Comparing the three samples, it can be seen that Pt diffraction peaks are evidentin the Pt/TiO_2/CNT catalyst, while no diffraction peak for TiO_2 was observed [238]. This indicates that the TiO_2 phase in the Pt/TiO_2/CNT catalyst was amorphous [235].The characteristic peaks of face centered cubic crystalline platinum at about 39, 45, 68, 82° 2θ corresponded to the Pt (111), (200), (220) and (311) planes, respectively. There was no shift in any of the diffraction peaks of

platinum in Pt/TiO_2/CNT. This means that the addition of $TiO_2$to the substrate had no effect on the crystalline lattice of platinum. As mentioned previously the characteristic diffraction peaks of the face centered cubic (*fcc*) Pt demonstrates that successful reduction of the Pt precursor to metallic form has been achieved during the conditions of synthesis and the in-house Pt/TiO_2/CNT catalyst is Pt (*fcc*) crystal structure.By use of the Scherrer equation (Equation [2-1]), it was confirmed that the Pt/TiO_2/CNT had a particle size 2.95 nm, which is in agreement with the result obtained from TEM observation (Section 5.4.2.2).

Figure 5.9 shows the XRD patterns for the catalysts, PtRu/TiO_2/CNT, PtRu/CNT and JM commercial PtRu/C.

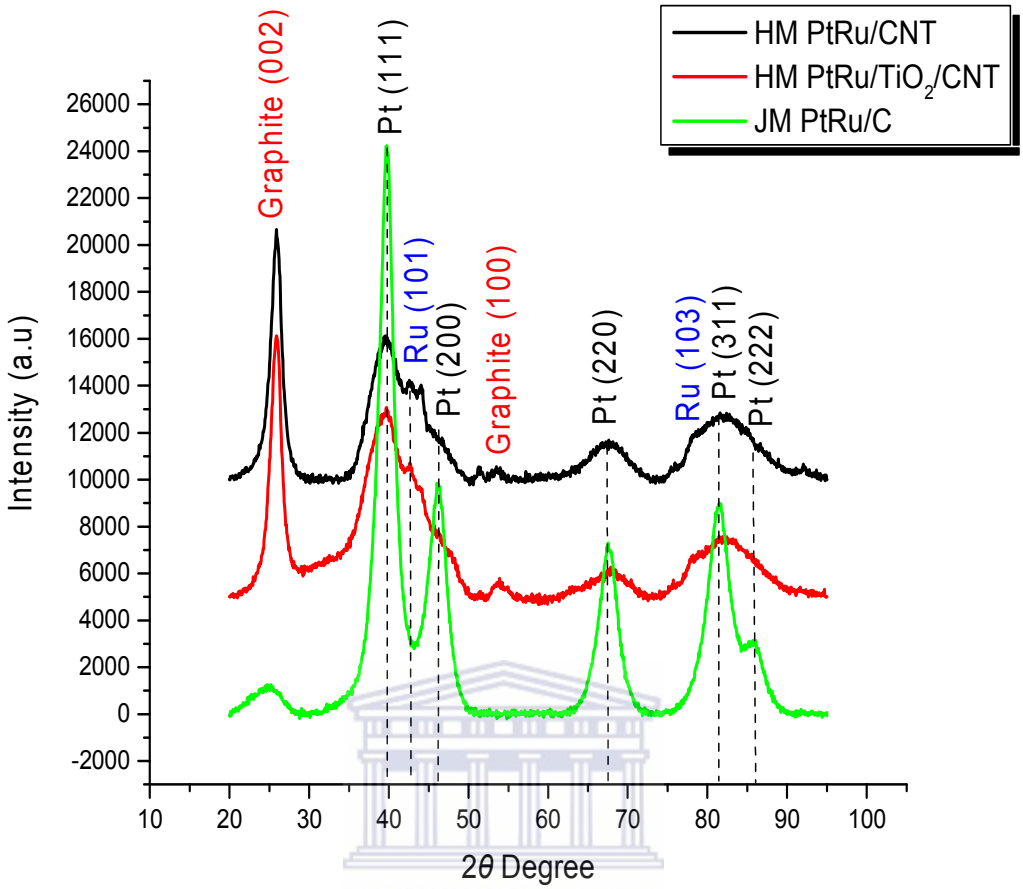

Figure 5.9: X-Ray diffraction patterns of JM PtRu/C, home-made PtRu/CNT and PtRu/TiO_2/CNT catalysts

In Figure 5.9it can be seen that the XRD pattern of PtRu/TiO_2/CNT is the same as that of PtRu/CNT. There are no obvious peaks that could be attributed to TiO_2 [238].This indicates that the TiO_2 phase in the PtRu/TiO_2/CNT catalyst was amorphous [235]. It also can be seen that there was no shift in any of the diffraction peaks of Pt-Ru in PtRu/TiO_2/CNT when compared with that commercial JM PtRu/C catalyst. This means that the addition of TiO_2 had no effect on the crystalline lattice of Pt-Ru [235]and also indicatesPtRu/TiO_2/CNT catalyst had the same face-centered structure as JM PtRu/C. However, in case of in-house PtRu/TiO_2/CNT small

diffraction peaks were observed at 43.5° (101) and 78.5° (103), those were assigned to the hcp structure of Ru while there is no diffraction peaks corresponding to the characteristic hexago-nal-closest-packing structure of Ru in the case of commercial PtRu/C catalyst.This results indicate that the commercial JM PtRu/C catalyst obtained complete alloying of Ru into the face-centered cubic lattice of Pt [217] while there may exist the separate phases of Pt and Ru [214] of home-made PtRu/TiO_2/CNT catalyst. It also can be seen that for the PtRu/TiO_2/CNT catalyst, the Pt (222) peak is not easy to identify while compared with commercial PtRu/C catalyst. It is because of the very small platinum particle sizes in the catalyst PtRu/TiO_2/CNT that the peak of the facet is broadened significantly [217].By using the Scherrer equation (Equation [2-1]), the average particle size of PtRu/TiO_2/CNT catalyst was 1.40 nm.

Figure 5.10 shows the XRD patterns for the catalysts PtRuFe/TiO_2/CNT andPtRuFe/CNT.

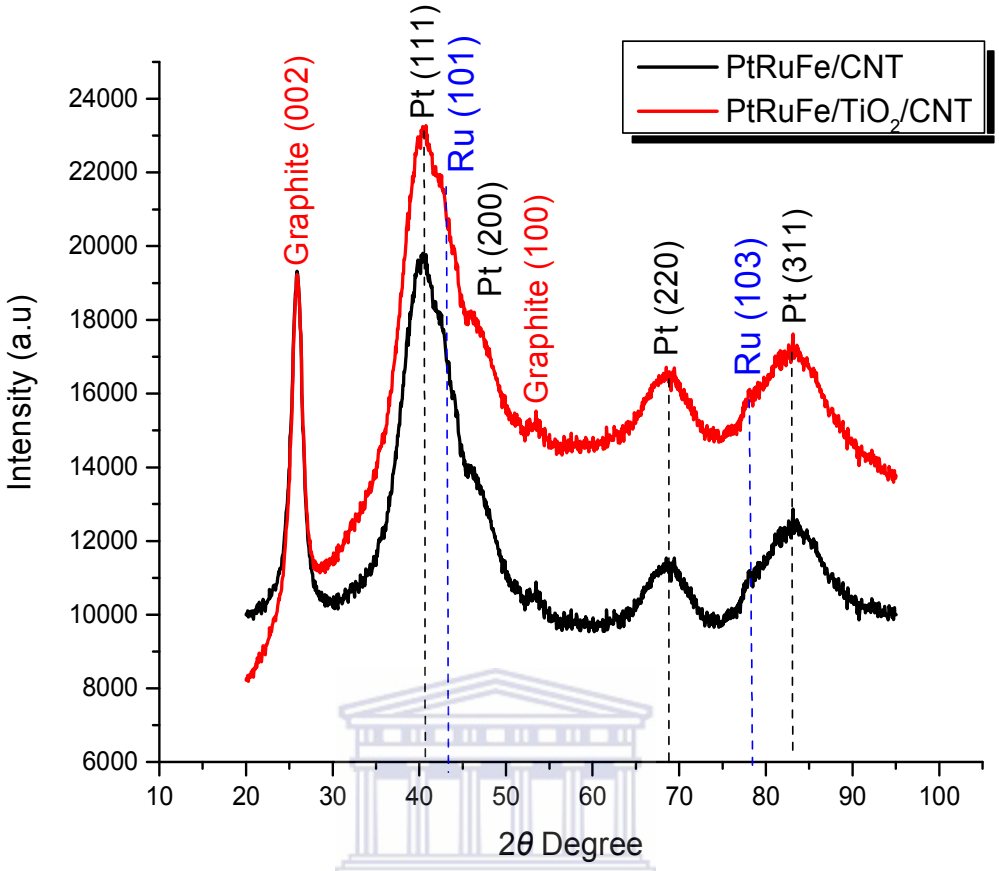

Figure 5.10: X-Ray diffraction patterns of PtRuFe/TiO_2/CNT and PtRuFe/CNT

Comparing the two samples in Figure 5.10, it can be seen that PtRuFe/TiO_2/CNT and PtRuFe/CNT catalysts showed the same structured pattern. Obvious graphite and Pt diffraction peaks can be observed in both catalysts and Ru peaks are seen as poorly defined shoulders on Pt peak (111) and Pt peak (311), however no Fe peaks are observed, while no diffraction peak of the TiO_2phase was visible [238]. This indicates that the PtRuFe/TiO_2/CNT catalyst obtained complete alloying of Fe into the face-centered cubic lattice of PtRu [217] and the deposited TiO_2phase on PtRuFe/CNT catalyst was amorphous. The characteristic peaks for Pt (111) and Pt (220) are observed at 2θ values, 41.0° and 69.5°, respectively. There was no shift

observed in any of the diffraction peaks of the Pt-Ru-Fe metals in PtRuFe/TiO_2/CNT when compared with that PtRuFe/CNT catalyst. This means that the addition of $TiO_2$to the substrate had no effect on the crystalline lattice of Pt-Ru-Fe [160]. By use of the Scherrer equation (see Equation [2-1]), it was confirmed that the particle size of PtRuFe/TiO_2/CNT is 1.31 nm. This result is similar to that of the TEM result (Section 5.4.2.2). It also can be seen that for the PtRuFe/TiO_2/CNT catalyst, the Pt (222) peak is not identified. It is because of the very small platinum particle sizes in the catalyst PtRuFe/TiO_2/CNT that the peak of the facet is broadened significantly [217].

Figure 5.11 shows the XRD pattern forPtRuCu/TiO_2/CNT and PtRuCu/CNT.

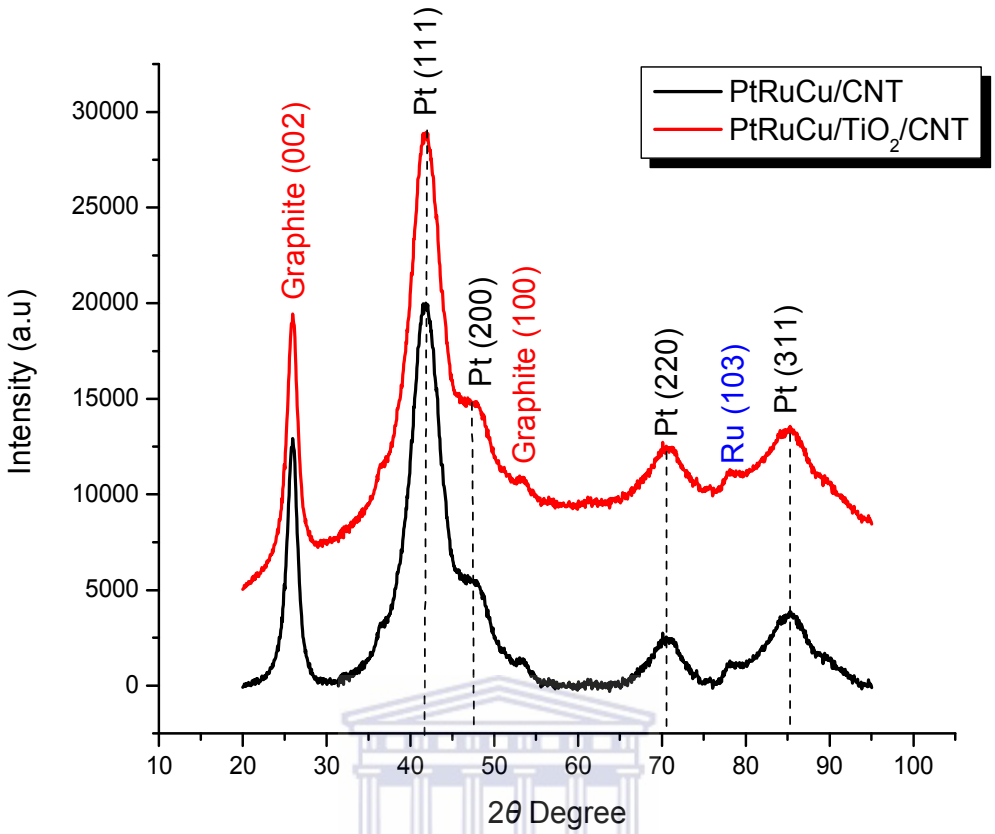

Figure 5.11: X-Ray diffraction patterns of PtRuCu/TiO_2/CNT and PtRuCu/CNT.

It can be seen in Figure 5.11that Cu or Cu oxide diffraction peaks were no visible in either the PtRuCu/TiO_2/CNT or the PtRuCu/CNT catalysts, indicating that alloying was relatively complete [217]. Nevertheless, the diffraction peak of Ru (103) is seen in both cases in the diffractogram. This suggests that separate phases of Pt and Ru may exist in both catalysts [214]. There are no obvious peaks attributed to TiO_2 in catalyst PtRuCu/TiO_2/CNT.This indicates that PtRuCu/TiO_2/CNT catalyst was amorphous [235]. It also can be seen that there was no shift in any of the diffraction peaks in PtRuCu/TiO_2/CNT when compared with that PtRu/CNT catalyst. This means that the addition of TiO_2 had no effect on the crystalline lattice of the catalyst

PtRuCu/TiO_2/CNT [235]. It also can be seen that for the PtRuCu/TiO_2/CNT catalyst, the Pt (222) peak is not identified. It is because of the very small platinum particle sizes in the catalyst PtRuCu/TiO_2/CNT that the peak of the facet is broadened significantly [217]. By use of the Scherrer equation (see Equation [2-1]), it was confirmed that the particle size of PtRuCu/CNT is 1.98 nm. This result corresponded to the TEM result (Section 5.4.2.2).

The XRD patterns for the catalysts PtRuV/TiO_2/CNT and PtRuV/CNT is shown in Figure 5.12.

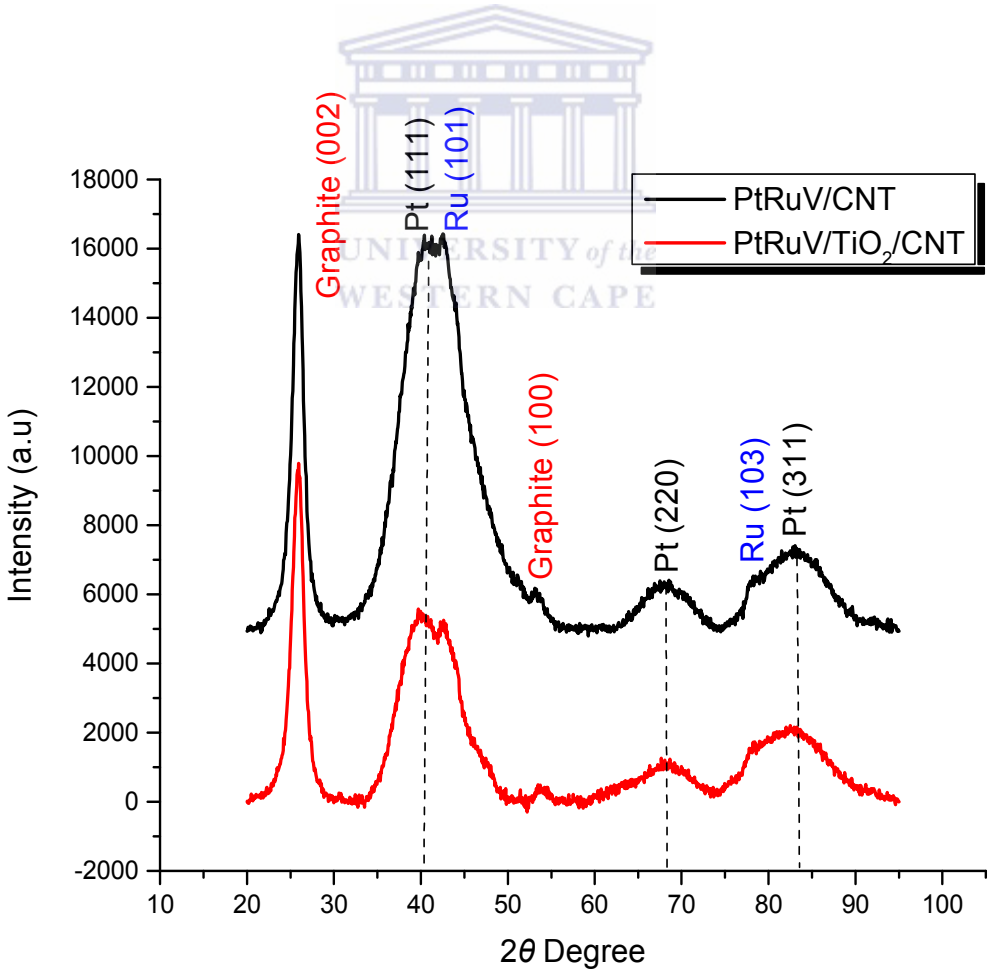

Figure 5.11: X-Ray diffraction patterns of PtRuV/TiO_2/CNT and PtRuV/CNT

Figure 5.11 shows that the V or V oxide diffraction peaks of tri-metallic PtRuV/CNTand PtRuV/TiO_2/CNT are not observed, which indicates that alloying was relatively complete [217]. Nevertheless, the diffraction peaks of Ru (101) and (103) are seen in the diffraction gram. These results indicate thatseparate phases may exist of Pt and Ru in the case of both catalysts [214]. Comparing the two samples, it can be seen that PtRuV/TiO_2/CNT and PtRuV/CNT catalysts showed the same structural pattern. Obvious Pt diffraction peaks can be observed in both catalysts, while no diffraction peak of TiO_2 was seen. This indicates that the depositeed TiO_2 on PtRuV/CNT catalyst was amorphous [235]. There was no shift in any of the diffraction peaks of Pt-Ru-V in PtRuV/TiO_2/CNT when compared with that of the PtRuV/CNT catalyst. This means that the addition of $TiO_2$to the substrate has no effect on the crystalline lattice of the catalyst [235]. It also can be seen that for the PtRuV/TiO_2/CNT catalyst, the Pt (222) peak is not identified. It is because of the very small platinum particle sizes in the catalyst PtRuV/TiO_2/CNT that the peak of the facet is broadened significantly [217]. By use of the Scherrer equation (Equation [2-1]), it was confirmed that the particle size of PtRuV/CNT is 1.30 nm. This result corresponded to the TEM result (Section 5.4.2.2).

5.3.2.4 Electrochemical activity of catalysts

The electrochemical (EC) activityand active surface area of the catalysts were evaluated by cyclic voltammetric (CV) as described in Section 3.2. 0.5M H_2SO_4 was used as electrolyte and followed by the addition of 0.5 M methanol which undergoes

oxidation on the platinum surface which was specified in Section 3.2. The measured potential range was from -0.2 to 1.0V (vs. Ag/AgCl) at a sweep rate of 50mV/s.

The cyclic voltammograms graphs for the JM commercial Pt/C catalyst and home-made PGM/TiO_2/CNT catalysts are presented in Figure 5.13.

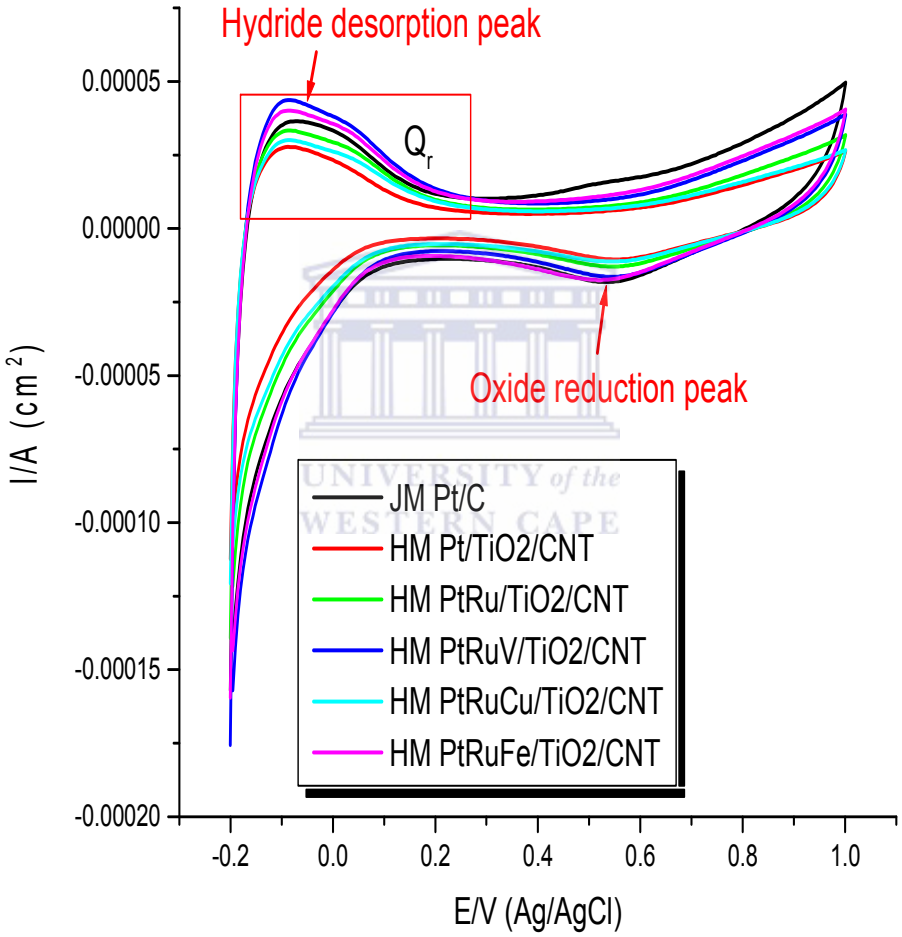

Figure 5.13: Cyclic voltammograms of commercial Pt/C and home-made PGM/TiO_2/CNT catalysts

It can be seen from Figure 5.13 that all catalysts showed the Pt-Hydride desorption peak around potential -0.21 to 0.10 V and the Pt-Oxide reduction peak from potential 0.30 to 0.80 V.

Table 5.6 summarize the charges $Q_r$and electrochemical active surface area of the catalysts.

Table 5.6: Electrochemical-active surface area parameters of electrocatalysts

Sample	**[metal loading] (mg/cm^2)**	**Q_r (µC)**	**S_e (m^2/g)**
JM Pt/C	0.0042	168	190
JM Pt Ru/C	0.0058	194	159
A12: $Pt/TiO_2/CNT$	0.0034	160	224
A13: $PtRu/TiO_2/CNT$	0.0034	165	231
A14: $PtRuFe/TiO_2CNT$	0.0032	172	255
A15: $PtRuCu/TiO_2/CNT$	0.0033	162	233
A16: $PtRuV/TiO_2CNT$	0.0032	175	260

[Metal loading]: consumed wt. % metal loading for the CV test from the working electrode of each catalyst (see Section 3.2)

The integrated peak areas of the catalysts, which are based on the area of hydrogen desorption peak (Q_r), were well defined by the Autolab software, and the electrochemical-active surface area were calculated by the equation [2-4], which was described in Section 2.7.5.

It can be seen from Table 5.6 that all the PGM supported on TiO_2/CNT catalysts showed significantly larger chemical-active surface areas (S_e) than that of the commercial JM Pt/C catalyst. Comparing between metal types, the bi-metallic catalyst showed a larger chemical active surface area than that of mono-catalyst, which were 231 and 224m^2/g, respectively, and the tri-metallic catalysts displayed even better results when compared with the bi-catalyst. The catalyst PtRuV/TiO_2/CNT showed the highest electrochemically active surface area (260 m^2/g**)** compared to the other catalysts, as it contained the smallest metal particle size (1.39 nm). This investigation is consistent with the conclusion in Chapter 4 that the additional metals incorporated with Pt can reduce the particle size and increase the active surface area of the catalysts. The interaction of the second or third metal can cause a positive enhancement of catalytic activity of the catalysts.

It isgenerally recognized that the active surface coverageS_e is an important indication in determiningthe electrochemical activity of a catalyst. The higher the surfacecoverage, the greater the electrochemical activity that can beobtained [216].

Methanol oxidation analyst for thePGM/TiO_2/CNT catalysts and commercial JM Pt/C catalyst were measured by cyclic voltammoetry in 0.5 M H_2SO_4 +0.5 M MeOH solution as is shown in Figure 5.14.

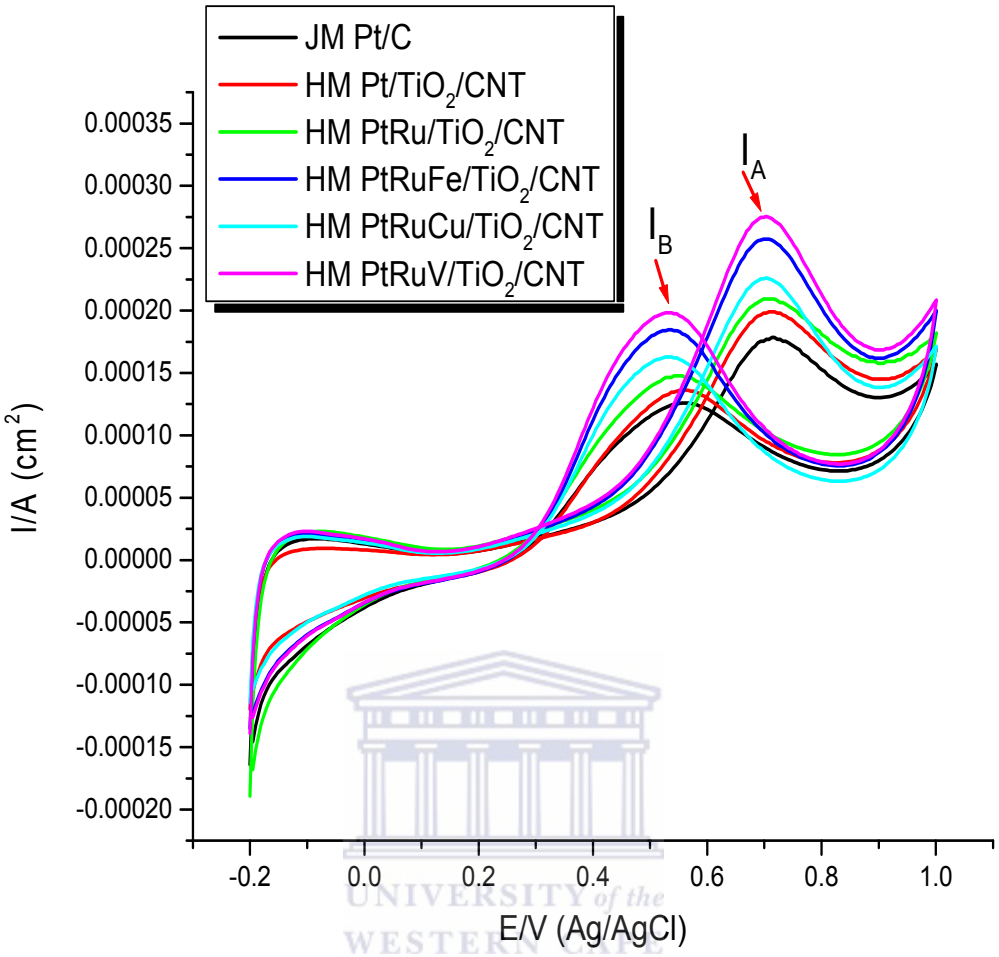

Figure 5.14: Cyclic voltammograms of JM Pt/C catalyst and home-made PGM/TiO_2/CNT electrocatalysts in 0.5 MH_2SO_4 + 0.5 M MeOH

Figure 5.14displays a comparison of methanol oxidation activity for standard JM Pt/C and in-house PGM/TiO2/CNT catalysts. It can be seen that all catalysts showed voltamperograms of methanol oxidation.

Table 5.7 summarizes the results obtained for the oxidation of methanol on the catalysts.

Table 5.7: Currents and potential for the oxidation and re-oxidation of methanol for the PGM/TiO_2/CNT catalysts

catalyst	**Direct Potential (V)**	**Direct Current (I_A) ($mAcm^{-2}$)**	**Inverse Current (I_B) ($mAcm^{-2}$)**	**I_B/I_A *100%**
JM Pt/C	0.72	182	130	71.4
JM Pt Ru/C	0.78	140	105	75.0
A12: Pt/TiO_2/CNT	0.72	200	145	72.5
A13: PtRu/TiO_2/CNT	0.71	210	151	71.9
A14: PtRuFe/TiO_2CNT	0.70	260	187	71.9
A15: PtRuCu/TiO_2/CNT	0.71	230	170	73.9
A16: PtRuV/TiO_2CNT	0.70	280	200	71.4

The highest direct current (280 mA/cm^2)at potential 0.70 V was observed in the case of PtRuV/TiO_2/CNT catalyst. Catalysts Pt/TiO_2/CNT, PtRu/TiO_2/CNT, PtRuFe/TiO_2/CNT and PtRuCu/TiO_2/CNT catalysts displayed currents of200mA/cm^2, 210 mA/cm^2, 260mA/cm^2 and 230 mA/cm^2 respectively while commercial JM Pt/C catalyst presented the lowest current at 182 mA/cm^2 during methanol oxidation reaction. The order of the current corresponded to calculated chemical active surface area of the catalysts (Table 5.6). The onset potential for methanol oxidation is very similar for all the catalysts (0.36-0.38 V). Hence, it can be seen that the direct oxidation peak potentials (V) for methanol oxidation of catalysts are slightly reduced with increasing direct current (I_A) (Table 5.7). The lower the peak potential, the better the electro-catalytic activity [216], thus these

results indicate that the PtRuV/TiO_2/CNT was the most active catalyst of the series PGM/TiO_2/CNT catalysts.

It is well known that the direct scan peak current (I_A) display the methanol oxidation and the reverse scan peak current (I_B) point the methanol re-oxidation. The difference between the forward and the reverse current also indicate the methanol oxidation activities of the catalysts. The bigger the ratio of I_B/I_A suggests that the lower poisoning effect and the better the tolerance of the electrode towards the strongly adsorbed intermediates [212].

Table 5.7 also lists the oxidation potentials for the direct conversion of methanol to CO_2, as well as the corresponding current intensities when the scan is switched towards cathodic potentials. For the catalysts Pt/TiO_2/CNT, PtRu/TiO_2/CNT, PtRuFe/TiO_2/CNT, PtRuCu/TiO_2/CNT and PtRuV/TiO_2/CNT, the ratio I_B/I_A contributed with 72.5%, 71.9% and 71.9%, 73.9% and 71.4%, respectively; whereas the commercial JM Pt/C catalyst the rationI_B/I_Acontributes with 71.4%. The I_B/I_A rate demonstrated the highest poisoning tolerance of the PtRuCu/TiO_2/CNT sample (73.5%) and the lowest poisoning tolerance was found for the of PtRuV/TiO_2/CNT sample. This result indicates that the oxidation of methanol to CO_2 is performed in a more selective way on the catalyst with bigger particle size than on the catalyst with smaller particles (Table 5.6) [216]. It can be also seen that all home-made PGM/TiO_2/CNT catalysts showed better CO_2poisoning tolerance than that of commercial Pt/C though these samples obtained smaller particle sizes.These results

confirmed that Pt or PtRu catalysts supported on TiO_2 exhibited excellent catalytic activity for methanol electro-oxidation because of the synergetic interaction between Pt and TiO_2 [156-157].

5.4 Conclusion

TiO_2 coated on CNTs as a new support for the PGM catalysts were studied in this chapter. EDS, FTIR, BET, HRTEM and XRD results showed that the additional TiO_2 is deposited as an amorphous phase on the CNTs. The OMCVD method was successfully developed to synthesize the PGM/TiO_2/CNT catalysts, which could be used to deposit metals on a substrate in a controlled manner. Physico-chemical analysis confirmed that the platinum group metals (PGM) supported on TiO_2/CNT support possessed the smaller particle sizes (1.39 – 2.63 nm) and larger chemical-active surface area (224 – 260m^2/g) , higher methanol oxidation activity (200 – 280$mAcm^{-2}$) and better CO poisoning tolerance (71.4 – 72.5 %) when compared with the catalysts of PGM supported on CNTs. The additional TiO_2showed as a good surface promoter for improving PGM activity towards methanol oxidation. This is because the chemical nature of the substrate (TiO_2) influences the quality of the deposit to a great extent at early stage of its growth during nucleation. It influences the properties of film adhesion and even the formation of the deposit itself [163].

The electrochemical results were confirmed that the methanol oxidation activity of electrocatalysts was increased at lower direct potential by an increased active

surface area. It also displayed that the oxidation of methanol to CO_2 is performed in a more selective way on the catalyst with bigger particle size than on the catalyst with smaller particles.

The characterization results for the PGM/TiO_2/CNT catalysts were in agreement with the finding in Chapter 4, which confirmed that the bi-metallic catalyst showed higher electrochemical activity than that of the monocatalysts and the tri-metallic catalysts displayed better electrochemical activity than that of the bi- catalyst.It showed that the addition metals incorporated with Pt could reduce the particle size and increase the active surface area of the catalysts. Catalyst PtRuV/TiO_2/CNT presented the best electrochemical activity of all the investigated electrocatalysts because of its increased chemically-active surface area, which are 280mAcm^{-2} and 260m^2/g, respectively. Overall, PtRuV/TiO_2/CNT has the highest catalytic activity when compared to the other home-made electrocatalysts even has a significant activity higher than commercial standard PtRu/C catalyst (140 mAcm^{-2}).

The use of the OMCVD method again successfully developed implemented in this study for producing PGM/TiO2/CNT electrocatalysts and producing consistent results that resulted in uniform particle size, high dispersion and high electrochemical activity.The method allows to simultaneous deposition of three metals and catalysts alloying is nearly complete. Finally, the easy and reproducible conditions of OMCVD method toprepare more active catalysts than by the classicalimpregnation method should attract the attention ofindustry.

CHAPTER 6:

Determination of Reducibility of Platinum Group Metal Electrocatalysts

In this chapter, the investigation of the reduction kinetics of metal oxides of the catalyst precursors will be provided by Temperature Programmed Reduction (TPR) technique. The metal-support interaction and bimetal formation will be also provided by TPR.

6.1 Introduction

Temperature programmed reduction determines the number of reducible species present on the catalyst surface and reveals the temperature at which the reduction of each species occurs [179].The catalytic activity or antipoison properties of platinum base catalysts were enhanced by the additional metal alloy. However, their mechanics in the reaction duration are far from clearly understood due to the measurement limitation. TPR technique is a sensitive tool to study the characteristics of additional metal components. This technique consists of heating the catalystwith a linear temperature ramp in a flow of hydrogenwhile monitoring the hydrogen consumption. In this way, fingerprintprofiles are obtained which allow one to study theinfluence of the support and of additional metal on the metal reducibility.Furthermore, the presence and amount of each of the reducible metal

species in the catalystand their degree of reduction can be derived from the integratedhydrogen consumption, and lumped kinetic parameterscan be estimated if an adequate model of the reductionprocess exists [248]. Peak temperatures observed during the reduction of unsupported compounds and supported precursors have been used to assess the strength of metal-support interactions. It has been proposed that higher reduction peak temperatures are indicative of stronger metal-support interactions [179].

6.2 Experimental Work

The synthesize procedures of bi- and tri- metallic electrocatalysts, PGM/CNT and PGM/TiO_2/CNT, were specified in Section 4.2 and Section 5.2. Synthesize procedure of catalysts Ru/TiO_2/CNT, Fe/TiO_2/CNT, Cu/TiO_2/CNT and V/TiO_2/CNT were detailed follow.

6.2.1 Materials

The chemicals employed to prepare the series of mono metallic catalysts are shown in Table 6.1.

Table 6.1 Chemicals for preparing non-platinum catalysts

Chemicals	**Specifications**	**source**
Multi-wall carbon nanotubes	95 wt.%, 20 -30 OD	Cheap Tubes Inc ©
Titanium acetylacetonate	97%	Sigma-Aldrich
Ruthenium acetylacetonate	97%	Sigma-Aldrich
Copper acetylacetonate	97%	Sigma-Aldrich
Iron acetylacetonate	97%	Sigma-Aldrich

6.2.2 Catalyst Synthesis

Non-platinum monoelectrocatalysts supported on TiO_2/CNT and synthesized by the using the methodologies given in the following subsections are tabulated in Table 6.2. The theoretical molar ratio of TiO_2:Pt1:1 was used in this study because it was described as the optimum molar ratio for TiO_2/Pt by H.Q. Song et a.l [160].

Table 6.2: Summary of prepared PGM/TiO_2/CNT electrocatalysts and non-platinum catalysts

catalyst	**Metal**	**Support**	**Metal Theoretic Loading (wt. %)**
A15	Ru	TiO_2/CNT	40
A16	Cu	TiO_2/CNT	40
A17	Fe	TiO_2/CNT	40

6.2.2.1 Synthesis TiO_2/CNT support

The same synthesis procedure as specified in Section 5.2.2.1 was used to produce the TiO_2/CNT support.

6.2.2.2 Synthesis of 40 wt. % $Ru/TiO_2/CNT$, $Fe/TiO_2/CNT$ and $Cu/TiO_2/CNT$ catalysts (A15-A17)

1313.53 mg Ruthenium acetylacetonate [$Ru(acac)_3$], 2106.81 mg Iron acetylacetonate [$Fe(acac)_3$] and 1372.97 mg and Copper acetylacetonate [$Cu(acac)_2$] were each individually mixed with the respective amount of 500 mg prepared TiO_2/CNT support and then the synthesis procedure specified in Section 5.2.2.2 was followed to produce the baseline series of mono metallic catalysts $Ru/TiO_2/CNT$ (A15), $Fe/TiO_2/CNT$ (A16) and $Cu/TiO_2/CNT$ (A17)

6.2.3 Characterization technique

The TPR was used in this study, which was conducted on a micrometrics Auto chem. Analyzer, a mixture of H_2/Ar was used during the experiment at a flow rate of 50 ml/min. The experimental procedure is specified in Section 3.1.7.

6.3 Results and Discussion

6.3.1 Temperature programmed reduction in H_2

The characterisation of active sites of platinum group metal catalysts supported on CNT and TiO_2/CNT was carried out by TPR. The term multi-metallic catalysts refer to combinationsof two or three metals having a relatively large surface area and their formation will be also studied using TPR. The TPR results of the PGM/CNT catalysts and monometallic catalysts, $Pt/TiO_2/CNT$, $Ru/TiO_2/CNT$,

Fe/TiO_2/CNTand Cu/TiO_2/CNT, will be presented as base lines for comparative purposes and bi- and tri-metallic catalysts, PtRu/TiO_2/CNT, PtRuFe/TiO_2/CNT and PtRuCu/TiO_2/CNT, will be then displayed and discussed in the following section.

TPR profiles of Pt/CNT, PtRu/CNT, Pt/TiO_2/CNT, Ru/TiO_2/CNT and PtRu/TiO_2/CNT catalysts are shown in Figure 6.1.

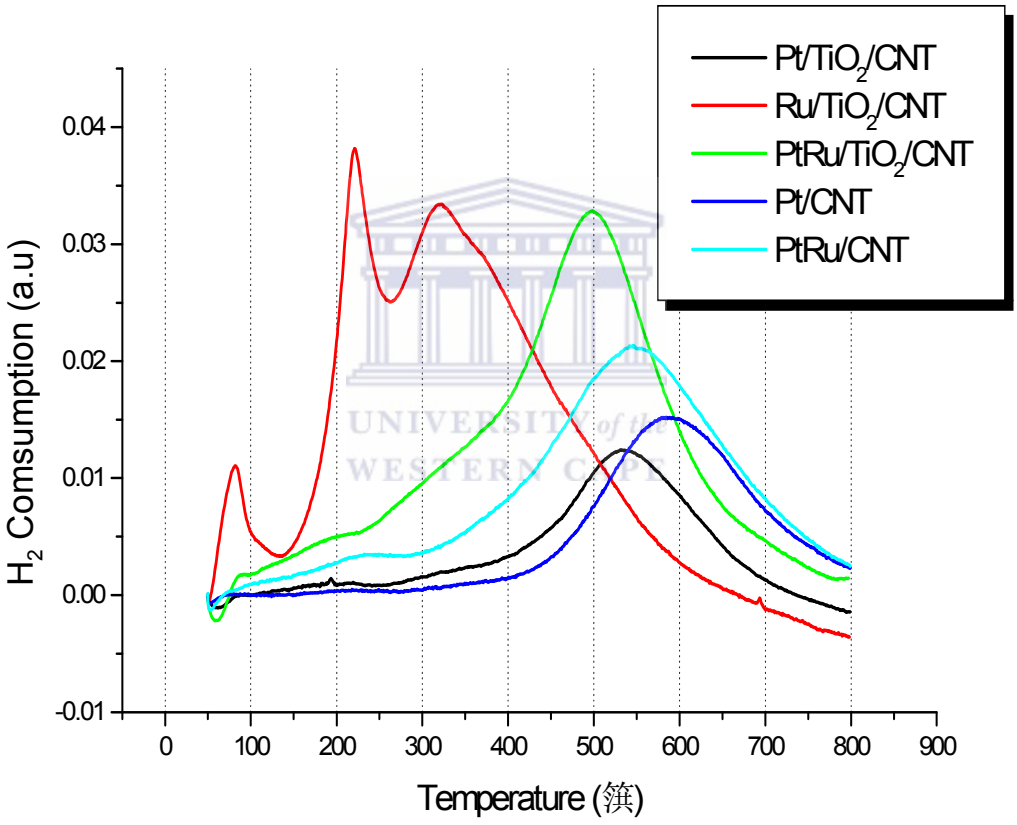

Figure 6.1: TPR spectra of Pt/CNT, PtRu/CNT, Pt/TiO_2/CNT, Ru/TiO_2/CNT and PtRu/TiO_2/CNT catalysts

It can be seen from Figure 6.1, for the catalyst Pt/TiO_2/CNT, the metal reduction appears at 540 °C with a weak signal, which means low H_2 consumption [249].

Metal Ru/TiO2/CNT showed three reduction peaks with a strong H_2 consumption signal, which were located at 90 °C, 220 °C and 320 °C, respectively, corresponding to intermediate oxides in the transformation of $Ru^{3+} \longrightarrow Ru^{2+} \longrightarrow Ru^{0}$.

The reduction peak of the binary catalyst PtRu/TiO_2/CNT is shown at 500 °C with a strong signal, which reveals that the addition of Ru on Pt changes the reducing temperature and the shape of the TPR spectrum of binary catalyst [250]. The appearance of a peak not seen in the monometallic systems has been used as a measure of bimetal formation. Another indication of bimetal formation that applies to the platinum-ruthenium system is the appearance/disappearance of the Ru oxidative peak. The disappearance of Ru reduction peaks can be used to identify bimetal formation [179]. The shifting of PtRu/TiO_2/CNTpeak of H_2consumption to a lower temperature as depicted in Figure 6.1 exhibits modification of the reduction behaviour of Pt oxide due to introduction of Ruoxide [251]. Additionally, a small shoulder at about 300 °C, which attributes to the ruthenium oxide, was observed in the profiles of the PtRu/TiO_2/CNT sample.

From the TPR results, it can be seen that Pt/CNT and PtRuCNT catalysts showed similar redox paeks as Pt/TiO_2/CNT and PtRu/TiO_2/CNT, which appeared at 585 °C and 550 °C, respectively. When compare the reduction temperature of Pt/CNT, PtRu/CNT with Pt/TiO_2/CNT and PtRu/TiO_2/CNT, it can be observed that redox peaks of catalysts supported TiO_2/CNT shifted to the lower temperature than catalysts supported on CNTs, which are from 585 °C to 540 °C of Pt and 550 °C to

500 °C of PtRu, respectively. This attributed to the highly dispersion of metal particles and the interacting between metal and the TiO_2/CNT support [252]. Theseresults are coresponed well with the conclusionin Chapter 5, wchih showed that PGM electrocatalysts support on TiO_2/CNT obtain better partical dispersion than PGM support on CNTs.

Figure 6.2 shows the TPR spectra of PtRuFe/CNT, Pt/TiO_2/CNT, Ru/TiO_2/CNT, Fe/TiO_2/CNT and PtRuFe/TiO_2/CNTcatalysts.

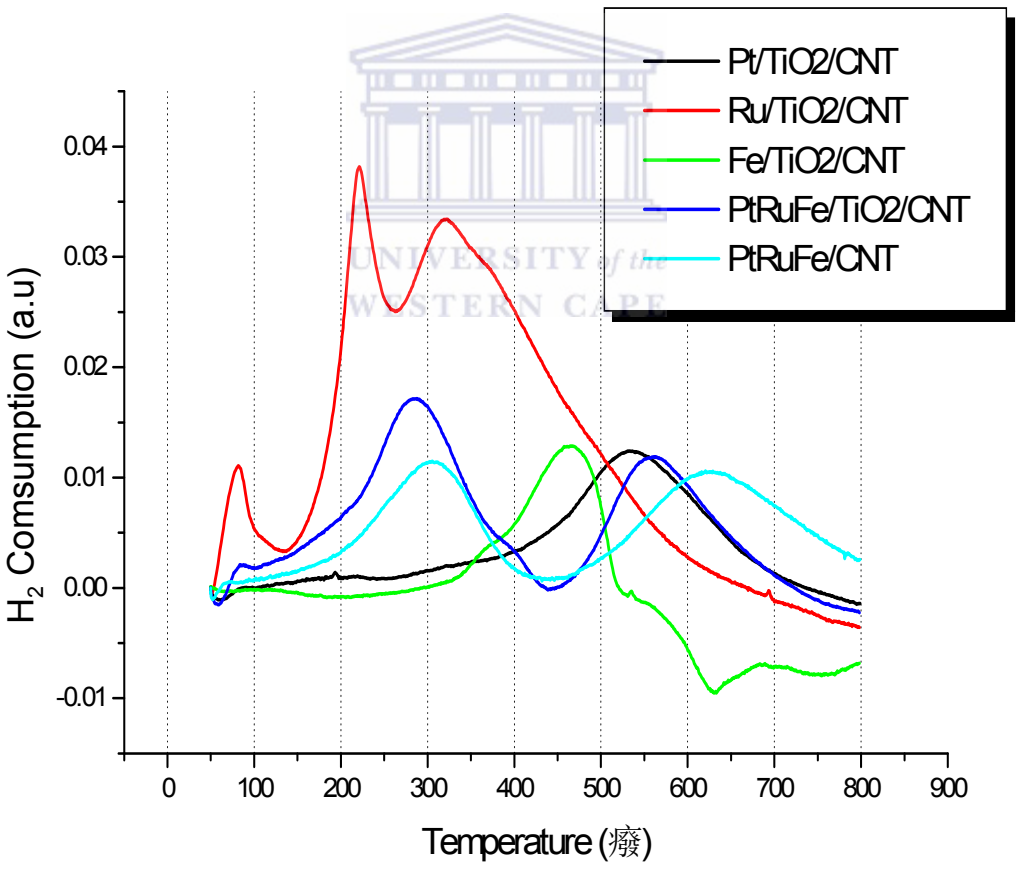

Figure 6.2: TPR spectra of PtRuFe/CNT, Pt/TiO_2/CNT, Ru/TiO_2/CNT,Fe/TiO_2/CNT and PtRuFe/TiO_2/CNT catalysts

From Figure 6.2, it can be observed thatthe metal reduction peak of catalyst $Fe/TiO_2/CNT$ appears at 460 °C with a weak signal, which means less H_2 consumption [249]. Ternary $PtRuFe/TiO_2/CNT$ catalyst showed three reduction peaks, which appeared at 90 °C, 280 °C and 560 °C, respectively. The first small reduction peak of $PtRuFe/TiO_2/CNT$ showed the same reduction temperature as $Ru/TiO_2/CNT$, which is assigned to the reduction of surface capping oxygen of ruthenium. The second reduction of $PtRuFe/TiO_2/CNT$was closer to 320 °C, in comparison with the single metal loaded on the support, which in this study is Ru. This peak is attributed to the reduction of ruthenium oxide, while the third peak seems to be closer to the Pt peak that appeared at 550°C. This third peak has been attributed to the reduction of platinum oxide. Additionally, a small shoulder at about 400 °C, which could be attributed to the iron oxide, was observed in the profiles of the $PtRuFe/TiO_2/CNT$ sample. The absence of reduction peak of Fe on the ternary catalyst indicates that Fe formed an alloy with Pt and Ru, which is confirmed by XRD results (Section 5.3.2.3) [251].

It can be seen from the TPR image that the PtRuFe/CNT catalyst showed similar redox peaks as $PtRuFe/TiO_2/CNT$. The second and third reduction peaks of PtRuFe/CNT were located at 300 °C and 640 °C, respectively, which temperature are higher than that $PtRuFe/TiO_2/CNT$. This is attributed to the high dispersion of metal particles and the interacting between metal and the TiO_2/CNT support [252]. These results are correspond well with the conclusion in Chapter 5, which showed

that PGM electrocatalysts support on TiO_2/CNT obtain better partical dispersion than PGM support on CNTs.

Figure 6.3 shows the TPR spectra of PtRuCu/CNT, Pt/TiO_2/CNT, Ru/TiO_2/CNT, Cu/TiO_2/CNT and PtRuCu/TiO_2/CNTcatalysts.

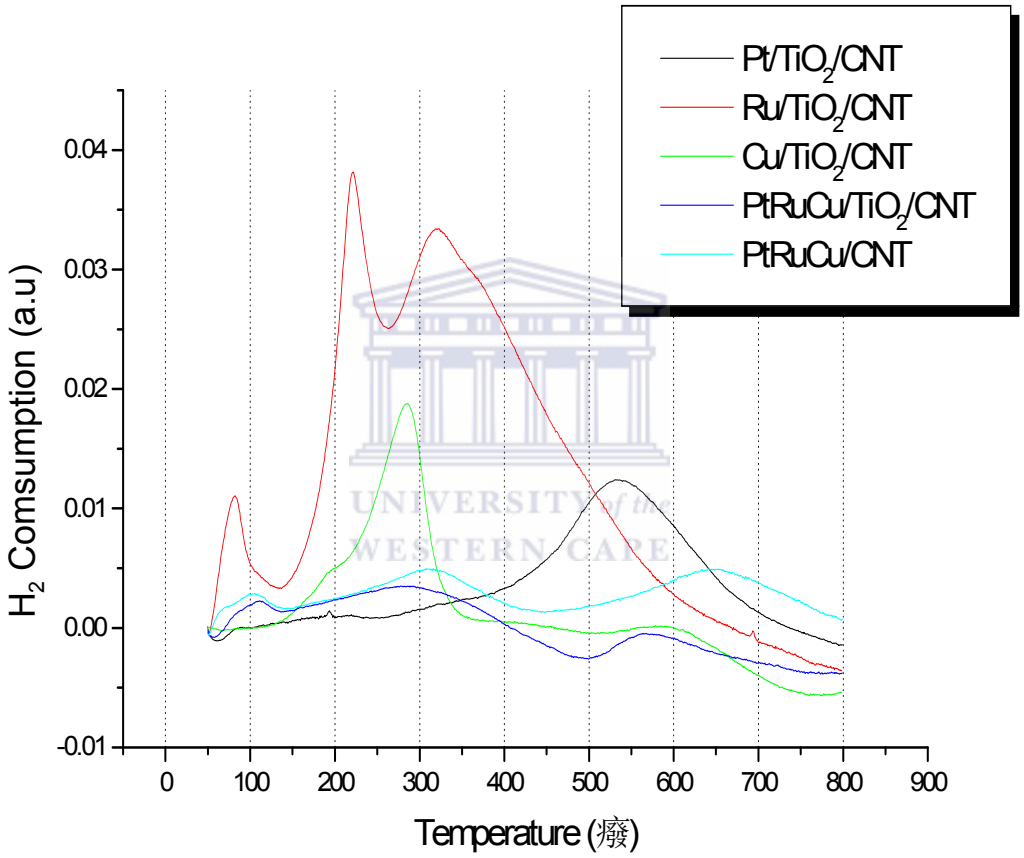

Figure 6.3: TPR spectra of PtRuCu/CNT, Pt/TiO_2/CNT, Ru/TiO_2/CNT, Cu/TiO_2/CNT and PtRuCu/TiO_2/CNT catalysts

From Figure 6.3, it can be observed thatthe metal reduction peak of catalyst Cu/TiO_2/CNT appears at 290 °C with a strong signal, which means high H2 consumption with less effect of the support [249]. The ternary catalyst

PtRuCu/TiO_2/CNT catalyst showed three reduction peaks with very weak signal, which appear at 90 °C, 300 °C and 560 °C, respectively. The first small reduction peak of PtRuCu/TiO_2/CNT showed the same reduce temperature (90 °C) as Ru/TiO_2/CNT, which is assigned to the reduction of surface capping oxygen of ruthenium. The second reduction of PtRuCu/TiO_2/CNTwas closer to 320 °C, in comparison with the single metal loaded on the support which in this study is Ru. This peak is attributed to the reduction of ruthenium oxide, while the third peak seems to be closer to the Pt peak that appeared at 550°C. This third peak has been attributed to the reduction of platinum oxide. The absence of the reduction peak of Cu on the ternary catalyst indicates that Cu formed alloy with Pt and Ru, which is confirmed by XRD results (Section 5.3.2.3).

It can be seen from TPR image that PtRuCu/CNT catalyst showed similar redox paeks as PtRuCu/TiO_2/CNT, which are appeared at 90 °C, 320 °C and 650 °C, respectively. The higher metal reduction temperature attributed to the highly dispersion of metal particles and the interacting between metal and the TiO_2/CNT support [252]. These results are coresponed well with the conclusion in Chapter 5, wchih showed that PGM electrocatalysts support on TiO_2/CNT obtain better partical dispersion than PGM support on CNTs.

6.4 Conclusion

TPR was used to study the reducibility of the catalysts in this chapter. The investigation showed thatthe addition of second or third metal changes the reducing

temperature and the shape of spectrum of monometallic catalysts.The disappearance of additional metal reduction peaks can be used to identify bi- or tri-metal formation. It is important to note that the metallic state of the metal deposited on the substrate for binary and ternary catalysts - it means that there were few metal oxides formed by OMCVD method. This is a very important finding as other techniques cause agglomeration when chemicals are used for reduction.

The TPR results also presented that the catalysts supported TiO_2/CNT showed lower metal reduction temperature, which could be attributed to the highly dispersion of metal particles and interacting function between metal and TiO_2. These results confirmed that PGM catalysts support on TiO_2/CNT can produce better particle size distribution than PGM support CNTs.

CHAPTER 7:

Conclusion and Recommendations

The summary of findings and the overall conclusions of the thesis are consolidated in this chapter. A summary of the contributions that this dissertation has made as well as recommendations for future research are then presented.

7.1 Conclusions

The ultimate scientific goal of the project was to successfully develop methodological approaches for the preparation of multicomponent electrocatalysts for practical application of the methanol electro-oxidation process. The requirements for a practical electrocatalyst includehigh intrinsic activity for the electrochemical oxidation of a fuel at the anode side and for the reduction of di-oxygen at the cathode side of a fuel cell. It also requires good durability and electrocatalysts should have good electrical conductivity to minimize resistive losses in the catalyst layer, be inexpensive to fabricate, and be manufacturable at high volume with good reproducibility. These targets were achievable through nano-engineering of Pt catalytic mantles onto the surface of the carbon material supports. Further, the hypothesis of the study was stated as follows:

Development of synthesize method, based on the Organometallic Chemical Vapour Deposition technique, for the "one-step" preparation of advance multicomponent electrocatalysts, based on Pt and Pt alloys, for the methanol electro-oxidation

application. The fabrication method should be efficient and produce electrocatalysts that should exhibit uniform particle size, high dispersion and high electrochemical activity.

In addressing the hypothesis the following research questions were investigated:

i. What is the most efficient/economical fabrication method?
ii. Which fabrication method produces the best catalytic behavior?
iii. Can multicomponent catalysts be prepared by using the simple synthesis method?
iv. Can the catalysts be prepared without agglomeration and with high dispersion and high catalytic activity?
v. Will the CNTs be a better support than Vulcan XC-72 for the catalysts?
vi. What is the optimal content for Pt catalysts?
vii. Will the electrochemical activity of Pt catalyst be enhanced by adding the additional second or third metals?
viii. Will the added additional metals reduce the cost of Pt catalysts?
ix. What is the structure of prepared binary and ternary PGM catalysts?
x. Can TiO_2 modify the CNTs as a new support for electrocatalysts?
xi. Will the catalytic activities of the catalysts be enhanced by supported on TiO_2/CNT

The synthetic approaches used, supports and Pt alloys that were used in this project allowed for tailoring of morphological properties of the manufactured electrocatalysts.

Experimental tasks and a detailed research work-plan were formulated to address the hypothesis and research questions. A set of physico-chemical properties governing the applicability of the electrocatalysts were identified in a comprehensive literature review. The novelties of the formulated research work-plan were also highlighted. Standard characterization tools were reviewed and used in the investigation of the characteristics of the prepared electrocatalysts, and included Scanning Electron Microscopy (SEM), X-ran Diffraction (XRD), Surface Area and Porosity Analysis (BET), Energy Dispersive X-ray Spectroscopy(EDS), Inductively Coupled Plasma Mass Spectroscopy (ICP-MS), Brunauer-Emmett-Teller N_2 adsorption technique (BET), Fourier Transform Infrared (FTIR), Temperature Programmed Reduction (TPR) and Cyclic Voltammetry (CV).

Results of the characterization of the electrocatalysts were collected and are summarized as follows:

1. The study was initiated by an investigation of the different methods (wet-chemical (WC) and Organometallic Chemical Vapour Deposition (OMCVD) method) and supports (Vulcan XC-72 and Multi-wall Carbon Nanotubes), which were used Platinum acetylacetonate as precursor, for preparing the platinum catalysts (A1-A4).Following an investigation of the effect of the following variables (deposition method, substrate type), the Pt catalysts prepared by the OMCVD method exhibited enhanced characteristics compared to the catalysts prepared by WC method. The physico-chemical

results showed that all the Pt catalysts were prepared with *fcc* structures and the particle sizes of the Pt catalysts prepared by OMCVD method were 2.0 ± 1.0 nm while the particle sizes of the catalysts prepared by WC method were 3.5 ± 2.0 nm. Electrochemical activities of the catalysts were measured by CV. According to the results, all the electrocatalysts were active for hydrogen and oxygen according to the areas of the reaction peak. The catalysts prepared by OMCVD method displayedlarger chemical-active surface area, which were 138 and 153 m^2/g, respectively, than that of the catalysts preparedby WC method, which were 91 and 107 m^2/g, respectively.These larger surface area of OMCVD catalysts resulted in higher methanol oxidation activity of the Pt catalysts.The methanol electro-oxidation positive peak current densities for the catalysts produced by OMCVD method were 99 and 115 mA/cm^2, respectively, while in the case of the catalysts produced by WC method the current densities were 79 and 82 mA/cm^2, respectively.The platinum catalysts supported on CNTs also displayed a larger chemical-surface area and better methanol oxidation activity than that of the Pt supported on Vulcan due to the highly crystalline structure of CNTs. The chemical-surface areas of the platinum supported on CNTs were 153 and 107 m^2/g, respectively and methanol electro-oxidation current densities were 115 and 82 mA/cm^2, respectively. On the other side, the catalysts supported on Vulcan XC-72 showed the chemical-surface areas of 138 and 91 m^2/g, respectively, and the methanol electro-oxidation current densities were 99 and 79 mA/cm^2,

respectively.

2. The effect of Pt content was also investigated for the purpose of optimal Pt wt. % to obtain the highest electro-catalytic activity. The properties of the 20, 40 and 60 wt.% platinum supported on CNTs catalysts were evaluated using physic-chemical and electrochemical characterizations techniques.

   It was found that the particle size of Pt was increased by increasing Pt wt.%. Different Pt wt.% loading catalysts were successfully produced by OMCVD method. HRTEM results showed that the average Pt particle sizes of 20, 40 and 60 wt. % Pt catalysts were 2.61, 2.77 and 3.22 nm, respectively. Electrochemical analysis showed that the electrochemical surface area of 20, 40 and 60 wt. % Pt catalysts were 170, 201 and 151 m^2/g, respectively, and the methanol electro-oxidation current densities for the catalysts were 149, 200 and 137 mA/cm^2, respectively. It was found that 40 wt. % Pt/CNT catalyst obtained the largest electrochemical surface area (201 m^2/g) and the highest methanol oxidation activity (200 mA/cm^2), which was compared higher to that of the commercial standard JM Pt/C catalyst (190 m^2/g and 182 mA/cm^2).

3. An investigation into the influence of Pt combined with additional metals (PtRu/CNT, PtRuFe/CNT, PtRuCu/CNT and PtRuV/CNT) was undertaken for the purpose of reducing theCO poisoning and enhancing catalytic performance by advanced electro-catalyst design relying on the bi-functional

mechanism. Significant influences of additional metals on the Pt catalysts were observed.

It was found that the added additional metals (Ru, Fe, Cu, V) could reduce the particles size of the catalysts and resulted in the larger chemical-active surface area and higher methanol electro-oxidation current. The average particle sizes were 1.75 nm, 2.31 nm, 1.66 nm and 1.58 nm for catalysts PtRu/CNT, PtRuCu/CNT, PtRuFe/CNT and PtRuV/CNT, respectively.All the binary and ternary metal catalysts were proved to be relatively complete alloy phases by XRD analysis. Electrochemical analysis showed that electrochemical surface area of catalysts PtRu/CNT, PtRuCu/CNT, PtRuFe/CNT and PtRuV/CNT were 215, 200, 222 and 238 m^2/g, respectively and methanol electro-oxidation current densities are for the catalysts were 205, 185, 210 and 228 mA/cm^2, respectively. It was found that PtRuV/CNT catalyst obtained the largest electrochemical surface area (238 m^2/g) and the highest methanol oxidation activity (228 mA/cm^2), which is compared significant better compared to that of the commercial standard JM PtRu/C catalyst (159 m^2/g and 140 mA/cm^2).

4. As $TiO_2$is known for its high catalytic activity and stability in acidic or alkaline solutions and was reported to exhibit excellent catalytic activity for methanol electro-oxidation because of the synergetic interaction between Pt and TiO_2, an approach was adopted to deposit TiO_2 on CNTs as a new

composite support substrate for deposition of the PGM catalysts, which were again prepared by using the OMCVD method,

In the first investigation, comparison between the characteristics of pre-treated CNTs and TiO_2 coating on CNTs (TiO_2/CNT) wasmade. It was found byphysic-chemical characterizations that the additional TiO_2 is deposited as an amorphous phase on the CNTs.

The investigations of PGM/TiO_2/CNT electrocatalysts were undertaken by ICP, HRTEIM, XRD, TPR and CV techniques. It was found that the OMCVD method could be successfully applied to synthesize the PGM/TiO_2/CNT catalysts, which method could be used to deposit various metals on a substrate in a controlled manner and addition, $TiO_2$was demonstrated to be a good surface promoter for the PGM catalysts. The average particle size for catalysts Pt/TiO_2/CNT, PtRu/TiO_2/CNT, PtRuFe/TiO_2/CNT, PtRuCu/TiO_2/CNT and PtRuV/TiO_2/CNT were 2.95, 1.40 1.31, 1.98 and 1.30 nm, respectively, which smaller compared to that of PGM catalysts which were supported only on CNTs. The additional TiO_2coating on the CNTs resulted in a smaller particle size of the PGM catalysts when compared with the catalysts supported only on CNTs. XRD and TPR results showed that PGM/TiO_2/CNT catalysts were alloys and additional metal changed the reducing temperature and the shape of spectrum of monometallic catalysts.The electrochemical characterization showed that the chemical-active surface areas were 224, 231, 255, 233 and

260 m^2/g and the methanol electro-oxidation current were 200, 210, 260, 230 and 280 mA/cm^2 for catalystsPt/TiO_2/CNT, PtRu/TiO_2/CNT, PtRuFe/TiO_2/CNT, PtRuCu/TiO_2/CNT and PtRuV/TiO_2/CNT, respectively. Overall, PtRuV/TiO_2/CNT was found to have the largest chemically-active surface area(260 m^2/g) and the highest methanol oxidation current density (280 mA/cm^2) when compared to the other home-made electrocatalysts as well as the commercial standard JM PtRu/C catalyst (159 m^2/g and 140 mA/cm^2).

To summarize, different approaches were used to prepare the platinum group metal electrocatalysts and the following conclusions can be made

- All the catalysts were successfully produced with different approaches by using OMCVD method
- A novel route is described to form plurimetallic nanophase electrocatalysts using the Organometallic Chemical Vapor Deposition (OMCVD) method, which was compared with the traditional wet-chemcial (WC) method. The OMCVD method resulted in the successful presentation of the PGM electrocatalysts with different supports, metal contents and combination metal alloys in a very simple synthesis procedure which was used to prepared new catalysts with high dispersion and electrocatalytic activity. The results showed that the OMCVD method is a powerful, efficiency, economic and environmental friendly method to control the deposition of the desired metal

phases upon the chosen substrates.

- CNTs is a better PGM catalysts support than Vulcan
- 40 wt.% Pt was found to be the optimal weight percentage for preparing the Pt catalysts upon CNTs because loading lower than 40 wt.% resulted in lower electrocatalytic activity and a higher wt.% than 40 would increase the cost of the catalyst whilst causing agglomeration, which resulted in a smaller chemical-active surface of catalysts and waste of PGM
- The binary and ternary PGM catalysts are alloys, which were proved by XRD analysis, and the additional metals in binary and ternary systems resulted in a smaller particle size of Pt alloys and increasing the electrochemical activity of the prepared PGM catalysts
- TPR technique also proved that the binary and ternary of PGM/TiO_2/CNT were alloy forms. Additionally, the investigation showed that the addition of second or third metal changes the reducing temperature and the shape of spectrum of monometallic catalysts.
- TiO_2 was deposited on CNTs as an amorphous phase via OMCVD and it was demonstrated to be a good surface promoter for improving PGM activity towards methanol oxidation. The PGM catalysts supported on TiO2/CNT showed the smallest particles sizes, which resulted in significantly improved chemical-active surface and higher methanol electro-oxidation current in the electrochemical investigation when compared with the PGM catalysts supported only on CNTs, as well as being significantly higher than the commercial

standard JM catalysts.

To conclude, in the course of addressing the hypothesis and research questions, the physico-chemical and electrochemical properties of the electrocatalysts, which were mainly prepared by the OMCVD method, have been evaluated. The OMCVD method was demonstrated as a powerful, fast and environmental friendly method as it produced mono, binary and plurimetallic catalysts without the multiple processing stages of impregnation, washing, drying, calcinations, and activation. The study has also aided in the understanding of the influence of the supports, Pt content and addition of metals of Pt alloys. In addition, a new approach in which $TiO_2$was deposited on CNTs as a new composite support substrate was also studied. It is important to note that the investigation of reducibility and structure of PGM/TiO_2/CNT catalysts showed that there were few metal oxides formed by OMCVD method. This is a very important finding as other techniques cause agglomeration when chemicals are used for reduction. The scientific goals of improving the electrocatalytic of electrocatalysts were addressed. The knowledge emanating from this project is expected to be used to implement the OMCVD method as means to synthesize superior catalysts with uniform particle size, high dispersion and high electrochemical activity.

7.2 Recommendations

Based on the analyses and conclusions of the study, a number of recommendations regarding future research directions of investigation were made:

- The fuel cell application and testing of the home-made catalysts should be implemented;
- The deposition on CNTs of different TiO_2 amount should be investigated;
- The dispersion of the composite nanophase catalysts in catalystic inks for screenprinted electrodes should be determined;
- The catalysts of PGM supported on TiO_2/CNT should be investigated as the photo catalysts for water treatment applications

Publications:

1) Papers:

1. S.Naidoo, Q.Naidoo, G. Vaivars, "Low Temperature Quaternary Catalysts Synthesis of Nano-sized for Fuel Cell Applications" , Journal of Integrated Ferroelectrics, 103:1-10, 2009
2. M.Willians, L.Khotseng, Q.Naidoo, L.Petrik, A.Nechaev, V.Linkov, "Applicability of analytical protocols for the characterisation of carbon-supported platinum group metal fuel cell electrocatalysts", South African Journal of Science 105, 2009
3. M.W. Davids, M. Lototskyya, A. Nechaev,Q. Nadioo, M. Williams, Y. Klochko, "Surface modification of TiFe hydrogen storage alloy with palladium by metal-organic chemical vapour deposition", Journal of Hydrogen Energy, Ref. No.: HE-D-11-00913R1, 2011

2) Conference Proceeding:

1. L.Petrik, Q.Y.Naidoo, S.Naidoo, P.Ndungu, "Characteristics of platinum group nano-alloy on carbon nanostructured materials", 1-4 February 2009, 3rd NanoAfrica 2009 Conference, Pretoria, South Africa (talk)
2. G. Vaivars, S. Naidoo, Q. Ying and V. Linkov. Low Temperature Quarternary Catalyst Synthesis used for Methanol and Hydrogen Oxidation on MWCNT. In: Abstr. FM&NT-2008, International Baltic Sea Region conference "Functional materials and nanotechnologies 2008" Riga, April 1-4, 2008. Riga: 2008. P.76.
3. S. Naidoo, Q. Y. Naidoo, G. Vaivars and V. Linkov, "Low Temperature Quarternary Catalyst Synthesis used for Methanol and Hydrogen

Oxidation on MWCNT", 9-11 July 2008, 1st International Symposium of ElectrochemSA, UWC, Cape Town, South Africa

4. L.Petrik, Q.Y.Naidoo, Z.G.Godongwana, M.Harting, DT.Britton, EI.Iwuoha, "PREPARATION AND ELECTROCHEMICAL CHARACTERIZATIONOF COMPOSITE ELECTROCATALYSTS", 9-11 July 2008, 1st International Symposium of ElectrochemSA, UWC, Cape Town, South Africa (First Price)
5. Q.Y.Naidoo, S.Naidoo, L.Petrik, G.Vaivars, "PREPARATION AND ELECTROCHEMICAL CHARACTERIZATION OF HIGYLY ACTIVE Pt/C ELECTROCATALYSTS", 30 November – 5 December 2008, 39th National Convention of the South Africa Chemical Insitute, Stellenbosch, South Africa
6. Q. Ying Naidoo, A. Nechaev, P. Leslie, P. Ndungu, S. Naidoo, "Titanium Dioxide Modified Carbon Nanotubes as Platinum Group Metal Catalyst Support", 16 – 21 January 2011, 40th National Convention of the South Africa Chemical Insitute, Johannesburg, South Africa

References:

[1] D.M. He, L.X. Yang, S.Y. Kuang, Q.Y. Cai, *Electrochem. Commun.* 9 (2007)2467

[2] S. Basri, S.K. Kamarudin, W.R.W. Daud, Z. Yaakub, *Int. J. Hydrogen Energy*35 (2010)7957

[3] M. Creamer, "The uses of platinum-group metals", (2005), [Online], Available: http://www.miningweekly.com/article/the-uses-of-platinumgroup-metals-2006-11-10

[4] PLATINUM TODAY, (2009), [Online], Available: http://www.platinum.matthey.com/applications/applications.html

[5] Mineweb, "Precious metals consultant CPM predicts record platinum prices will persist" (2007), [Online], Available: http://www.mineweb.co.za/mineweb/view/mineweb/en/page35?oid=22650&sn=Detail

[6] J. Rolnitzky, "Catalysts at the nanoscale", [ONLINE], AVAILABLE: http://tahan.com/charlie/nanosociety/course201/, 2005

[7] C.Y. Wang, H.Y. Du, Y.T. Tsai, C.P. Chen, C.J. Huang, L.C. Chen, *J.Power Sources* 171 (2007) 55

[8] H. Pereza, A. Morin, L. Akroura, C. Cremona, B. Baret, J. Haccoun, *Electro. Acta* (2009)

[9] P. Pannopard, P. Khongpracha, M. Probst, J. Limtraku. *J. MolecularGraphics and Modelling*28 (2009) 62.

[10] K. Sasaki, J.X.Wang, M. Balasubramanian, J. McBreen, F. Uribe, R.R. Adzic, *Electro Acta* 49 (2004) 3873

[11] D. Sebastia´n, I. Suelves, M.J. La´zaro, R. Moliner,*J. Power Sources*192 (2009) 51

[12] Y. Shao, G. Yin, Y. Gao,*J. Power Sources*171 (2007) 558

[13] R.I. Jafria, N. Sujathaa, N. Rajalakshmib, S. Ramaprabhu,*Int. J. Hydrogen Energy*34 (2009) 6371

[14] Z.Konya, V.F.Puntes, I.Kirisci, J.Zhu, P.Alivisatos, G.A.Somorjai,*Catal.Lett.,* 81 (2002) 137

[15] "Catalyst", (2002), [Online], Available: http://www.princeton.edu/~chm333/2002/spring/FuelCells/Catalysts.shtml,

[16] Thomsett. D. (2003) "Catalysts for the Proton Exchange Membrane Fuel Cell, Fuel Cell Technology Handbook", Florida, CRC Press LLC, 6: 1-23.

[17] "Catalysis", (2008),[Online], Available: http://en.wikipedia.org/wiki/Catalyst

[18] "Nanomaterials", (2008) [Online], Available: http://en.wikipedia.org/wiki/Nanomaterials

[19] National Nanotechnology Infrastructure Network, NNIN Document: NNIN-1106, (2007), [Online], Available:http://www.nnin.org

[20] G. Hoogers, (2003), "Fuel Cell Technology Handbook", by CRC Press LLC

[21] H. Hoster, T. Iwasita, H. Baumgartner, W. Vielstich, *J. Electrochem. Soc.*, (2001), 148 (5), A496

[22] Z.B. He, J.H. Chen, D.Y. Liu, H.H. Zhou, Y.F. Kuang, *Diamond Relat. Mater.* 13 (2004) 1764

[23] M. Hepel, I. Dela, T. Hepel, J. Luo, C.J. Zhong, Electrochim. Acta 52 (2007) ü 5529.

[24]S. Wasmus, A. Küver,*J. Electroanal. Chem.*461 (1999) 14

[25] Z.L. Liu, X.Y. Ling, X.D. Su, Y.J. Lee,*J. Phys. Chem.* B 108 (2004) 8234

[26] Y. Takasu, H. Itaya, T. Kawaguchi, W. Sugimoto, Y. Murakami, *Stud. Surf.Sci. Catal*.145 (2003) 279

[27] C. Burda, X.B. Chen, R. Narayanan, M.A. El-Sayed,*Chem.Rev* .105 105 (2005) 1025

[28] U.A. Paulus, A. Wokaun, G.G. Scherer, T.J. Schmidt, V. Stamenkovic¡ä,V. Radmilovic, N.M. Markovic¡ä, P.N. Ross, *J. Phys. Chem.* B 106 (2002) 4181

[29]J.R. Chang, S.L. Chang, T.B. Lin, *J. Catal.*169 (1997) 338

[30] A. Stanislaus, B.H. Cooper, *Catal. Re . Sci. Eng.* 36 (1994) 75

[31]S.H. Zhou, B. Varughese, B. Eichhorn, G. Jackson, K. McIlwrath, *Angew. Chem., Int. Ed.* 44 (2005) 4539.V

[32] L. Yang, J.H. Chen, X.X. Zhong, K.Z. Cui, Y. Xu, Y.F. Kuang, Colloids Surf. A 295 (2007) 21

[33] Y.B. Lou, M.M. Maye, L. Han, J. Luo, C.J. Zhong, *Chem. Commun.*473 (2001)

[34] M.M. Maye, Y.B. Lou, C.J. Zhong, *Langmuir*16 (2000) 7520

[35] J.H. Zeng, J.Y. Lee, J. Power Sources 140 (2005) 268

[36] L. Xiong, A.J. Manthiram, *Mater. Chem.*14 (2004) 1454

[37] A. Crown, I.R. Moraes, A. Wieckowski, J. Electroanal. Chem. 500 (2001) 333

[38] J.T. Moore, D. Chu, R.Z. Jiang, G.A. Deluga, C.M. Lukehart, *Chem. Mater.* 15 (2003) 1119

[39] C.E. Lyman,R.E. Lakis, H.G. Stenger,*Jr.Ultramicroscopy*58 (1995) 25

[40] G. Treglia, B. Legrand, *Phys. Re* .B 35 (1987) 4338

[41] M. Wu, D. Chen, T. Huang, *Langmuir* 17 (2001) 3877

[42] I. Srnova-Sloufova, B. Vlckva, Z. Bastl, T.L. Hasslett, *Langmuir* 20

(2004) 3407

[43] A. Henglein, *J. Phys. Chem.* B 104 (2000) 2201

[44] M. Wu, L. Lai,*Colloid Surf*. A 204 (2004) 149

[45] S.K. Ghosh, M. Mandal, S. Kundu, S. Nath, T. Pal, *Appl. Catal.*A 268

(2004) 61

[46] M.T.M. Koper, T.E. Shubina, R.A. van Santen, *J. Phys. Chem.*106 (2002) 686

[47] M. Watanabe, S. Motoo, *J. Electroanal. Chem.* 60 (1975) 267

[48] E. Herrero, K. Fanaszczuk, A. Wieckowsik, *J. Electroanal. Chem.* 361 (1993) 269

[49] C. Vericat, M. Wakisaka, R. Haasch, P.S. Bagus, A. Wieckowski, *J. Solid State Electrochem.* 8 (2004) 794

[50] C. Lu, R.I. Masel, *J. Phys. Chem.* B 105 (2001) 9793

[51] K.A. Friedrich, K.P. Geyzers, U. Linker, U. Stimmimg, J. Stumper, *J. Electroanal. Chem.* 402 (1996) 123

[52] U.A. Paulus, U. Endruschat, G.J. Feldmeyer, T.J. Schmidt, H. Bonnemann,

R.J. Behm, *J. Catal.* 195 (2000) 383

[53] S. Wasmus, A. Kuver, *J. Electroanal. Chem.* 461 (1999) 14

[54] K.Y. Chen, P.K. Shen, A.C.C. Tseung, *J. Electrochem. Soc*. 142 (1995) L185

[55] M. Gotz, H. Wendt, *Electrochim. Acta* 43 (1998) 3637

[56] C. Roth, M. Goetz, H. Fuess, *J. Appl. Electrochem.* 31 (2001) 793

[57] D.C.Papageorgopoulos, M.Keijzer, F.A.deBruijn, *Electrochim. Acta*48 2002) 197

[58] R. Venkataraman, H.R. Kunz, J.M. Fenton, *J. Electrochem. Soc.* 150 (2003) A278

[59] C. He, H.R. Kunz, J.M. Fenton, *J. Electrochem. Soc.* 150 (2003) A1017

[60]P.Strasser,Q.Fan,M.Devenney,W.H.Weinberg,P.Liu,J.K.Norskov,*J. Phys. Chem.* B 107 (2003) 11013.

[61] G. Lu, J.S. Cooper, P.J. McGinn, *J. Power Sources* 161 (2006) 106

[62] W. Zhou, Z. Zhou, S. Song, W. Li, G. Sun, P. Tsiakaras, Q. Xin, *Appl. Catal.* B 46 (2003) 273

[63] W.Zhou,W.Li, S.Song, Z.Zhou, L.Jang, G.Sun, Q.Xin, K.Poulianitis, S. Kontou, P. Tsiakaras, *J. Power Sources* 131 (2004) 217.

[64] S. Tanaka, M. Umeda, H.Ojima, Y. Usui,O. Kimura,I. Uchida,*J. Power Sources* 152 (2005) 34

[65] E.V. Spinace¡ä, M. Linardi, A. Oliveira Neto, *Electrochem. Commun.* 7 (2005) 365

[66] S.Rousseau, C.Coutanceau, C.Lamy, J.-M.Leger, *J.PowerSources*158 (2006) 18

[67] E. Antolini, F. Colmati, E.R. Gonzalez, *Electrochem. Commun.* 9 (2007) 398

[68] F. J. Luczak, D.A. Landsman, US Patent 4,447,506 (1984)

[69] A.K.Shukla,M.Neergat,P.Bera,V.Jayaram,M.S.Hegde,*J.Electroanal. Chem*. 504 (2001) 111

[70] M.Neergat, A.K.Shukla, K.S.Gandhi, *J.Appl.Electrochem.*31(2001)373

[71] F.J. Luczak, D.A. Landsman, US Patent 4,806,515 (1989)

[72] F.J. Luczak, D.A. Landsman, US Patent 4,711,829 (1987)

[73] K.E. Deluca, F.J. Luczak, K. Deluca, EP 665985-A (1994)

[74] A. Seo, J. Lee, K. Han, H. Kim, *Electrochim. Acta* 52 (2006) 1603

[75] G. Tamizhmani, G.A. Capuano, *J. Electrochem. Soc.* 141 (1994) L132

[76] J.Cho, W.Roh,D.Kim,J.Yoon,J.Choy,H.Kim,*J.Chem.Soc.,Faraday Trans.*94 (1998) 2835

[77] A. Lima, C. Coutanceau, J.M. Le´ger, C. Lamy, *J. Appl.Electrochem.* 31 (2001)

379

[78] M. Go¨ tz, H. Wendt, *Electrochim.Acta* 43 (1998) 3637.

[79] G.L. Holleck, D.M. Pasquariello, S.L. Clauson, in: S. Gottesfeld, T.F. Fuller (Eds.), Proton Conducting Membrane Fuel Cells, PV 98-27, The Electrochemical Society Proceedings Series, Pennington, NJ (1999) 151.

[80] E. Auer, A. Freund, T. Lehmann, K.A. Starz, R. Schwarz, U.Stenke, US Patent 6007 (1999) 934

[81] S. Mukherjee, J.L. Moran-Lopez, *Surf. Sci.* 189_/190 (1987) 1135

[82] A. Hamnett, *Catalysis Today* 38 (1997) 445-457

[83] M.P. Hogarth, T.R. Ralph, *Platinum metals Rev*. 46 (2002) 146

[84] L. Li, Y.C. Xing, *Energies*, 2 (2009) 789

[85] R. Ferrando, J. Jellinek, R. Johnston, *Chemical Review*, (2006), Vol. 108, No. 3

[86] R.L. Johonston, "Computational Nanoscience: From Clusters to Proteins via Nature-Inspired Computation", Ceria Workshop: Computational Intelligence in Cheminformatics, Birmingham, (2006)

[87] H. S. Liu, C. J. Song, L. Zheng, J. J. Zhang, H. J. Wang, D. P. Wilkinson, *J. Power Source* 155 (2006) 95-100

[88]H. Zeliger, *J. Electrochem. Soc.* (1967), 114, 144

[89] J. Bett, J. Lundquise, E. Washington, P. Stoneheart, *Electrochimica acta.* (1973), 18, 343

[90] W.M. Vogel, J.M. Baris, *Electrochimica Acta,* (1977), 22, 1259

[91] H.R. Kunz, G.A. Gruver, *J. Electrochem. Soc.,* (1975), 112, 1279

[92] K.F. Bluton, P.Greenburg, *J. Electrochem. Soc*., (1972), 119, 489

[93] L.J. Brogeli, *Electrochimica Acta.*, (1978), 23, 489

[94] M. Peuckert, T. Yoneda, *J. Electrochem, Soc.*, (1986), 113, 944

[95] F. Parmigiani, E. Kay, P.S. Bagus, *J. Electron Spectrose. Relat. Phenom*, (1990), 50:39

[96] T. Frelink, W. Visscher, J.A.R. Van Veen, *J. Electroanal. Chem.,* (1995), 385:65

[97] M.K. Min, J. Cho, K. Cho, H. Kim, J. Electro. Acta., (2000), 45:4211-4217

[98] L. Geni¨¨s, R Faure, R. Durand, *J. Electro. Acta*., (1998), 44:1371-1327

[99] P.N. Ross, *J. Electrochem. Soc.*, (1970), 117, 328

[100] M.S. Wilson, F.H. Farzon, K.E. Sickafus, S. Gottesfeld, *J. Eletrochem. Soc*. 140 (1993)2872

[101] S. Y. Cha, W. M. Lee, *J. Electrochem. Soc*. 146 (11) (1999)4055

[102] "Chemisorption: Active Sites", [Online], Available: www.dct.tudelft.nl/race/education/st4081/catcat09.ppt

[103] S. G. Sun, J. Clavilier, *J. Electroanal. Chem*., 236 (1987)95

[104] B. Beden, S. Juanto, J. M. Leger, *J. Electroanal. Chem*., 238 (1987) 323

[105] Y. Kinomoto, S. Watanabe, M. Takahashi, M. Ito.*Surf. Sci.*242 (1991) 538

[106] Y. Morimoto, E. Yeager, *J. Electroanal. Chem.*, 441 (1998)77

[107] H. Hoster, T. Iwasita, H. Baumgartner, W. Vielstich, *J. Electrochem. Soc.*, A 148 (5) (2001)496

[108] A.V. Ruban, H.L. Skriver, Norskov, *J. K. Phys. Re* .B 59 (1999) 15990.

[109] G. Bozzolo, J. Ferrante, R.D. Noebe, B. Good, F.S. Honecy, P. Abel, *Comput. Mater. Sci.*15 (1999) 169

[110] A.M. Molenbroek, S. Haukka, B.S. Clausen,*J. Phys. Chem.* B 102 (1998)10680

[111] G. Schmid, P. Braunstein, L.A. Oro, P.R. Raithby, Eds. Wiley-VCH: Weinheim, 3 (1999) 1325

[112] N. Toshima, M. Harada, T. Yonezawa, T. Kushihashi, K. Kushihashi,K. Asakura, *J. Phys. Chem.* 95 (1991) 7448

[113]S.H. Zhou, B. Varughese, B. Eichhorn, G. Jackson, K. McIlwrath, *Angew. Chem., Int. Ed.*44 (2005) 4539V

[114] Q.Ying, "Preparation and characterization of highly active nano Pt/C electrocatalysts for proton exchange membrane fuel cell", Published Master Thesis, University of the Western Cape, South Africa, (2006)

[115] W.j. Zhou, "Research on Anode Catalysts for Low-Temperature Direct Alcohol Fuel Cell", Published PhD. Thesis, Dalian Institute of Chemical Physics, (2003)

[116] H. Q. Song, X. P. Qiu, X. X. Li, F. S. Li, W. T. Zhu, L. Q. Chen, *J.Power Sources* 170 (2007) 50

[117] J. Prabhuram, X.Wang, C.L. Hui, I.M. Hsing, *J. Phys. Chem.* B 107 (2003) 11057

[118] J.T. Moore, J.D. Corn, D. Chu, R. Jiang, D.L. Boxall, E.A. Kenik, C.M. Lukehart, *Chem. Mater.* 15 (2003) 3320

[119] H. Tang, J.H. Chen, L.H. Nie, D.Y. Liu,W. Deng, Y.F. Kuang, S.Z. Yao, *J. Colloid Interface Sci.* 269 (2004) 26.

[120] F.B. Su, X. Li, L. Lv, X.S. Zhao, *Carbon* 44 (2006) 799

[121] M.X. Liu, L.H. Gan, C. Tian, J.C. Zhu, Z.J. Xu, Z.X. Hao, L.W. Chen, *Carbon* 45 (2007) 3045. 15

[122] P. Ndungu, Z.G. Godongwana, L.F. Petrik, A. Nechaev, S. Liao, V. Linkov, *Microporous and Mesoporous Materials* 116 (2008) 593

[123] K.T. Jeng, C.C. Chien, N.Y. Hsu, S.C. Yen, S.D. Chiou, S.H. Lin, W.M. Huang, *J. Power Sources*, 160 (2006) 97

[124] W. Li, C. Liang, J. Qin, H. Li, G. Sun, Q. Xin, *Carbon*, (2004), 42: 436-439

[125] M. Wang, J. Chen, Z. Fen, H. Tand, G. Deng, D. He, Y. Kuang, *Carbon* (2004), 42: 3257-3260

[126] E. Frackowiak, G. Lota, T.Cacciaguerra, F. Béguin, *Elcrtro. Communications*, 8 (2006)129

[127] N. Rajalakshmi, Hojin Ryu, M.M. Shaijumon, S. Ramaprabhu, *J. Power Sources,*140 (2005)250

[128] Z. Liu, L. Gan, L. Hong, W. Chen, J. Y. Lee, *J. Power Sources,*139 (2005) 73

[129] M.Carmo, V.A. Paganin, J.M. Rosolen, E.R. Gonzalez, *J. Power Sources*, 142 (2005)169

[130] W. Li, C. Liang, J. Qin, W. Zhou, H. Han, Z. Wei, G. Sun, Q. Xin, *Carbon*, 40 (2002)791

[131] Y. Lin, X. Cui, *J. Phys. Chem.* B 109 (2005) 14410

[132] J.H. Chen, M.Y.Wang, B. Liu, Z. Fan, K.Z. Cui,Y.F.Kuang, *J. Phys. Chem.* B 110 (2006) 11775

[133] Q. Ying, Published Master Thesis, University of the Western Cape, (2006)

[134]CCOHS, basic information on carbon black, (2005), [Online], Available:

http://www.ccohs.ca/oshanswers/chemicals/chem_profiles/carbonbl/basic_cb.html

[135] L.R. Jordan, A.K. Shukla, J. Behrsing, N.R. Avery, B.C. Muddle, M. Forsyth ,*J. Applied Electrochemistry*, 30 (2000) 641

[136] E. Budevski, *J. Optoelectronics and Advanced Materials*5 (5) (2003)1319

[137] S. Iijima,*Natur* 354 (1991)56

[138] T.W. Ebbessen, P.M. Ajayan, *Nature*358 (1992) 220

[139] M. Terrones, W.K. Hsu, A. Schilder, H. Terrones, N. Grobert, J.P. Hare, *Appl Phys A. Mate Sci Process*66 (1998) 307

[140] F. Darkrim, D. Levesque,*J Phys Chem*104 (2000) 6773

[141] R. H. Baughman, A. A. Zakhidov, W. A. De Heer, *SCIENCE*, 297(2002)787

[142] "Carbon Nanotube", (2008), [Online], Available: http://en.wikipedia.org/wiki/Carbon_nanotube

[143] P. Serp, M. Corrias, P. Kalck, *Applied Catalysis* A 253 (2003) 337

[144] Z.G. Chen, X.P. Qiu, B. Lu, S.C. Zhang, W.T. Zhu, L.Q. Chen, *Electrochem.Commun*. 7 (2005) 593

[145] L. Cao, F. Scheiba, Ch. Roth, F. Schweiger, C. Cremers, U. Stimming, H. Fuess, L.Q. Chen, W.T. Zhu, X.P. Qiu, Angew. *Chem. Int. Ed.* 45 (2006) 5315

[146] H.B. Suffredini, V. Tricoli, L.A. Avaca, N. Vatistas, *Electrochem.Commun.* 6 (2004) 1025

[147] A.L. Santos, D. Profeti, P. Olivi, *Electrochim. Acta* 50 (2005) 2615

[148] L.H. Jiang, G.Q. Sun, Zh.H. Zhou, Sh.G. Sun, Q. Wang, Sh.Y. Yan, H.Q. Li, J. Tian, J.S. Guo, B. Zhou, Q. Xin, *J. Phys. Chem.* B 109 (2005) 8774

[149] Y.X. Bai, J.J. Wu, J.Y. Xi, J.Sh. Wang, W.T. Zhu, L.Q. Chen, X.P. Qiu, *Electrochem. Commun.* 7 (2005) 1087

[150] Ch.W. Xu, P.K. Shen, *J. Power Sources* 142 (2005) 27

[151] Ch.W. Xu, P.K. Shen, X.H.e. Ji, R. Zeng, Y.L. Liu, *Electrochem.Commun.* 7 (2005) 1305

[152] K. Thamaphat, P. Limsuwan, B. Ngotawornchai, *Kasetasar J.(Nat. Sci.)* 42 (2008) 357

[153] "Titanium dioxide", (2011), [Online], Available: http://en.wikipedia.org/wiki/Titanium_dioxide

[154] "Titanium Dioxide – Titania", (2011), [Online], Available:http://www.azom.com/article.aspx?ArticleID=1179

[155] H. Matusiewicz, E. Stanisz, *Microchem. J.* 86 (2007) 9

[156] K.W. Park, S.B. Han, J.M. L´eger, *Electrochem.Commun.* 9 (2007) 1578

[157] M. Hepel, I. Dela, T. Hepel, J. Luo, C.J. Zhong, *Electrochim. Acta* 52 (2007) 5529

[158] G.L. Puma, A. Bono, D. Krishnaiah, J.G. Collin, *J. Hazardous Maerials* 157 (2008) 209

[159] W.Z. Li, "The research of cathode carbon support platinum catalyst for direct methanol fuel cell", Published PhD. thesis, Dalian Institute of Chemical Physics, China (2003)

[160] H. Bönnemann, *J. Power Sources* 84 (1994)161

[161] J. Haber, J. H. Block, B. Delmon, *Pure & Appl. Chem.*, 67 (1995), Nos 8/9, 1257

[162] C. R. K. Rao, D. C. Trivedi, *Coordination Chemistry Review* 249 (2005) 613-631

[163] C. Thurier, P. Doppelt, *Coordination Chemistry Review*, 252 (2008)155

[164] Chemical vapor deposition, (2010), [Online], Available: http://en.wikipedia.org/wiki/Chemical_vapor_deposition

[165] E.C. Marboe, US Patent US2430520 (1947)

[166] M.J. Rand, *J. Electrochem. Soc.* 120 (1973) 686

[167] B.S. Kwak, P.N. First, A. Erbil, B.J. Wilkens, J.D. Budai, M.F. Chisholm,

L.A. Boatner, *J. Appl. Phys.* 72 (1992) 3735

[168] G. Malandrino, R. Lo Nigro, I.L. Fragal`a, *Chem. Vap. Depos.*(1999) 59

[169] M. Utriainen, M. Kröger-Laukkanen, L.S. Johansson, L. Niinistö, *Appl. Surf. Sci.* 157 (2000) 151

[170] G. Jacobs, F. Ghadiali, A. Pisanu, A. Borgna, W. E. Alvarez, D. E. Resasco, *Appl. Catal*. A 188 (1999), 79

[171] G. Jacobs, W. E. Alvarez, D. E. Resasco, *Appl. Catal.*A 206 (1999), 267

[172] S. B. Hong, E. Mielczarski, M. E. Davis, *J. Catal*.134 (1992), 349

[173] "Transmission electron microscopy", (2010), [Online], Available:http://en.wikipedia.org/wiki/Transmission_electron_microscopy

[174] S. Swapp, "Scanning Electron Microscopy (SEM)", (2011), [Online], Available:http://serc.carleton.edu/research_education/geochemsheets/techniques/SEM.html

[175] S.J. Bradley, Schmid, G., Ed. VCH: Weinheim, (1994) 459

[176] "Voltammetry", (2010), [Online], Available:http://en.wikipedia.org/wiki/Voltammetry

[177] J. H. Hirschenhofer, D.B. Stauffer, R.R.Engliman, I.G. Klett, "Fuel Cell Handbook - Fuel Cell Description", November, (1998), [Online], Available: http://www.hydrogencommerce.com/FCHandbook/TechOver1-1FCDesc.htm

[178] X. Wand, W.Z. Li, Z.W. Chen, M. Waje, Y. Yan, *J. Power Sources*, 158 (2006) 154

[179] S. Subramanian, *Platinum metal Rev*. 36 (2) (1992) 98

[180] R.W. McCabe, R.K. Ober, H.S. Gandhi, *J. Cata.* 151 (1995) 385

[181] K.L. Siefering, G.L. Griffin, *J. Electrochemistry. Society* 137 (1990) 1206

[182] S. Kim, J. Park, D. Choi, *Thin Solid Films,* 315 (1998) 229

[183] J. M. Lee, C.S. Hwang, H.J. Cho, C.G. Suk, H.J. Kim, *J. Electro. Chem. Society,* 145 (1998) 1066

[184] B. Lecohire, B. Calpini, J.M. Philippoz, H. Bergh, *J. Appl. Phy.* 72 (1992) 2022

[185] L.M. Liz-Marzan, M. Giersig, P. Mulvaney, *Langmuir* 12 (1996) 4329

[186] M. Brust, M. Walker, D. Bethell, D.J. Schiffrin, R. Whyman, *J. Chem. Soc., Chem. Commun.* (1994) 801

[187] T. Yonezawa, K. Yasui, N. Kimizuka, *Langmuir* 17 (2001) 271

[188] F. Pinna, Catalysis Today, 41 (1998) 129

[189] C. Dossi, R. Psaro, A. Bartsch, E. Brivio, A. Galasco, P. Losi, *Catalysis Today*, 17 (1993) 527

[190] C. Dossi, a. Fusi, S. Recchia, M. Anghileri, R. Psaro, *Chem. Comm.* (1994) 1245

[191] S. Feast, M. Englisch, A. Jentys, J.A. Lercher, *Appl. Cata.* A174 (1998) 155

[192] C. Dossi, R. Psaro, A. Bartsch, A. Fusi, L. Sordelli, R. Ugo, M. Bellatreccia, R. Zanoni, G. Vlaic, *J. Cata.*A 145 (1994) 377

[193] P. Atanasova, J. Wise, M. Fallbach, T. Kodas, M. Hampden-Smith, Preparation of catalysis VII: proceedings of the 7th international symposium on scientific bases for the preparation of heterogeneous catalysts, (1998) 73

[194] A. Guerrero-Ruiz, P. Badense, I. Rodriguez-Ramos, *Appl. Cata*. A173 (1998) 313

[195] H.P. Chu, L. Lei, X. Hu, P.L. Yue, *Energy and Fuels*, 12 (1998) 1108

[196] S. Suvanto, T.A. Pakkanen, L. Backman, *Appl. Cata*. A 177 (1999) 25

[197] J.S. Yoo, *Catalysis Today*, 41 (1998) 409

[198] Wikipedia, "Inductively coupled plasma mass spectrometry", (2010), [Online], Available: http://en.wikipedia.org/wiki/Inductively_coupled_plasma_mass_spectrometry

[199] W. Vielstich, A. Lamm, H. Gasteiger, "Handbook of Fuel Cells, Fundamentals Technology and Applications", 2 (2005) 508, Printed and bound in Great Britain by Antony Rowe, Chippenham, Wiltshire

[200] H.F. Xu, Y.Z. Lin, Y.L. Qiu, Q. Tang, *Chinese Journal of Catalysis*, 24 (2) (2003)143

[201] W. Li, C. Liang, W. Zhou, J. Qin, Z. Zhou, G. Sun, Q. Xin, *J. Phys. Chem.* B 107 (2007) 6292

[202] A. Sep´ulveda-Escribano, F. Coloma, F. Rodr´ıguex-Reinoso, *Appl. Catal.* A173 (1998), 247

[203] Y. Takasu, T. Kawaguchi, W. Sugimoto, Y. Murakami, *Electrochim. Acta* 48 (2003)3861

[204] T. Frelink, W. Visscher, J.A.R. van Veen, *J. Electroanal. Chem.* 382

[205] R.W. Pekala, *J. Mater. Sci.* 24 (1989) 3221

[206] R.W. Pekala, S.T. Alviso, X. Lu, J. Gross, J. Fricke, *J. Non-Cryst. Solids* 188(1995)34

[207] A. Pozio, M. De Francessco, A. Cemmi, F.Cardellini, L. Giorgi, J. Power. Sources 105 (2002) 13

[208] G.W. Yand, G.Y. Gao, G.Y. Zhao, H.L. Li, *Carbon*, 45 (2007) 3036

[209] S. Yin, P.K, Shen, S. Son, S.P. Jiang, *Elecrochemica Acta*, 54 (2009) 6954

[210] D.S. Austin, J.A. Polta, T.Z. Polta, A.P.-C. Tang, T.D. Cabelka, D.C. Johnson,*J. Electroanal. Chem.* 25 (1984) 227

[211] S. Trasatti, O.A. Petrii, *Pure Appl. Chem*. 63 (1991) 711

[212] T. Maiyalagan, *J. Power Sorces* 179 (2008) 443

[213] E.I. Santiago, S.M. Batista, E.M. Assaf,*J. Electrochem. Soc.*151 (2004), A944

[214] A.L. Ocampl, M. Miranda-Hernández, J. Morgado, J.A. Montoya, P.J. Sebastian, *J. Power Sources* 160 (2006) 915

[215] M.K. Jeon, J.S. Cooper, P.J. McGinn, *J. Power Sources* 185 (2008) 913

[216] Y. Marquez-Návarro, L. Galicia, V.H. Lara, G. Del Ángel, *J. Mexico Chem. Soc.* 52 (1) (2008) 67

[217] L. Brewer, in: P. Rudman, J. Stringer, R.I. Haffee (Eds.), Phase Stability in Metals andAlloys, McGraw-Hill, New York, (1967) 39

[218] M.K. Jeon, J.S. Cooper, P.J. McGinn, *J. Power Sources* 185 (2008) 913

[219] L. Yang, D. He, Q.Y. Cai, *J. Phys. Chem*. C 111 (2007)8214

[220] Y. Chen, J.C. Crittenden, S. Hackney, L. Sutter, D.W. Hand, *Environ. Sci. Technol.*39 (2005) 1201

[221] H.Q. Song, P. Xiao, X.P. Qiu, W.T. Zhu, *J. Power Sources* 195 (2010)1610

[222] Z.Y. Wang, G. Chen, D.G. Xia, L.J. Zhang, *J. Alloy and Compounds* 450 (2008) 148

[223] S.Q. Liu, A.C. Chen, *Langmuir* 21 (2005) 8409

[224] O. Varghese, X. Yang, J. Kendig, M. Paulose, K. Zeng, C. Palmer, K. Ong, C.A.Grimes, *SensorLett*. 4 (2006) 120

[225] O. Varghese, D. Gong, M. Paulose, K. Ong, C.A. Grimes, *Sens. Actuators* B 93 (2003) 338

[226] P. Paunović, A.T. Dimitrov, O. Popovski, D. Slavkov, *Macedonian Journal of Chemistry and Chemical Engineering*, 26 (2) (2007) 87, ISSN 1857 - 5552

[227] Y. Wang, E.R. Fachini, G. Cruz, Y. Zhu, Y. Ishikawa, J.A. Colucci, C.R.

Cabrera, *J. Electrochem. Soc.* 148 (2001) C222

[228] N.F.P. Ribeiro, F.M.T. Mendes, C.A.C. Perez, M.M.V.M. Souza, M. Schmal, *Appl. Catal.* A 347 (2008) 62

[229] T. Ioroi, T. Akita, S. Yamazaki, Z. Siroma, N. Fujiwara, K. Yasuda, *Electrochim. Acta* 52 (2006) 491

[230] A.S. Arico, S. Srinivasan, V. Antonucci, *Fuel Cells* 2 (2001) 133

[231] H.P. Yuan, D.J. Guo, X.P. Qiu, W.T. Zhu, L.Q. Chen, *J. Power Sources*, 188 (2009) 8

[232] K.W. Park, S.B. Han, J.M. L´eger, Electrochem.Commun. 9 (2007) 1578

[233] M. Hepel, I. Dela, T. Hepel, J. Luo, C.J. Zhong, Electrochim. Acta 52 (2007) 5529

[234] D.M. He, L.X. Yang, S.Y. Kuang, Q.Y. Cai, *Elecrochem. Commun*, 9 (2007) 2467

[235] H. Song, X. Qiu, F. Li, *Electrochimica Acta* 53 (2008) 3708

[236] Z.C. Di, J. Ding, X.J. Peng, Y.H. Li, Z.K. Luan, J. Liang, *Chemosphere* 62 (2006) 861

[237] S. Anandan, M. Yoon, *J. Photochem.Photobiol.* C4 (2003) 5

[238] Z.Y. Wang, G.Chen, D.G. Xia, L.J. Zhang, *J. Alloys and Compounds* 450 (2008) 148

[239] K. Hirakawa, M. Inoue, T. Abe, *Electrochimica Acta* 55 (2010) 5874

[240] F. Aviles, J.V. Cauich-Rodriguez, L. Moo-Tah, A. May-Pat, R. Vargas-Coronado,*Carbon* 47 (2009) 2970

[241] S. Wang, L.J. Ji, B. Wu, Q.M. Gong, Y.F. Zhu, J. Liang, *Applied Surface Surface Science*, 255 (2008) 3263

[242] L. Chen, X.J. Pang, G. S. Yu, J.M. Zhang, *Advanced Materials Letters*, 1 (2010) 75

[243] K. Zhang, F.J. Zhang, M.L. Chen, W.C. Oh, *Ultrasonics Sonochemistry*, xxx (2010) xxx

[244] Z.Y. Ryn, J.T. Zheng, M.Z. Wang, B.J. Zhang, *Carbon* 37 (1999) 1257

[245] M. L. Chen, F. J. Zhang, W.C. Oh, *J. the Korean Ceramic Society*, 47 (2010) 269

[246] R.L. Jia, C.Y. Wang, "Preparation of platinum supported on carbon blacks with different surface chemical characteristics", in Proceedings of The third International Conference on Fuel Cell Science, Engineering and Technology, May (2005), Fuel Cell, 74138

[247] Y.H. Yin, C.H. Huang, *Chinese Year of Semiconductor* (in Chinese), 18 (2) (1997) 97

[248] S. Besselmann, C. Freitag, O. Hinrichsen, M. Muhler, *Phys. Chem. Chem. Phys.*, 3 (2001) 4633, DOI: 10.1039/B105466j

[249] S. Velu, L. Wang, M. Okazak, K. Suzuk, S. Tomura, *Microporous and Mesoporous Materials,* 5 (1-2) (2002) 113

[250] H. Zhu, S.J. Liao, "TPR investigation for the effect of several promoters on the carbon supported platinum catalyst", [Online], Available:http://event09.ise-online.org/cdrom/online/files/ise082990.pdf

[251] Istadi, N.A.S. Amin, *J. Molecular Catalysis* A: Chemical 259 (2006) 61

[252] A. Nie, H.S. Yand, Q. Li, X.Y. Fan, F.M. Qiu, X.B. Zhang, Industrial & Engineering Chemistry Research, (2011), DOI: 10. 1021/ie200568a,

Appendix:

1. Calculations for initial theoretical Platinum and other metal contents in home-made electrocatalysts, which synthesized using OMCVD method, (wt. %) is described as follows:

1) 10% Pt/CNT catalyst:

Mole of Pt = mole of Pt $(acac)_2$

= [mass of Pt $(acac)_2$] / [molecular weight of Pt $(acac)_2$]

= 0.11205 / 393.29

= 2.85×10^{-4} mol

Mass of Pt = (molecular weight of Pt) × (mole of Pt)

= 195 × (2.85×10^{-4})

= 55.57 mg

Wt.% loading of Pt = { (mass of Pt) / [(mass of Pt) + (mass of CNTs)] } × 100%

= [55.57 / (55.57+500)] ×100%

= 10 %

2) The calculation procedure specified in 1) was followed to obtaincontent of 20, 40, 60wt. % Pt/CNT catalysts

3) 20 % Pt 20 % Ru/CNT:

Mole of Pt = mole of Pt $(acac)_2$

= [mass of Pt $(acac)_2$] / [molecular weight of Pt $(acac)_2$]

= 0.335 / 393.29

= 8.52×10^{-4} mol

Mass of Pt = (molecular weight of Pt) × (mole of Pt)

= 195 × (8.52×10^{-4})

= 166.14 mg

Mole of Ru = mole of Ru $(acac)_2$

= [mass of Ru $(acac)_2$] / [molecular weight of Ru $(acac)_2$]

= 0.65478 / 381.43

= 1.72×10^{-3} mol

Mass of Ru = (molecular weight of Ru) × (mole of Ru)

= $101.07 \times (1.72 \times 10^{-3})$

= 173.84 mg

Wt.% loading of Pt = { (mass of Pt) / [(mass of Pt) + (mass of Ru) + (mass of CNTs)] } × 100%

= [166.14 / (166.14 + 173.84 + 500)] ×100%

= 19.8%

Wt.% loading of Ru = { (mass of Ru) / [(mass of Pt) + (mass of Ru) + (mass of CNTs)] } × 100%

= [173.84 / (166.14 + 173.84 + 500)] ×100%

= 20.0 %

4) The calculation procedure specified in 3) was followed to obtain the content of PtRuFe/CNT, PtRuCu/CNT and PtRuV/CNT catalysts

2. Demonstration for obtaining the hydrogen desorption area on Auto lab software:

1) **Impor the plot into the Auto-lab**
2) **“Analysis”**
3) **“Peak search”**
4) **“Manual”**
5) **“Linear free cursor”**
6) **Choose the area of hydrogen desoption**
7) **Obtain the peak area (C) automatically from the software**